

**Editor**

N Viswanadham

*Indian Institute of Science, Bangalore*

**Consulting Editor**

R Narasimha

*National Institute of Advanced studies, Bangalore*

**Associate Editor**

Gangan Prathap

*National Aerospace Laboratories, Bangalore*

**Editorial Board**

V S Borkar, *Indian Institute of Science, Bangalore*

S C Dutta Roy, *Indian Institute of Technology, New Delhi*

K S Gandhi, *Indian Institute of Science, Bangalore*

M Gaster, *Queen Mary & Westfield College, London*

F Hussain, *University of Houston, Houston, TX*

Y Jaluria, *Rutgers University, New Brunswick, NJ*

B D Kulkarni, *National Chemical Laboratory, Pune*

R Narayana Iyengar, *Central Building Research Institute, Rourkee*

B C Nakra, *Indian Institute of Technology, New Delhi*

M A Pai, *University of Illinois, Urbana-Champaign, IL*

P Ramachandra Rao, *National Metallurgical Laboratory, Jamshedpur*

A Roshko, *California Institute of Technology, Pasadena, CA*

V V S Sarma, *Indian Institute of Science, Bangalore*

S Sathiya Keerthi, *Indian Institute of Science, Bangalore*

R K Shyamasundar, *Tata Institute of Fundamental Research, Bombay*

A Sridharan, *Indian Institute of Science, Bangalore*

J Srinivasan, *Indian Institute of Science, Bangalore*

**Editor of Publications of the Academy**

N Mukunda

*Indian Institute of Science, Bangalore*

**Subscription Rates**

(Effective from 1996)

**All countries except India**

(Price includes AIR MAIL charges)

**Institutional**

US\$100

**Individuals**

US\$40

**India**

Rs. 150

Rs. 75

All correspondence regarding subscription should be addressed to **The Circulation Department** of the Academy.

**Editorial Office**

Indian Academy of Sciences, C V Raman Avenue  
P.B. No. 8005, Sadashivanagar  
Bangalore 560 080, India

Telephone: (080) 3342546, 3342943  
Telefax: 91-80-3346094

e-mail: sadhana@ias.ernet.in

# Recent Results in Signal Processing and Communications

## Foreword

This special issue consists of ten papers which have been selected from among those presented at the Conference on Signal Processing, Communications and Networking, held at the Indian Institute of Science, Bangalore during July 16–19, 1997. These papers report some new results in the fields of signal processing and communication. They cover a wide spectrum of topics of current interest, namely, parameter estimation in the presence of Ricean fading, transformations for mapping circular array manifold to that of uniform linear array and the associated errors, use of fractal models and multiresolution framework in image reconstruction and interpretation, group codes with rotational invariance property, use of group delay function in power spectrum estimation of complex signals, analysis of stochastic gradient lattice algorithm, adaptive notch filters, schemes for I-Q imbalance correction, application of cosine-modulated filter banks in reconstruction of periodic errors in bursts in oversampled data and performance analysis of two versions of TCP over mobile radio links.

Use of sensor arrays in the field of mobile communication to improve the performance of a cellular system has been an active area of research. Recently, maximum likelihood and least squares based techniques have been proposed for estimating direction-of-arrival (DOA) of the received signal from a mobile unit and the associated angular spread due to scattering in the presence of Rayleigh fading using a linear array. The first paper by Han and Otterson addresses a similar problem for a Ricean fading channel.

Recently, several high resolution DOA estimation methods and the effect of certain pre-processing schemes, known as smoothing techniques, on the performance of these methods have been studied by many authors. Most of these studies have been restricted to uniform linear arrays because several of the high resolution methods and smoothing schemes are applicable only to such arrays. However, in practical applications where 360° coverage is required, we use uniform circular arrays. One can apply a transformation based on phase mode excitation concept, to the data from the circular array and use the techniques applicable to uniform linear arrays. The second paper by Maheswara Reddy and Umaphathi Reddy discusses the errors arising out of this transformation and their effect on the performance of the DOA estimation.

In computer-aided tomography, the objective is to reconstruct a cross-section of an object from measurements that are strip integrals of some property of the object. A popular technique for image reconstruction is the filtered back projection. The third paper by Chowdhury, Barman and Ramakrishnan addresses the problem of reconstruction from noisy projections, restricting their discussion to parallel beam tomography. One of the

advantages of their approach is the reduction in the time of exposure to the p radiation.

Digital communication over additive white Gaussian noise channel can be model transmission of a point from a finite set of points of a finite-dimensional vector space. The problem of signal set design then reduces to choosing a specified number of points in a space of specified dimension in such a way that the minimum distance between points is maximum. One can obtain good signal sets in large dimension starting with a signal set of small dimension using group codes. The fourth paper by Jyoti Bali and Rajan reports rotational invariance properties of coded signal sets obtained by the construction for a class of two- and four-dimensional signal sets.

Spectrum estimation is a highly researched field. The basic periodogram spectrum estimate (PSE), which has good resolution, low bias and gives good signal detectability from large variance. A group delay approach, with modification for the group delay, preserves the advantages of PSE and reduces the variance of the estimate. The fifth paper by Narasimhan, Plotkin and Swamy applies the group delay function with modifications to complex signals to estimate the power spectrum, and discusses its application based on Wigner–Ville distribution.

Adaptive IIR notch filters provide superior performance at lower computational cost relative to their FIR counterparts in suppressing narrowband interference and provides line enhancement. A diverse choice of biquad designs are proposed for performing the above functions by several authors. The sixth paper by Krishna and Hiremath provides a lucid presentation on how all these designs are equivalent in their asymptotic performance.

The adaptive lattice filter has several desirable characteristics such as orthogonality of the input, faster convergence and simple stability checking criteria. The steepest gradient lattice algorithm is commonly used for adapting the FIR lattice filter coefficients because of its low computational complexity. The seventh paper by Negi and Prasad presents some theoretical results on bias in reflection coefficient and convergence of the algorithm.

In a coherent receiver, In-phase and Quadrature phase signals are derived by demodulating the IF signal. Practical demodulators give rise to some amplitude and phase imbalance in I-Q signals. The eighth paper by Sivannarayana and Veerabhadra Rao suggests a method in time and frequency domains for I-Q imbalance correction.

The restoration of erasure bursts in oversampled multimedia data has assumed increasing significance in the context of cell loss in ATM networks. Many heuristic methods such as linear interpolation, repetition, muting, and systematic approaches have been considered in recent years. The ninth paper by Jayasimha and Hiremath presents a low-complexity approach, based on cosine modulated filter banks, for reconstructing periodic erasure bursts.

versions of TCP (the original, and the Tahoe version) over a Rayleigh fading radio link; the analysis reveals the effect of vehicle speed, and the average SNR required for achieving adequate throughputs.

We would like to express our thanks to Prof. N. Viswanadham, Editor, *Sādhanā*, for inviting us to bring out this special issue, and also special thanks to the editorial staff of the journal for their effort and cooperation in bringing out this issue.

February 1998

V UMAPATHI REDDY  
ANURAG KUMAR  
Guest Editors



# Parameter estimation using a sensor array in a Ricean fading channel\*

K V S HARI<sup>1</sup> and BJÖRN OTTERSTEN<sup>2</sup>

<sup>1</sup>Department of Electrical Communication Engineering, Indian Institute of Science, Bangalore 560 012, India

<sup>2</sup>Department of Signals, Sensors and Systems, Royal Institute of Technology, S-100 44 Stockholm, Sweden

e-mail: hari@ece.iisc.ernet.in; otterste@s3.kth.se

**Abstract.** The estimation of the Direction-Of-Arrival (DOA) and the variance of the angular spread, using an array of sensors in the case of a Ricean channel is considered, using the Maximum-Likelihood, Least-Squares and Weighted Least Squares criteria. The Cramér–Rao bound is also obtained for the problem of interest. Simplification of the cost functions to reduce the dimension of the problem has been carried out and the performance of the methods has been studied based on numerical experiments.

**Keywords.** Antenna arrays; fading channels; spatially distributed sources.

## 1. Introduction

The use of sensor arrays in the field of mobile communication to improve the performance of a cellular system has been an active area of research recently. An important issue is to efficiently use the available channel bandwidth to provide services to as many users as possible. Techniques using an array of sensors have been proposed which estimate the Direction-Of-Arrival (DOA) of the received signal from a mobile unit and the associated angular spread due to scattering, to form multiple beams on the same channel and increase user capacity (Yeh & Reudink 1982; Anderson *et al* 1991; Balaban & Salz 1992; Ohgane *et al* 1993; Zetterberg & Ottersten 1995). Estimation of DOA and angular spread of scattered field using a Uniform Linear Array (ULA) has been carried out for a Rayleigh fading channel using the Maximum Likelihood and least squares criteria.

criteria. A comparison of the performance of these methods is carried out using simulations.

## 2. Data model

In a mobile communication scenario, the narrowband signal from a source received at the base station using a sensor-array, is assumed to be a sum of *large* number of signals with different strengths and arriving from angles relative to the direction of the source. This model has been verified by experiments showing the scattering effects of the channel (Adachi *et al* 1986). In this report, a uniform linear array (ULA) with an inter-sensor distance,  $d_\lambda$  (in wavelengths) is considered. The response of the  $k$ th sensor to a unit-amplitude narrowband signal impinging from a direction  $\theta$  (relative to the broadside of the array), is known as the *array response vector* for  $\theta$ , denoted by  $\mathbf{a}(\theta)$  and its  $k$ th element is defined as<sup>1</sup>

$$[\mathbf{a}(\theta)]_k = \exp[j2\pi d_\lambda(k - 1) \sin(\theta)].$$

Assume that a single source is transmitting a narrowband signal at an angle  $\theta$  which is being received by the ULA due to scatterers in the vicinity. The noiseless output of the  $k$ th sensor as a function of time  $t$ , can be written as

$$y_k(t) = \left( \sum_n g_n(t) e^{j\alpha_n(t)} e^{(j2\pi d_\lambda(k-1) \sin(\theta + \theta_n))} \right) s(t),$$

where  $g_n(t)$ ,  $\alpha_n(t)$  are the amplitude and phase factors due to the  $n$ th scatterer,  $\theta_n$  is the deviation with respect to  $\theta$  due to the  $n$ th scatterer. Stacking the outputs of all sensors into a vector,  $\mathbf{y}(t)$ , the *snapshot* of the array output can be written as

$$\mathbf{y}(t) = \mathbf{h}(t) s(t),$$

$$\mathbf{h}(t) = \sum_n g_n(t) e^{j\alpha_n(t)} \mathbf{a}(\theta + \theta_n),$$

where  $\mathbf{h}(t)$  denotes the *channel response vector* at time instant  $t$ .

### 2.1 Fading channels

A channel is said to be a *fading channel* if the amplitudes and phases of the scatterers and the directions of the scatterers are random and vary with time (Braun & Dersch 1991). Further, if these are independent and identically distributed, and the number of scatterers is very large, the Central-Limit Theorem can be applied to the channel response vector.

signal amplitudes, phases and the directions needs to be done. Trump & Ottersten (1996) have assumed that

$$\begin{aligned} E[g_n(t)e^{j\alpha_n(t)}g_m(s)e^{-j\alpha_m(s)}] &= 0, \quad n \neq m, \quad t \neq s, \\ &= 1, \quad \text{otherwise}, \\ E[e^{j\alpha_n(t)}] &= 0. \end{aligned}$$

Based on these assumptions,  $Cov[\mathbf{h}(t), \mathbf{h}(\tau)] = \mathbf{C}_h \delta(t - \tau)$ . Many distributions of  $\theta_n$  have been proposed by Anderson *et al* (1991), Parsons & Turkmani (1991), Proakis (1991) and Trump & Ottersten (1996) and in this paper it is assumed that  $\theta_n$  is small and  $\theta_n \sim \mathcal{N}(m_\theta, \sigma_\theta)$ .

2.1a *Rayleigh fading channel:* In an urban environment, usually, there is no direct path between the mobile unit and the base station sensor array and it is assumed that  $\mathbf{m}_h(t) = E[\mathbf{h}(t)] = \mathbf{0}$  (Zetterberg & Ottersten 1995; Trump & Ottersten 1996) and such a channel is known as a Rayleigh fading channel (Proakis 1989). Assuming,  $m_\theta = 0$ ,  $\mathbf{C}_h$  is given as (Trump & Ottersten 1996)

$$\mathbf{C}_h = \mathbf{R}_a \bullet \mathbf{B}(\theta, \sigma_\theta),$$

where the  $kl$ th element of  $\mathbf{B}$  is given by

$$[\mathbf{B}]_{kl} = \exp\{-2[\pi(k-l)d_\lambda]^2\sigma_\theta \cos^2(\theta)\},$$

and

$$\mathbf{R}_a = \mathbf{a}(\theta) \mathbf{a}^H(\theta).$$

*Model M1* – Let  $s(t)$  be a random signal uncorrelated with  $\mathbf{h}(t)$  and  $s(t) = \alpha \exp[j\phi_s(t)]$  with  $\alpha$  being a deterministic quantity and  $\phi_s(t)$  being distributed uniformly between 0 and  $2\pi$ . Then  $\mathbf{m}_y(t) = \mathbf{0}$ ,  $\mathbf{C}_y(t) = \mathbf{C}_h |\alpha|^2$ .

It can be easily shown using elementary probability theory, that  $\mathbf{y}(t) \sim \mathcal{N}(\mathbf{0}, \mathbf{C}_y(t))$  for model M1.

*Remark 1.* It is to be noted that if  $s(t)$  is Gaussian,  $\mathbf{y}(t)$  is no longer Gaussian.

*Model M2* – If  $s(t)$  is a deterministic signal, then  $\mathbf{m}_y(t) = \mathbf{0}$ ,  $\mathbf{C}_y(t) = \mathbf{C}_h |s(t)|^2$  and  $\mathbf{y}(t) \sim \mathcal{N}(\mathbf{0}, \mathbf{C}_y(t))$ .

## 2.2 Ricean fading channel

*Case 1:* Let  $\gamma$  be a deterministic but unknown quantity.

*Case 2:* Let  $\gamma \sim N(\gamma_0, \sigma_\gamma)$  independent of other parameters. Since  $\alpha$  is assumed,  $\gamma_0 \neq 0$ . It is clear that the new channel response vector in both cases has a non-zero mean of the form  $\gamma\mathbf{a}(\theta)$ . This channel is said to be a *Ricean fading channel* because the envelope has a Rice distribution (Proakis 1989).

*Model M3* – Let  $s(t)$  be a *random* signal uncorrelated with  $\mathbf{h}(t)$  and  $\mathbf{m}_y(t) = \mathbf{0}$ ,  $\mathbf{C}_y(t) = (\mathbf{C}_h + \mathbf{m}_h\mathbf{m}_h^H)|\alpha|^2$ . As in the case of Gaussian.

*Model M4* –  $s(t)$  is a *deterministic* signal. Then  $\mathbf{m}_y(t) = \mathbf{m}_h s(t)$ ,  $\mathbf{C}_y(t) \sim \mathcal{N}(\mathbf{m}_y(t), \mathbf{C}_y(t))$ .

### 2.3 Noisy data

Consider the noisy array output as

$$\mathbf{x}(t) = \mathbf{y}(t) + \mathbf{n}(t),$$

where  $\mathbf{n}(t)$  is the additive noise vector which is zero-mean Gaussian,  $E[\mathbf{n}(t)\mathbf{s}(t)] = \mathbf{0}$ ,  $E[\mathbf{n}(t)\mathbf{n}^H(t)] = \sigma_n \mathbf{I}$  and  $E[\mathbf{n}(t)\mathbf{n}^T(\tau)] = \mathbf{0}$ . Then  $\mathbf{C}_x(t) = \mathbf{R}_x + \sigma_n^2 \mathbf{I}$  for any of the above models. In this paper, the Ricean fading channel (models M3 and M4) with  $\gamma$  being deterministic but unknown. The covariance matrices for  $\mathbf{x}(t)$  belonging to these models can be obtained as

$$\mathbf{R}_x = \sigma_\gamma \sigma_s \mathbf{R}_a + \sigma_s \mathbf{R}_b + \sigma_n \mathbf{I},$$

$$\mathbf{C}_x = \sigma_s \mathbf{R}_b + \sigma_n \mathbf{I},$$

where  $\sigma_\gamma = |\gamma|^2$ ,  $\sigma_s = E|s(t)|^2$  and  $\mathbf{m}_x$  is the mean of  $\mathbf{x}(t)$ .

## 3. Parameter estimation

It is clear that there are two cases of interest: (i) Random source (model M3) and (ii) Deterministic source (model M4). The estimation of parameters for the channel assuming a random source (model M1) was carried out (Trumpf et al. 1997). In this paper, the estimation of the parameters for models M3 and M4 using Maximum Likelihood and Weighted Least Squares criteria is presented.

*Problem statement.* Given  $N$  snapshots of the array outputs,  $\mathbf{x}(t_1), \mathbf{x}(t_2), \dots, \mathbf{x}(t_N)$ , estimate the parameter vector  $\boldsymbol{\eta} = [\theta, \sigma_\theta, \sigma_s, \sigma_n, \sigma_\gamma]^T$  for model M3 and  $\boldsymbol{\eta} = [\theta, \sigma_\theta, \sigma_s, \sigma_n]^T$  for model M4.

$$E\{(\boldsymbol{\eta} - \hat{\boldsymbol{\eta}})(\boldsymbol{\eta} - \hat{\boldsymbol{\eta}})^T\} \geq \mathbf{J}_{\boldsymbol{\eta}}^{-1},$$

where  $\mathbf{J}_{\boldsymbol{\eta}}$  is the *Fisher Information Matrix*. For model M3, the  $kl$ th element of  $\mathbf{J}_{\boldsymbol{\eta}}$  is (Trump & Ottersten 1996)

$$[\mathbf{J}_{\boldsymbol{\eta}}]_{kl} = N \operatorname{Tr} \left[ \mathbf{R}_x^{-1} \frac{\partial \mathbf{R}_x}{\partial \boldsymbol{\eta}_k} \mathbf{R}_x^{-1} \frac{\partial \mathbf{R}_x}{\partial \boldsymbol{\eta}_l} \right], \quad (1)$$

where  $\partial(\cdot)/\partial \boldsymbol{\eta}_k$  denotes differentiation with respect to the  $k$ th parameter of  $\boldsymbol{\eta}$ . For model M4, the  $kl$ th element of  $\mathbf{J}_{\boldsymbol{\eta}}$  can be easily shown to be

$$[\mathbf{J}_{\boldsymbol{\eta}}]_{kl} = N \operatorname{Tr} \left[ \mathbf{C}_x^{-1} \frac{\partial \mathbf{C}_x}{\partial \boldsymbol{\eta}_k} \mathbf{C}_x^{-1} \frac{\partial \mathbf{C}_x}{\partial \boldsymbol{\eta}_l} + 2 \mathbf{C}_x^{-1} \frac{\partial \mathbf{m}_x}{\partial \boldsymbol{\eta}_k} \frac{\partial \mathbf{m}_x^H}{\partial \boldsymbol{\eta}_l} \right]$$

where  $\mathbf{m}_x$ ,  $\mathbf{C}_x$  and  $\mathbf{R}_x$  denote the mean, covariance matrix and the correlation matrix of  $\mathbf{x}(t)$ .

## 5. Maximum-likelihood estimation

Given the Gaussian nature of  $\mathbf{x}(t_1), \mathbf{x}(t_2), \dots, \mathbf{x}(t_N)$ , the negative log-likelihood function for model M3 is given as

$$l_{ML}(\theta, \sigma_\theta, \sigma_s, \sigma_n, \sigma_\gamma) = \log(\det(\mathbf{R}_x)) + \operatorname{Tr}[\mathbf{R}_x^{-1} \hat{\mathbf{R}}]$$

and the conditional negative log-likelihood function for model M4 is given as

$$\begin{aligned} l_{ML}(\theta, \sigma_\theta, \sigma_n, \sigma_\gamma, s(t), t = 1, \dots, N) \\ = \log(\det(\mathbf{C}_x)) + \operatorname{Tr}[\mathbf{C}_x^{-1} \mathbf{M}], \end{aligned}$$

where  $\mathbf{M}$  is defined as

$$\mathbf{M} = \hat{\mathbf{R}} + \mathbf{m}\mathbf{m}^H - 2\mathbf{m}\hat{\mathbf{m}}^H$$

with

$$\hat{\mathbf{R}} = \frac{1}{N} \sum_{t=1}^N \mathbf{x}(t)\mathbf{x}^H(t),$$

$$\hat{\mathbf{m}} = \frac{1}{N} \sum_{t=1}^N \mathbf{x}(t).$$

$\hat{\mathbf{R}}$  is the data correlation matrix<sup>2</sup> and  $\hat{\mathbf{m}}$  is the sample mean of  $\mathbf{x}(t)$ . The maximum likelihood (ML) estimate of  $\boldsymbol{\eta}$  is obtained by minimizing  $l_{ML}$  in the parameter space of  $\boldsymbol{\eta}$ . Results from estimation theory guarantee that the ML estimates are asymptotically efficient.

## 6. Least squares estimation

As the solution to the ML problem is computationally expensive, a look at other criteria like the least squares criterion is worthwhile.

### 6.1 Weighted least squares

The general form of least squares is the weighted least squares (WLS) cost function which can be expressed as

$$\begin{aligned} l = l_{\text{WLS}}(\boldsymbol{\eta}) &= \|\mathbf{W}^{H/2}(\mathbf{R}_x - \hat{\mathbf{R}})\mathbf{W}^{1/2}\|_F^2 \\ &= \text{Tr}[(\mathbf{R}_x - \hat{\mathbf{R}})\mathbf{W}(\mathbf{R}_x - \hat{\mathbf{R}})\mathbf{W}], \end{aligned}$$

where  $\mathbf{W}$  is a positive definite *weighting* matrix. The choice of  $\mathbf{W}$  is usually such that the error-covariance of the parameter vector,  $\boldsymbol{\eta}$ , is minimized. Denoting the estimate of  $\boldsymbol{\eta}_0$  as  $\hat{\boldsymbol{\eta}}$ , the error in the parameter vector is given by

$$\tilde{\boldsymbol{\eta}} = (\boldsymbol{\eta}_0 - \hat{\boldsymbol{\eta}}) \approx -\mathbf{H}^{-1}(\boldsymbol{\eta}_0) \frac{\partial l}{\partial \boldsymbol{\eta}},$$

where  $\mathbf{H}$  is the Hessian of the cost function given by

$$[\mathbf{H}]_{ij} = \frac{\partial^2 l}{\partial \boldsymbol{\eta}_i \partial \boldsymbol{\eta}_j}.$$

The  $i$ th element of the gradient vector  $\mathbf{l}'$ , of the cost function can be obtained as

$$\begin{aligned} \mathbf{l}' &= \frac{\partial l}{\partial \boldsymbol{\eta}_i} = 2 \text{Tr}[(\mathbf{R}_x - \hat{\mathbf{R}})\mathbf{D}_i], \\ \mathbf{D}_i &= \mathbf{W} \frac{\partial \mathbf{R}_x}{\partial \boldsymbol{\eta}_i} \mathbf{W}. \end{aligned}$$

Following the development by Trump & Ottersten (1996),

$$\sqrt{N} \mathbf{l}' \sim \text{As } \mathcal{N}(\mathbf{0}, \mathbf{Q}),$$

where

$$\mathbf{Q} = \lim_{N \rightarrow \infty} N E[\mathbf{l}' (\mathbf{l}')^T].$$

Hence, the asymptotic distribution of the estimation error is given by

$$\sqrt{N} \tilde{\boldsymbol{\eta}} \sim \text{As } \mathcal{N}(\mathbf{0}, \mathbf{C}),$$

The  $ij$ th element of  $\mathbf{Q}$  is given as

$$\begin{aligned} E \left[ \frac{\partial l}{\partial \eta_i} \frac{\partial l}{\partial \eta_j} \right] &= 4 E[\text{Tr}\{(\mathbf{R}_x - \hat{\mathbf{R}}) \mathbf{D}_i\} \\ &\quad \times \text{Tr}\{(\mathbf{R}_x - \hat{\mathbf{R}}) \mathbf{D}_j\}] \\ &= 4 \text{Tr}\{\mathbf{R}_x \mathbf{D}_i\} \text{Tr}\{\mathbf{R}_x \mathbf{D}_j\} \\ &\quad - 4 \text{Tr}\{\mathbf{R}_x \mathbf{D}_i\} E[\text{Tr}\{\hat{\mathbf{R}}_x \mathbf{D}_j\}] \\ &\quad - 4 E[\text{Tr}\{\hat{\mathbf{R}} \mathbf{D}_i\}] \text{Tr}\{\mathbf{R}_x \mathbf{D}_j\} \\ &\quad + 4 E[\text{Tr}\{\hat{\mathbf{R}} \mathbf{D}_i\} \text{Tr}\{\hat{\mathbf{R}} \mathbf{D}_j\}] \\ &= 4 E[\text{Tr}\{\hat{\mathbf{R}} \mathbf{D}_i\} \text{Tr}\{\hat{\mathbf{R}} \mathbf{D}_j\}] \\ &\quad - 4 \text{Tr}\{\mathbf{R}_x \mathbf{D}_i\} \text{Tr}\{\mathbf{R}_x \mathbf{D}_j\} \end{aligned}$$

as  $E[\hat{\mathbf{R}}] = \mathbf{R}$ . The second term in the above equation can be written as

$$\begin{aligned} &= 4 E[\text{Tr}\{\hat{\mathbf{R}} \mathbf{D}_i\} \text{Tr}\{\hat{\mathbf{R}} \mathbf{D}_j\}] \\ &= \frac{4}{N^2} \sum_{t \neq l \neq m \neq o} E[\mathbf{x}_l^*(t) \mathbf{x}_m(t) \mathbf{x}_o^*(\tau) \mathbf{x}_p(\tau)] [\mathbf{D}_i]_{op} [\mathbf{D}_j]_{lm}. \end{aligned} \quad (2)$$

**6.1a Random source (model M3):** For the random source case, since  $\mathbf{m}_x(t) = \mathbf{0}$ , the above product of four Gaussian random variables with zero mean can be expressed as

$$\begin{aligned} &= \frac{4}{N^2} \sum_{t \neq l \neq m \neq o} (E[\mathbf{x}_l^*(t) \mathbf{x}_m(t)] E[\mathbf{x}_o^*(\tau) \mathbf{x}_p(\tau)]) \\ &\quad + E[\mathbf{x}_l^*(t) \mathbf{x}_p(\tau)] E[\mathbf{x}_o^*(\tau) \mathbf{x}_m(t)] [\mathbf{D}_i]_{op} [\mathbf{D}_j]_{lm} \\ &= 4 \text{Tr}\{\mathbf{R}_x \mathbf{D}_i\} \text{Tr}\{\mathbf{R}_x \mathbf{D}_j\} + \frac{4}{N} \text{Tr}\{\mathbf{R}_x \mathbf{D}_i \mathbf{R}_x \mathbf{D}_j\}. \end{aligned}$$

Thus

$$E \left[ \frac{\partial l}{\partial \eta_i} \frac{\partial l}{\partial \eta_j} \right] = \frac{4}{N} \text{Tr} \left\{ \mathbf{R}_x \mathbf{W} \frac{\partial \mathbf{R}_x}{\partial \eta_i} \mathbf{W} \mathbf{R}_x \mathbf{W} \frac{\partial \mathbf{R}_x}{\partial \eta_j} \mathbf{W} \right\}.$$

It was shown (Göransson 1995) that  $\mathbf{W} = \mathbf{R}_x^{-1}$  would yield

$$[\mathbf{C}^{-1}]_{ij} = \text{Tr} \left\{ \frac{\partial \mathbf{R}_x}{\partial \eta_j} \mathbf{R}_x^{-1} \frac{\partial \mathbf{R}_x}{\partial \eta_i} \mathbf{R}_x^{-1} \right\},$$

Differentiating w.r.t.  $\sigma_s$ ,  $\sigma_\gamma$ ,  $\sigma_n$ , setting to zero, and simplifying, the hold,

$$\begin{aligned} a_{11}\sigma_\gamma\sigma_s + a_{12}\sigma_s + a_{13}\sigma_n &= b_1, \\ a_{21}\sigma_\gamma\sigma_s + a_{22}\sigma_s + a_{11}\sigma_n &= b_2, \\ a_{22}\sigma_\gamma\sigma_s + a_{32}\sigma_s + a_{12}\sigma_n &= b_3, \end{aligned}$$

where  $a_{11} = \text{Tr}[\hat{\mathbf{R}}^{-1}\mathbf{R}_a\hat{\mathbf{R}}^{-1}]$ ,  $a_{12} = \text{Tr}[\hat{\mathbf{R}}^{-1}\mathbf{R}_b\hat{\mathbf{R}}^{-1}]$ ,  $a_{13} = \text{Tr}[\hat{\mathbf{R}}^{-1}\mathbf{R}_a\hat{\mathbf{R}}^{-1}\mathbf{R}_a]$ ,  $a_{22} = \text{Tr}[\hat{\mathbf{R}}^{-1}\mathbf{R}_b\hat{\mathbf{R}}^{-1}\mathbf{R}_a]$ ,  $a_{32} = \text{Tr}[\hat{\mathbf{R}}^{-1}\mathbf{R}_b\hat{\mathbf{R}}^{-1}\mathbf{R}_a]$ ,  $b_2 = \text{Tr}[\hat{\mathbf{R}}^{-1}\mathbf{R}_a]$ ,  $b_3 = \text{Tr}[\hat{\mathbf{R}}^{-1}\mathbf{R}_b]$ , Using the above equations, o sions for the three parameters as

$$\begin{aligned} \hat{\sigma}_n &= \frac{a_{22}b_1 - a_{11}b_3 - \sigma_s[a_{12}a_{22} - a_{32}a_{11}]}{[a_{13}a_{22} - a_{12}a_{11}]}, \\ \hat{\sigma}_\gamma &= \frac{a_{11}b_1 - a_{13}b_2 - \sigma_s[a_{11}a_{12} - a_{13}a_{22}]}{\sigma_s[a_{11}^2 - a_{13}a_{21}]}, \\ \hat{\sigma}_s &= \frac{c_1 + c_2 + c_3}{c_4}, \end{aligned}$$

where

$$\begin{aligned} c_1 &= b_1 \left( 1 - \frac{a_{11}^2}{[a_{11}^2 - a_{13}a_{21}]} - \frac{a_{13}a_{22}}{[a_{13}a_{22} - a_{12}a_{11}]} \right), \\ c_2 &= b_2 \left( \frac{a_{13}a_{11}}{[a_{11}^2 - a_{13}a_{21}]} \right), c_3 = b_3 \left( \frac{a_{13}a_{11}}{[a_{13}a_{22} - a_{12}a_{11}]} \right), \\ c_4 &= \left( a_{12} - \frac{a_{11}[a_{11}a_{12} - a_{13}a_{22}]}{[a_{11}^2 - a_{13}a_{21}]} - \frac{a_{13}[a_{12}a_{22} - a_{32}a_{11}]}{[a_{13}a_{22} - a_{12}a_{11}]} \right). \end{aligned}$$

The weighted least-squares cost function can now be recast as

$$l_{WLS}(\theta, \sigma_\theta) = \text{Tr}((\hat{\sigma}_\gamma\hat{\sigma}_s\mathbf{R}_a + \hat{\sigma}_s\mathbf{R}_b + \hat{\sigma}_n\mathbf{I})\hat{\mathbf{R}}^{-1} - \mathbf{I})^2],$$

and the search is now over a two-dimensional space of  $[\theta, \sigma_\theta]$  which less expensive than before.

**6.1b Deterministic source (Model M4):** For the model M4, the r have non-zero means and thus

$$E[\text{Tr}\{\hat{\mathbf{R}}\mathbf{D}_i\}\text{Tr}\{\hat{\mathbf{R}}\mathbf{D}_j\}] = \frac{1}{\pi^2} \sum_{m=-\infty}^{\infty} \{E[\mathbf{x}_i^*(t)\mathbf{x}_m(t)]E[\mathbf{x}_j^*(t)\mathbf{x}_m(t)]\}$$

After some tedious calculations, the  $ij$ th element of  $\mathbf{Q}$  for this case is given as

$$[\mathbf{Q}]_{ij} = \frac{4}{N} \text{Tr}\{\mathbf{R}_x \mathbf{D}_i\} \text{Tr}\{\mathbf{R}_x \mathbf{D}_j\} + \frac{4}{N} \text{Tr}\{\mathbf{R}'_x \mathbf{D}_i\} \text{Tr}\{(\mathbf{R}'_x)^T \mathbf{D}_j\} \\ - 8 \text{Tr}[\mathbf{m}_x \mathbf{m}_x^H \mathbf{D}_i] \text{Tr}[\mathbf{m}_x \mathbf{m}_x^H \mathbf{D}_j],$$

where

$$\mathbf{R}'_x = E[\mathbf{x}(t) \mathbf{x}^T(t).] = \mathbf{m}_x(t) \mathbf{m}_x^T(t).$$

*Remark 2.*

- It is difficult to obtain  $\mathbf{W}$  from the above equation for  $\mathbf{Q}$ , which minimizes  $\mathbf{C}$ .
- The same result holds good for model M2 also, with the appropriate correlation matrix

6.1c *Least squares:* A more popular criterion, which is simpler, is the least square criterion, defined for  $\mathbf{W} = \mathbf{I}$  as

$$l_{LS} = \text{Tr}[(\hat{\mathbf{R}} - \mathbf{R}_x)(\hat{\mathbf{R}} - \mathbf{R}_x)^H]$$

*Random source (Model M3)* – As in the case of the WLS criterion, since the cost function is quadratic in  $\sigma_s$ ,  $\sigma_\gamma$ ,  $\sigma_n$ , these parameters can be separated. Using some simple identities, one can obtain

$$\hat{\sigma}_n = \frac{\beta \text{Tr}[\hat{\mathbf{R}}] - L \text{Tr}[\hat{\mathbf{R}} \mathbf{R}_b] - \sigma_s L (\beta - \text{Tr}[\mathbf{R}_b \mathbf{R}_b^H])}{L(\beta - L)}, \\ \hat{\sigma}_\gamma = \frac{\text{Tr}[\hat{\mathbf{R}} \mathbf{R}_a] - \text{Tr}[\hat{\mathbf{R}}] - \sigma_s (\beta - L)}{\sigma_s L(L-1)}, \\ \hat{\sigma}_s = \frac{\text{numerator}}{\text{denominator}},$$

where

$$\text{numerator} = \text{Tr}[\hat{\mathbf{R}}]((L^2 - 2L + \beta)/((\beta - L)(L - 1))) \\ - \text{Tr}[\hat{\mathbf{R}} \mathbf{R}_a](1/(L - 1)) + \text{Tr}[\hat{\mathbf{R}} \mathbf{R}_b](L/(\beta - L)), \\ \text{denominator} = L - (L(\beta - \text{Tr}[\mathbf{R}_b \mathbf{R}_b]))/(\beta - L) - (\beta - L)/(L - 1).$$

The least-squares cost function can now be recast as

**Table 1.** Mean squared error ( $\text{deg}^2$ ) in the DOA ( $=10 \text{ deg}$ ) vs  $L$  for  $\sigma_\theta = 1$ 

L	ML	LS
4	$1.2560e-02$	$1.2512e-02$
6	$4.4170e-03$	$4.3335e-03$
8	$3.7610e-03$	$3.7726e-03$
10	$2.3106e-03$	$2.2610e-03$

## 7. Numerical study

An experiment to study the performance of the algorithms based on various criteria, is presented next.

*Experiment.* A scenario with  $\theta = 10^\circ$ ,  $\sigma_s = 10$ ,  $\sigma_n = 1$ ,  $\sigma_\gamma = 0$  and ULA is considered. Various values of  $\sigma_\theta$ ,  $L$  are considered as  $\sigma_\theta = 0, 1, 2, 3, 4, 5, 6, 7, 8, 9, 10$  and  $L = 4, 6, 8, 10, 12$ .

The estimates of  $\theta$  and  $\sigma_\theta$  are obtained for each of the above combinations of  $\sigma_\theta$  and  $L$  using the ML, LS and WLS criteria using the same data vectors. In this research work, the Levenberg–Marquardt search method is used to obtain the parameters. The updated vector of the estimate at the  $k$ th iteration is given by

$$\hat{\eta}(k+1) = \hat{\eta}(k) - \mu(k) \mathbf{H}^{-1} \mathbf{g},$$

where  $k$  denotes the iteration,  $\mathbf{H}$  is the Hessian and  $\mathbf{g}$  is the gradient of the cost function. The initial estimate of  $\theta$  is obtained by using the ESPRIT algorithm and the initial estimate of  $\sigma_\theta = 0$ . The sample statistics of the estimates are obtained from 200 independent runs.

*Effect of number of sensors:* Table 1 presents the MSE in the DOA as a function of  $L$  for a particular value of the angular spread,  $\sigma_\theta$ .

- The MSE decreases as  $L$  increases for all methods which agrees with the theoretical results.
- For any value of  $L$ , the performance of the LS method is very close to the ML method while the WLS method performs poorly in comparison with the other two methods. This could be due to use of the estimate of the correlation matrix as the weighting matrix.

Table 2 presents the MSE in the DOA as a function of the angular spread,  $\sigma_\theta$  for a particular value of  $L$ .

**Table 2.** Mean squared error( $\text{deg}^2$ ) in the DOA ( $=10 \text{ deg}$ ) vs  $\sigma_\theta$  for  $L = 10$

- It is clear that the performance deteriorates as the angular spread increases, for all methods.
- As observed before, WLS performs poorer than LS and ML while the performance of ML is the best among the methods.

### 3. Conclusions

Estimation of parameters, the DOA and the variance of the angular spread, using an array of sensors in the case of a Ricean channel is considered, using the maximum-likelihood least-squares and weighted least squares criteria. The Cramér–Rao bound is also obtained for the problem of interest. Due to the quadratic nature of the least-squares criteria, simplification of the cost functions to reduce the dimension of the problem has been carried out. The performance of the methods (in terms of the mean-squared error in the estimates of the parameters) has been studied based on numerical experiments which show that the maximum-likelihood and least-squares methods perform comparably while the weighted least squares method is slightly poorer than the other methods. This could be due to the use of an estimated correlation matrix as the weighting matrix instead of the true one.

### References

Adachi F, Feeny M T, Williamson A G, Parsons J D 1986 Crosscorrelation between the envelopes of 900 MHz signals received at a mobile radio base station site. *Inst. Elec. Eng. Proc.* 133: 506–512

Anderson S, Millnert M, Viberg M, Wahlberg B 1991 An adaptive array for mobile communication systems. *IEEE Trans. Vehicular Technol.* 40: 230–236

Balaban P, Salz J 1992 Optimum diversity combining and equalization in digital data transmission with applications to cellular mobile radio. *IEEE Trans. Commun.* 40: 865–907

Braun W R, Dersch U 1991 A physical mobile radio channel model. *IEEE Trans. Vehicular Technol.* 40: 472–482

Göransson B 1995 Parametric methods for source localization in the presence of spatially correlated noise. Technical report TRITA-S3-SB-9503, Department of Signals, Sensors and Systems, Royal Institute of Technology, Stockholm

Mendel J M 1989 *Lessons in digital estimation theory* (Englewood Cliffs, NJ: Prentice-Hall)

Ohgane T, Shimura T, Matsuzawa N, Sasaoka H 1993 An implementation of a CMA adaptive array for high speed GMSK transmission in mobile communications. *IEEE Trans. Vehicular Technol.* 42: 282–288

Parsons J D, Turkmani A M D 1991 Characterization of mobile radio signals; model description. *Inst. Elec. Eng. Proc. I-138*: 549–555

Proakis J G 1989 *Digital communications* 2nd edn (Singapore: McGraw-Hill)



# Spatial smoothing with uniform circular arrays

K MAHESWARA REDDY \* and V U REDDY

Electrical Communication Engineering Department, Indian Institute of Science, Bangalore, India

\*Present address: Centre for Aeronautical Systems Studies and Analysis, Defence Research and Development Organisation, New Tippasandra, Bangalore 560 075, India

e-mail: mahesh@cassa.ernet.in; vur@ece.iisc.ernet.in

**Abstract.** In this paper, we extend and analyse spatial smoothing with uniform circular arrays (UCA's). In particular, we study the performance of the Root-MUSIC with smoothing in the presence of correlated sources, finite data perturbations and errors in transformed steering vector that arise due to some approximations made to enable the extension of the Root-MUSIC and smoothing to UCA. Expressions are derived for the asymptotic performance of the Root-MUSIC with smoothing applied to the transformed UCA data. An attempt has been made to bring out the impact of both forward and forward-backward smoothing. Computer simulations are provided to demonstrate the usefulness of the analysis.

**Keywords.** Uniform circular arrays; phase modes; direction of arrival estimation; spatial smoothing.

## 1. Introduction

Uniform circular arrays (UCA's) are commonly employed when  $360^\circ$  coverage is required in the plane of the array. Circular arrays are non-uniform linear arrays, and hence, the rooting techniques and preprocessing schemes like spatial smoothing cannot be directly applied to these arrays. Tewfik & Hong (1992) showed that it is possible to extend the Root-MUSIC to UCA using the phase mode excitation concept. Mathews & Zoltowski (1994) proposed real beamspace MUSIC to UCA (UCA-RB-MUSIC) which yields reduced computation and better resolution. They also studied the direction of arrival (DOA) estimation performance of the UCA-RB-MUSIC.

While extending the rooting techniques to UCA, all the authors assumed that some of the terms in the transformed steering vector of UCA, where the transformation is performed

DOA estimates obtained with the Root-MUSIC even when the number of snapshots goes to infinity, and we analyse the effect of these errors in this paper. We also extend the forward-backward smoothing to UCA and analyse the effect of smoothing in the presence of correlated noise and finite data perturbations. We discuss the impact of both forward and forward-backward smoothing.

In § 2, we provide a brief background. We propose in § 3 forward spatial smoothing highlighting the assumptions made for extending the Root-MUSIC and spatial smoothing to UCA and the errors associated with these assumptions. In § 4, we analyse the performance of the Root-MUSIC with forward and forward-backward smoothing applied to transformed UCA data. We present the results of computer simulations in § 6 and conclude the paper in § 7.

## 2. Background

Consider a UCA with  $L$  identical and omni-directional sensors. Let  $r$  be the radius of the array and  $d$  be the circumferential spacing between the elements. Let  $\theta$  denote the azimuth angle measured in the plane containing the elements. We assume for simplicity that the sources are in the same plane as the UCA. The steering vector of the array at the centre of the array can then be expressed as<sup>1</sup>

$$\mathbf{a}_c(\theta) = [e^{j\xi \cos \theta}, e^{j\xi \cos(\theta - 2\pi/L)}, \dots, e^{j\xi \cos(\theta - 2\pi(L-1)/L)}]^T$$

where  $\xi = 2\pi r/\lambda$ ,  $\lambda$  is the wavelength and  $(.)^T$  represents the transpose of  $(.)$ .

Consider the phase mode excitation of the UCA. The weight vector that excites the array with  $m$ th phase mode is given by (Davies 1983)  $\mathbf{w}_m^H = (j^{-|m|}/L)[1, e^{j\xi \cos(2\pi m(L-1)/L)}]$ . The array pattern for the  $m$ th phase mode can be shown to be (Davies 1983; Mathews & Zoltowski 1994)

$$f_m(\theta) = \mathbf{w}_m^H \mathbf{a}_c(\theta) = J_{|m|}(\xi) e^{jm\theta}$$

$$+ j^{-|m|} \sum_{q=1}^{\infty} [j^g J_g(\xi) e^{-jg\theta} + j^h J_h(\xi) e^{jh\theta}]; \quad -\mathcal{D} \leq m \leq \mathcal{D}$$

where  $\mathcal{D}$  is the maximum number of phase modes given by (Davies 1983)  $\mathcal{D} \leq L/2$ .  $J_m(\xi)$  is the Bessel function of the first kind of order  $m$ ,  $h = Lq + m$ ,  $g = Lq - m$  represents the complex conjugate transpose of  $(.)$  and  $\lfloor x \rfloor$  denotes the largest integer less than or equal to  $x$ . The first term in (2), the principal term, becomes dominant when  $|m| > 0.5\lambda$ . In our analysis, we consider  $d < 0.5\lambda$  and assume the second term to be negligible.

The normalised transformation matrix  $\mathbf{F}$  to excite the array patterns corresponds to

where

$$\begin{aligned}\mathbf{J}_\xi &= \sqrt{L} \operatorname{diag}[J_{\mathcal{D}}(\xi), \dots, J_1(\xi), J_0(\xi), J_1(\xi), \dots, J_{\mathcal{D}}(\xi)], \\ \mathbf{a}(\theta) &= [e^{-j\mathcal{D}\theta}, e^{-j(\mathcal{D}-1)\theta}, \dots, 1, \dots, e^{j(\mathcal{D}-1)\theta}, e^{j\mathcal{D}\theta}]^T,\end{aligned}\quad (4)$$

and  $\Delta \mathbf{a}(\theta)$  is the contribution due to the second term in (2). Note that the vector  $\mathbf{a}(\theta)$  has a structure similar to that of the steering vector of a uniform linear array (ULA). This suggests that we can extend the spatial smoothing to UCA provided the term  $\Delta \mathbf{a}(\theta)$  is negligible. We treat  $\Delta \mathbf{a}(\theta)$  as the error in the transformed steering vector, caused due to approximation.

### 3. Forward spatial smoothing with UCA

Assume that  $M$  sources are impinging on the UCA and the DOA's of these sources are  $\theta_1, \theta_2, \dots, \theta_M$ . If we assume that the signal and noise are uncorrelated and noise is spatially white with variance  $\sigma^2$ , then the covariance matrix at the output of UCA can be expressed as

$$\mathbf{R}_c = \mathbf{A}_c \mathbf{S} \mathbf{A}_c^H + \sigma^2 \mathbf{I}, \quad (5)$$

where  $\mathbf{S}$  is the signal covariance matrix,  $\mathbf{I}$  is an identity matrix and  $\mathbf{A}_c$  is the matrix of direction vectors of the UCA. From (5) and (3), the covariance matrix that we obtain after applying the transformation  $\mathbf{F}$  can be shown to be

$$\mathbf{R}^t = \mathbf{F}^H \mathbf{R}_c \mathbf{F} = \mathbf{J}_\xi \mathbf{A} \mathbf{S} \mathbf{A}^H \mathbf{J}_\xi + \sigma^2 \mathbf{I} + \Delta \mathbf{R}, \quad (6)$$

where  $\mathbf{A} = [\mathbf{a}(\theta_1), \dots, \mathbf{a}(\theta_M)]$  and  $\Delta \mathbf{R} = \Delta \mathbf{A} \mathbf{S} \mathbf{A}^H \mathbf{J}_\xi + \mathbf{J}_\xi \mathbf{A} \mathbf{S} \Delta \mathbf{A}^H + \Delta \mathbf{A} \mathbf{S} \Delta \mathbf{A}^H$  with  $\Delta \mathbf{A} = [\Delta \mathbf{a}(\theta_1), \dots, \Delta \mathbf{a}(\theta_M)]$ . Note that the size of  $\mathbf{R}^t$  is  $(2\mathcal{D}+1) \times (2\mathcal{D}+1)$ , and hence the number of sources ( $M$ ) should be less than  $(2\mathcal{D}+1)$  for any MUSIC-type algorithm to be applied to  $\mathbf{R}^t$ .

Spatial smoothing is a preprocessing scheme originally proposed for ULA to alleviate the ill effects of correlation. This scheme can be extended to UCA by applying the transformation  $\mathbf{J}_\xi^{-1}$  to the covariance matrix  $\mathbf{R}^t$  provided the term  $\Delta \mathbf{R}$  is negligible. If the source are in the same plane as the UCA or if all the sources are at the same but known elevation angle, then  $\mathbf{J}_\xi^{-1}$  is a known matrix.

Let  $K$  be the number of virtual subarrays (since the subarrays are not physically available). Then, the forward smoothed covariance matrix  $\mathbf{R}_f^t$  is given by

$$\mathbf{R}_f^t = \frac{1}{K} \sum_{l=1}^K \mathbf{Z}_l^T \mathbf{J}_\xi^{-1} \mathbf{R}^t \mathbf{J}_\xi^{-1} \mathbf{Z}_l, \quad (7)$$

where the prewhitening matrix  $\mathbf{R}_{nw} = [\frac{1}{K} \sum_{l=1}^K \mathbf{Z}_l^T \mathbf{J}_\xi^{-1} \mathbf{J}_\xi^{-1} \mathbf{Z}_l]^{-1/2}$ , equal to the number of coherent signals present, then the forward spatial smoothing up the rank of the smoothed signal covariance matrix and makes it non-singular (Reddy et al., 1985).

Using the structure of  $\mathbf{a}(\theta)$  as given in (4), it can be shown (Reddy et al., 1985) that the effective correlation coefficient ( $\rho_f$ ) between the sources after forward spatial smoothing, in the case of UCA, is given by (assuming  $\Delta\mathbf{R}$  to be negligible)

$$|\rho_f| = \left| \rho \frac{\sin(K(\theta_i - \theta_j)/2)}{K \sin((\theta_i - \theta_j)/2)} \right|,$$

where  $\theta_i$  and  $\theta_j$  are the DOA's of the  $i$ th and  $j$ th sources respectively, and  $\rho$  is the effective correlation coefficient between these sources before smoothing. Note from (9) that the effective correlation coefficient depends on the individual directions of the sources, but is dependent only on the angular separation between them. If this angular separation is  $90^\circ$ , then  $\rho_f$  becomes zero for  $K=4$ . On the other hand, if the angular separation is  $180^\circ$ , then two subarrays ( $K=2$ ) are enough to force  $\rho_f$  to be zero. It can also be shown from (9) that  $\rho_f$  is independent of the spacing between the elements provided the spacing is less than  $\lambda/2$  (making  $\Delta\mathbf{a}(\theta)$ , and hence,  $\Delta\mathbf{R}$  to be negligible). In the case of ULA, the effective correlation coefficient between the sources is dependent on the individual directions of the sources and also on the spacing between the elements.

#### 4. Performance of the Root-MUSIC with smoothing

In this section, we analyze the performance of the Root-MUSIC with forward and backward spatial smoothing applied to the transformed UCA data.

##### 4.1 Forward spatial smoothing

Consider the smoothed covariance matrix after prewhitening (see (6)). Substituting (6) and (7) in (1) along with (6) and (7), we obtain

$$\begin{aligned} (\mathbf{R}_f^t)_w &= \frac{1}{K} \sum_{l=1}^K \mathbf{R}_{nw} \mathbf{Z}_l^T \mathbf{A} \mathbf{S} \mathbf{A}^H \mathbf{Z}_l \mathbf{R}_{nw}^H + \sigma^2 \mathbf{I} \\ &\quad + \frac{1}{K} \sum_{l=1}^K \mathbf{R}_{nw} \mathbf{Z}_l^T \mathbf{J}_\xi^{-1} \Delta \mathbf{R} \mathbf{J}_\xi^{-1} \mathbf{Z}_l \mathbf{R}_{nw}^H \\ &= \mathbf{R}_F + \Delta \mathbf{R}_F, \end{aligned}$$

and

$$\begin{aligned}\Delta \mathbf{R}_F &\equiv \frac{1}{K} \sum_{l=1}^K \mathbf{R}_{nw} \mathbf{Z}_l^T \mathbf{J}_\xi^{-1} \Delta \mathbf{R} \mathbf{J}_\xi^{-1} \mathbf{Z}_l \mathbf{R}_{nw}^H \\ &= \frac{1}{K} \sum_{l=1}^K \mathbf{R}_{nw} \mathbf{Z}_l^T [\mathbf{J}_\xi^{-1} \Delta \mathbf{A} \mathbf{S} \mathbf{A}^H + \mathbf{A} \mathbf{S} \Delta \mathbf{A}^H \mathbf{J}_\xi^{-1}] \mathbf{Z}_l \mathbf{R}_{nw}^H.\end{aligned}\quad (12)$$

$\mathbf{S}_f$  is the smoothed signal covariance matrix and  $\mathbf{A}_f$  is the virtual subarray direction matrix. In writing the RHS of (12), we assumed  $\Delta \mathbf{A}$  to be small and neglected the terms containing more than one  $\Delta \mathbf{A}$ . Note that  $\mathbf{R}_F$  is the smoothed covariance matrix that we would get if  $\Delta \mathbf{a}(\theta)$  (see (3)) is zero. In practice, however, this term may be small but non-zero, thereby resulting in errors in the DOA estimates when we apply the Root-MUSIC to  $(\mathbf{R}_f^t)_w$ . We now analyse the effect of this term (i.e.,  $\Delta \mathbf{R}_F$ ) and that due to finite data perturbations on the DOA estimates.

Let  $(\hat{\mathbf{R}}_f^t)_w$  denote the estimated covariance matrix from finite number of snapshots. This can be expressed as

$$(\hat{\mathbf{R}}_f^t)_w = (\mathbf{R}_f^t)_w + \Delta \mathbf{R}_p = \mathbf{R}_F + \Delta \mathbf{R}_F + \Delta \mathbf{R}_p,\quad (13)$$

where  $\Delta \mathbf{R}_p$  represents the perturbation due to finite data. Note that  $\Delta \mathbf{R}_p$  is random while  $\Delta \mathbf{R}_F$  is deterministic. If we assume that the noise at the output of the sensors is complex circularly Gaussian distributed, then the mean square error (MSE) in  $i$ th DOA estimate due to both the finite data perturbations and the error due to approximation (i.e. due to  $\Delta \mathbf{R}_F$ ), can be shown to be (Rao & Hari 1990)

$$E[\Delta \theta_i^2]_f = \frac{\Gamma_{\alpha\alpha\beta\beta} + Re(\Gamma_{\alpha\beta\alpha\beta}) + 2[Re(\alpha^H \Delta \mathbf{R}_F \beta)]^2}{2[\mathbf{v}_{f_1}^H(\theta_i) \mathbf{R}_{nw}^H \mathbf{P}_n \mathbf{R}_{nw} \mathbf{v}_{f_1}(\theta_i)]^2}. \quad (14)$$

$$\Gamma_{\alpha\alpha\beta\beta} = \frac{1}{NK^2} \sum_{p=1}^K \sum_{q=1}^K \alpha^H \mathbf{R}_{pq} \alpha \beta^H \mathbf{R}_{qp} \beta;$$

$$\Gamma_{\alpha\beta\alpha\beta} = \frac{1}{NK^2} \sum_{p=1}^K \sum_{q=1}^K \alpha^H \mathbf{R}_{pq} \beta \alpha^H \mathbf{R}_{qp} \beta. \quad (15)$$

$$\begin{aligned}\alpha &= \mathbf{P}_n \mathbf{R}_{nw} \mathbf{v}_{f_1}(\theta_i); \quad \beta = (\mathbf{R}_F)_s^\# \mathbf{R}_{nw} \mathbf{v}_f(\theta_i); \\ (\mathbf{R}_F)_s &= \mathbf{R}_{nw} \mathbf{A}_f \mathbf{S}_f \mathbf{A}_f^H \mathbf{R}_{nw}^H,\end{aligned}\quad (16)$$

where  $\mathbf{R}_{pq} = \mathbf{R}_{qp}^H = E[\mathbf{y}_p(t) \mathbf{y}_q^H(t)]$ ,  $\mathbf{y}_p(t)$  is the output vector obtained from the  $p$ th virtual subarray after prewhitening,  $N$  is the number of snapshots,  $\mathbf{P}_n$  is the projection matrix onto the noise subspace of  $\mathbf{R}_F$ ,  $\mathbf{v}_{f_1}(\theta)$  is the derivative of  $\mathbf{v}_f(\theta)$  w.r.t.  $\theta$  with  $\mathbf{v}_f(\theta)$

Reddy & Reddy (1996a) showed that the smoothing reduces the noise to finite data in addition to reducing the correlation among the impinging signals.

As the number of snapshots tends to infinity, the MSE in the DOA estimate due to the error due to the approximation (cf. (3)). This error, which is the asymptotic error in the DOA estimate, is deterministic and given by

$$E[\Delta\theta_i^2]_f = \Delta\theta_i^2 = \frac{[Re(\alpha^H \Delta \mathbf{R}_F \beta)]^2}{[\mathbf{v}_{f_1}^H(\theta_i) \mathbf{R}_{nw}^H \mathbf{P}_n \mathbf{R}_{nw} \mathbf{v}_{f_1}(\theta_i)]^2}.$$

Note that this error increases as  $d$  tends to  $\lambda/2$  since  $\Delta \mathbf{A}$  becomes large for small values of  $d$ . Let us first assume that the sources are uncorrelated. Then the error expression can be shown to be (see Reddy & Reddy 1996b)

$$\Delta\theta_i^2 = \frac{1}{L_o} \frac{[Re(\alpha^H \mathbf{R}_{nw} \Delta \mathbf{a}_f(\theta_i))]^2}{[\mathbf{v}_{f_1}^H(\theta_i) \mathbf{R}_{nw}^H \mathbf{P}_n \mathbf{R}_{nw} \mathbf{v}_{f_1}(\theta_i)]^2},$$

where

$$\Delta \mathbf{a}_f(\theta_i) = \frac{1}{K} \sum_{l=1}^K \mathbf{Z}_l^T \mathbf{J}_\xi^{-1} \Delta \mathbf{a}(\theta_i) \mathbf{e}^{-j(l-1)\theta_i},$$

which we define as the effective error along the direction of the  $i$ th source steering vector due to the approximation. Note from (19) that the asymptotic  $i$ th DOA estimate is dependent only on the effective error vector  $\Delta \mathbf{a}_f(\theta_i)$ . This vector can be shown to decrease with spatial smoothing (see Appendix A of Reddy & Reddy 1996b). Thus, we can expect the smoothing to improve the asymptotic DOA estimate. Root-MUSIC applied to the transformed UCA data. Expression (19), however, holds only when the sources are uncorrelated. For the case of correlated sources, the expression (18) leads to lengthy expressions even for a two-source case, and hence we do not present it here.

#### 4.2 Forward-backward spatial smoothing

Forward-backward spatial smoothing (William *et al* 1988) can also be used by applying the transformation  $\mathbf{J}_\xi^{-1}$  to the covariance matrix  $\mathbf{R}^t$  (given in (18)). Since the term  $\Delta \mathbf{R}$  is negligible. If  $K$  is the number of virtual subarrays, then the smoothed covariance matrix is given by

$$\mathbf{R}_{fb}^t = \frac{1}{2K} \sum_{l=1}^K \mathbf{Z}_l^T [\mathbf{J}_\xi^{-1} \mathbf{R}^t \mathbf{J}_\xi^{-1} + \tilde{\mathbf{I}} (\mathbf{J}_\xi^{-1} \mathbf{R}^t \mathbf{J}_\xi^{-1})^* \tilde{\mathbf{I}}] \mathbf{Z}_l,$$

shown (Williams *et al* 1988; Pillai & Kwon 1989) that the forward-backward smoothing can handle up to  $\lfloor 2(2D + 1)/3 \rfloor$  coherent signals in contrast to the forward smoothing which handles up to  $\lfloor (2D + 1)/2 \rfloor$  coherent signals only.

Taking into account the structure of  $\mathbf{a}(\theta)$  given in (4), it can be shown that the effective correlation coefficient ( $\rho_{fb}$ ) between the sources after forward-backward smoothing, in the case of UCA, is given by (assuming  $\Delta\mathbf{R}$  to be negligible)

$$|\rho_{fb}| = |\rho| \left| \frac{\sin(K(\theta_i - \theta_j)/2) \cos \psi}{K \sin((\theta_i - \theta_j)/2)} \right|, \quad (22)$$

where  $\rho = |\rho| e^{j\psi}$ . Observe from (22) and (9) that the effective correlation with forward-backward smoothing is same as that with forward smoothing only, when  $\psi$  is zero, i.e.,  $\rho$  is real. When  $\psi$  is an odd multiple of  $\pi/2$ , the effective correlation with forward-backward smoothing reduces to zero for all  $K$ .

The mean square error (MSE) in the  $i$ th DOA estimate that we obtain by applying the Root-MUSIC with forward-backward smoothing to the transformed UCA data, due to both the finite data perturbations and the error due to approximation (cf. (3)), can be shown to be (see Rao & Hari 1990)

$$\begin{aligned} E[\Delta\theta_i^2]_{fb} &= \frac{1}{NK^2 2[\mathbf{v}_{f_1}^H(\theta_i) \mathbf{R}_{nw}^H \mathbf{P}_n \mathbf{R}_{nw} \mathbf{v}_{f_1}(\theta_i)]^2} \\ &\times \sum_{p=1}^K \sum_{q=1}^K [[\alpha^H \mathbf{R}_{pq} \alpha \beta^H \mathbf{R}_{qp} \beta + |\alpha^H \mathbf{R}_{pq} \beta|^2] \\ &+ 2[Re(\alpha^H \Delta\mathbf{R}_{FB} \beta)]^2]. \end{aligned} \quad (23)$$

$$\alpha = \mathbf{P}_n \mathbf{R}_{nw} \mathbf{v}_{f_1}(\theta_i); \quad \beta = (\mathbf{R}_{FB})_s^\# \mathbf{R}_{nw} \mathbf{v}_f(\theta_i), \quad (24)$$

$$(\mathbf{R}_{FB})_s = \mathbf{R}_{nw} \mathbf{A}_f \mathbf{S}_{fb} \mathbf{A}_f^H \mathbf{R}_{nw}^H; \quad \Delta\mathbf{R}_{FB} = \frac{\Delta\mathbf{R}_F + \tilde{\mathbf{I}}(\Delta\mathbf{R}_F)^* \tilde{\mathbf{I}}}{2}, \quad (25)$$

where  $\mathbf{P}_n$  and  $\mathbf{S}_{fb}$  are the noise projection matrix and the signal covariance matrix, respectively, obtained with the forward-backward smoothing. The first two terms in (23) are due to finite data perturbations and the third term is because of the error due to the approximation. The performance with forward-backward smoothing is the same as that with forward smoothing when  $\mathbf{S}$  is real. Hence, the expression (19) can be used for the asymptotic performance of the Root-MUSIC with forward-backward smoothing also, when the sources are uncorrelated.

The analysis carried out, so far, assumes omni directional sensors. Spatial smoothing can also be extended to UCA with directional sensors (see Reddy & Reddy 1998) and the analysis of Section 4 is applicable for UCA with directional elements.

## 5. Numerical and simulation results

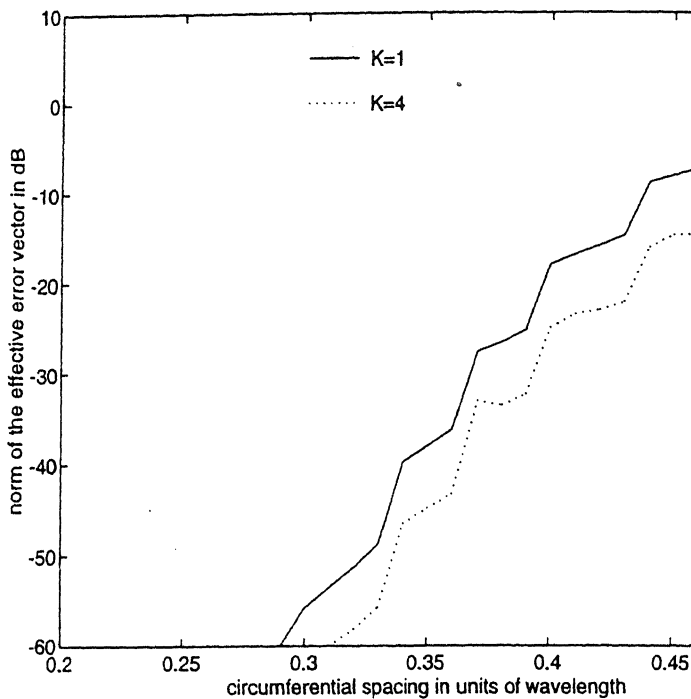


**Figure 1.** Norm of the effective error vector in the transformed steering vector as a function of circumferential spacing ( $L = 30$ ).

vector was the sum of noise and signal vectors which were generated separately. The noise vector consisted of zero mean, unit variance, independent complex circularly Gaussian random variables. In the case of uncorrelated signals, the signal vector consisted of zero mean, independent complex circularly Gaussian random variables with variance  $\sigma_s^2$ , where  $\sigma_s^2$  was chosen to give the desired signal powers. In the case of correlated signals, the second signal  $s_2(t)$  was generated as  $s_2(t) = \rho s_1(t) + \sqrt{1 - \rho^2} n(t)$ , where  $n(t)$  is a noise vector with zero mean, independent complex circularly Gaussian random variables with variance  $\sigma_n^2$  and  $\rho$  is the correlation coefficient between  $s_1(t)$  and  $s_2(t)$ . The DOA's were obtained by averaging over 100 Monte Carlo runs. The number of virtual subarrays, the total array size and the particulars of the array are described in the captions of figures and tables. The SNR indicated in the figures refers to the value at the input of the sensor element. For spectral MUSIC, the search was conducted in steps of  $0.002^\circ$ .

Figure 1 shows variation of the norm of the effective error vector in the transformed steering vector (see (20)). Note that as the spacing between the elements

**Table 1.** Performance of the Root-MUSIC applied to transformed UCA data as a function of the circumferential spacing between the elements (without smoothing) ( $L = 30$ ,  $N = 100$ , DOA's =  $0^\circ$  and  $7^\circ$ , SNR = 3 dB,  $\rho = 0.0$ ).

Circumferential spacing between the elements ( $d$ )	MSE in DOA estimate ( $\text{deg}^2$ )		
	Spectral MUSIC applied to UCA data	Root-MUSIC applied to transformed UCA data	
		Simulation	Evaluation of (14)
$0.32\lambda$	0.2275	0.07972	0.08477
$0.34\lambda$	0.1570	0.06487	0.05793
$0.36\lambda$	0.1104	0.06454	0.05382
$0.38\lambda$	0.07045	0.04952	0.03762
$0.40\lambda$	0.04468	0.03284	0.02803
$0.42\lambda$	0.03259	0.03140	0.02736
$0.44\lambda$	0.02222	0.04897	0.03515
$0.46\lambda$	0.01627	0.08968	0.07188
$0.48\lambda$	0.01116	0.30931	0.25090

the results. The performance of the spectral MUSIC improves as the spacing increases. This is because of the increased aperture that we get with increasing value of  $d$ . The performance of the Root-MUSIC is better than that of the spectral MUSIC when the spacing between the elements is less than  $0.42\lambda$ . But, as the spacing is increased further, the Root-MUSIC performance degrades and becomes worse as  $d$  approaches  $\lambda/2$ . This is because, at larger spacings, the error in the transformed steering vector is quite large (see figure 1). The simulation results agree reasonably well with the theoretical values obtained from the numerical evaluation of (14) when  $d$  is less than  $0.46\lambda$ . For larger values of  $d$ , however, the difference between the two increases since the theoretical expression (14) is less accurate when the term  $\Delta \mathbf{R}_F$  becomes large.

To see if the smoothing reduces the effect of the error introduced due to the approximation (cf. (3)) in the case of both uncorrelated and correlated scenarios, and to evaluate the utility of the theoretical result (18) and (19), we applied the Root-MUSIC with forward smoothing to the covariance matrix  $(\mathbf{R}_f^t)_w$ . The result so obtained from this is referred to as the asymptotic performance from the algorithm. Table 2 gives this result along with the theoretical values evaluated from (18) and (19) for various values of subarrays. Note from the results of table 2 that the MSE is maximum for  $K = 1$  (no smoothing) and it drops significantly with smoothing. Consider the results shown in the table for uncorrelated source scenario. As the smoothing is increased beyond  $K = 8$ , the performance starts deteriorating because of the reduction in the aperture. The results predicted from (19) are not identical to those obtained from the algorithm since the theoretical expressions are accurate for small values of errors and  $\Delta \mathbf{a}(\theta)$ , the error in the present case, is not small as discussed in (2). The overall performance is better than that of the unsmoothed case for all values of  $K$  considered.

Number of virtual subarrays, ( $K$ )	Asymptotic performance of the Root-MUSIC with forward smoothing ( $\Delta\theta_i^2$ in deg $^2$ )		
	$\rho = 0.0$	From the algorithm	Evaluation of (19)
1	$0.4852 \times 10^{-1}$	$0.5359 \times 10^{-1}$	$0.4852 \times 10^{-1}$
2	$0.1110 \times 10^{-1}$	$0.1148 \times 10^{-1}$	$0.2929 \times 10^{-1}$
3	$0.2002 \times 10^{-1}$	$0.2018 \times 10^{-1}$	$0.4686 \times 10^{-1}$
4	$0.4491 \times 10^{-2}$	$0.4684 \times 10^{-2}$	$0.2819 \times 10^{-2}$
5	$0.3120 \times 10^{-3}$	$0.3594 \times 10^{-3}$	$0.7611 \times 10^{-3}$
6	$0.5329 \times 10^{-3}$	$0.5958 \times 10^{-3}$	$0.9496 \times 10^{-3}$
7	$0.2543 \times 10^{-2}$	$0.2624 \times 10^{-2}$	$0.2612 \times 10^{-2}$
8	$0.1255 \times 10^{-3}$	$0.1524 \times 10^{-3}$	$0.5241 \times 10^{-3}$
9	$0.2663 \times 10^{-3}$	$0.3085 \times 10^{-3}$	$0.7199 \times 10^{-3}$
10	$0.3612 \times 10^{-3}$	$0.4167 \times 10^{-3}$	$0.8421 \times 10^{-3}$
11	$0.5708 \times 10^{-3}$	$0.6524 \times 10^{-3}$	$0.1081 \times 10^{-2}$
12	$0.1155 \times 10^{-2}$	$0.1289 \times 10^{-2}$	$0.1653 \times 10^{-2}$

the case of correlated sources are also given in table 2. Since the real, these results hold for both the forward and forward-backward improves the performance in this case too. However, the improv with uncorrelated sources.

To see the differential impact of forward and forward-backwardence of highly correlated and closely spaced sources with finite dario with  $\rho = 0.95e^{j\pi/4}$  and  $N$  (number of snapshots) = 100, ke nearly equal to the beamwidth of the UCA, and evaluated the M Table 3 gives the simulation results and the theoretical values pre Note that the forward-backward smoothing yields much superior p

**Table 3.** Finite data performance of the Root-MUSIC with smoothing applied with omni directional elements for correlated sources. ( $L = 50$ ,  $d = 0.34\lambda$ ,  $10^\circ$ ,  $\rho = 0.95e^{j\pi/4}$ , SNR = 3 dB)

Number of virtual subarrays, ( $K$ )	Spectral MUSIC applied to UCA data	MSE in DOA estimate (deg $^2$ )		
		Root-MUSIC with smoothing applied		
		Forward-Backward smoothing		Simulation
1	0.02485	0.003313	0.003058	0.01
2		0.003419	0.003223	0.01
3		0.003568	0.003449	0.01
4		0.004373	0.004053	0.01
5		0.007673	0.007213	0.02
6		0.01883	0.01789	0.05
7		0.01569	0.01582	0.04
8		0.01462	0.01556	0.03
9		0.01817	0.02131	0.05
10				

to the forward smoothing only. Further, the Root-MUSIC with forward-backward smoothing applied to the transformed UCA data performs better than the spectral MUSIC applied to the UCA data for all values of  $K$  (and much better at lower values of  $K$ ). When  $K$  increases, the aperture comes down and the performance will start degrading when the aperture effect becomes predominant. The difference between the simulation results and the predicted values (particularly in the forward smoothing case) can be attributed to the fact that the smoothing reduces the effect of finite data perturbations in addition to reducing the correlation among the sources, and hence, the actual MSE will be less than the value given by (14) (see Reddy & Reddy 1996a for discussion on this issue).

## 6. Conclusions

This paper extends the spatial smoothing to UCA and analyzes the DOA estimation performance of the Root-MUSIC with smoothing applied to the transformed UCA data. It is shown that the smoothing helps in reducing the effect of the errors that arise while extending the Root-MUSIC to UCA, in addition to reducing the correlation among the sources and the effect of noise perturbations due to finite data.

## References

Davies D E N 1983 *The handbook of antenna design* (London: Peter Peregrinus) vol. 2, chap. 11.

Mathews C P, Zoltowski M D 1994 Eigenstructure techniques for 2-D angle estimation with uniform circular arrays. *IEEE Trans. Signal Process.* 42: 2395–2407

Pillai S U, Kwon B H 1989 Forward/backward spatial smoothing techniques for coherent signal identification. *IEEE Trans. Acoust. Speech Signal Process.* 37: 8–15

Rao B D, Hari K V S 1990 Effect of spatial smoothing on the performance of MUSIC and minimum-norm method. *Inst. Elec. Eng. Proc.* 137: 449–458

Reddy K M, Reddy V U 1996a Further results in spatial smoothing. *Signal Process.* 48: 217–224

Reddy K M, Reddy V U 1996b Analysis of interpolated arrays with spatial smoothing. *Signal Process.* 54: 261–272

Reddy K M, Reddy V U 1998 Analysis of spatial smoothing with uniform circular arrays. *IEEE Trans. Signal Process.* (submitted)

Reddy V U, Paulraj A J, Kailath T 1987 Performance analysis of the optimum beamformer in the presence of correlated sources and its behaviour under spatial smoothing. *IEEE Trans. Acoust. Speech Signal Process.* 35: 927–936

Shan T J, Wax M, Kailath T 1985 On spatial smoothing for directions of arrival estimation of coherent signals. *IEEE Trans. Acoust. Speech Signal Process.* 33: 806–811

Tewfik A H, Hong W 1992 On the application of uniform linear array bearing estimation techniques to uniform circular arrays. *IEEE Trans. Signal Process.* 40: 1008–1011

Williams R T, Prasad S, Mahalanabis A K, Sibul L H 1988 An improved spatial smoothing technique for bearing estimation in a multipath environment. *IEEE Trans. Acoust. Speech Signal Process.* 36: 425–431



# Region-of-interest reconstruction from noisy projections using fractal models and Wiener filtering \*

AMIT K ROY CHOWDHURY<sup>1</sup>, KAUSHIK BARMAN<sup>2</sup> and  
K R RAMAKRISHNAN

Department of Electrical Engineering, Indian Institute of Science, Bangalore  
560 012, India

Present address: <sup>1</sup> Motorola India Electronics Limited, 33A "The Senate"  
Ulsoor Road, Bangalore 560 002, India

<sup>2</sup> Silicon Automation Systems (India), 3000, 12th B Main, HAL II Stage  
Indiranagar, Bangalore 560 008, India

e-mail:amitrc@miel.mot.com; kaushikb@sasi.com; krr@ee.iisc.ernet.in

**Abstract.** In this paper, we present a method for region-of-interest (ROI) tomography using noisy projections. A wavelet decomposition down to the coarsest level is done on the noisy signal. The signal at various levels is estimated using a Wiener filter. By assuming that the projections are  $1/f$  processes, the Wiener filtering reduces to a scalar multiplication. Using the Wiener filter and regularity property of the wavelets, we combine the estimation and localisation of the noisy projections for ROI imaging. Experimental results are shown on Shepp-Logan phantom and actual CT images. The validity of the  $1/f$  model for projections of real life images is also shown.

**Keywords.** Region-of-interest reconstruction; noisy projection; fractal models; Wiener filtering.

## 1. Introduction

In computer-aided tomography, the objective is to reconstruct the cross-section of an object from measurements that are strip integrals of some property of the object. In transmission X-ray tomography, the measurements consist of integrals (projections) of the attenuation coefficient  $\mu(x, y)$  of the object along strips which represent the path of the X-rays through the object. A popular technique for image reconstruction is the Filtered Back Projection (FBP) (Kak & Roberts 1986).

In this work, we are concerned with the problem of reconstructing a portion of the image from noisy projections. The discussions in this paper are restricted to parallel beam

tomography. Reconstruction of only a portion of the cross-section (ROI tomography or local tomography) leads to reduction in dose to the patient and savings in computation (compared to FBP of the whole image).

However, the problem of local tomography is complicated by the fact that it is not uniquely solvable in even dimensions (Natterer 1986). Most of the work has been conducted in 2-D and the reconstruction formula becomes globally non-unique due to the nature of the integrals of the object. Using wavelets is one method of solving this problem.

The FBP algorithm does not produce satisfactory reconstruction results in ROI tomography. The work reported here combines the ideas of multiresolution analysis and wavelets to estimate the projections using wavelets. We use a  $1/f$  model for the object and a Wiener filter for the estimation. It is further shown that this algorithm performs well in the case of ROI tomography.

## 2. Preliminaries

### 2.1 Radon transform and its inversion

The two-dimensional Radon transform,<sup>1</sup>  $\mathbf{f}(r, \theta)$ , of a function  $f(x, y)$  is defined as the function parameterized by  $(r, \theta)$  such that  $r = x \cos \theta + y \sin \theta$  is defined as

$$\mathbf{f}(r, \theta) = \int_{\mathbb{R}^2} f(x, y) \delta(r - x \cos \theta - y \sin \theta) dx dy.$$

The one-dimensional function  $f(r, \theta)$  is termed as the projection of the function  $f(x, y)$  along the angle  $\theta$ . The back-projection operator denoted as  $\mathcal{B}$  is defined as (Kak & Slaney 1988)

$$h_B(x, y) = \mathcal{B}h(r, \xi) = \int_0^\pi h(x \cos \theta + y \sin \theta, \xi) d\theta.$$

Then it can be shown that

$$f(x, y) = \mathcal{B}\mathcal{F}^{-1}[|\omega| \mathcal{F}\mathbf{f}(r, \theta)].$$

Equation (3) is the filtered back-projection implementation of the Radon transform. It means that we filter each projection by a  $|\omega|$  filter and then perform the inverse Fourier transform. This is the most common form of the Radon inversion algorithm.

**2.1a Nonlocality of the Radon inversion:** The Radon inversion algorithm can be represented as follows (Olsen 1996):

$$f(x, y) = \mathcal{R}^{-1}\mathbf{f}(r, \theta) = \mathcal{B}\mathcal{H}_r \frac{\partial}{\partial r} \mathbf{f}(r, \theta),$$

The Hilbert transform imposes a discontinuity on the Fourier transform of any function whose average value is not zero and also discontinuities on the higher derivatives which are not zero at the origin (Olsen 1996). This is because

$$\mathcal{FH}f(t) = \mathcal{F}\left(f(t) * \frac{1}{\pi t}\right) = \frac{1}{i} \operatorname{sign}(\omega) F(\omega). \quad (6)$$

Because of the discontinuities in the frequency domain, there is a spreading of the support of the function in the time domain (Olsen & DeStefano, 1994). However, this spreading of the function's support will not occur if the function's Fourier transform and the higher derivatives of it are zero at the origin (Olsen & DeStefano, 1994). If the Fourier transform or higher derivatives of it have zeroes at the origin, it implies that the function has a number of zero moments. Hence functions with arbitrarily high zero moments will have their support unchanged by the Hilbert transform. It is in this context that the wavelet transform is used. Wavelets are usually constructed with many zero moments (Daubechies 1988). Thus local properties of the high resolution components of a wavelet transform remain local after applying the Hilbert transform. It has been shown in (Olsen & DeStefano, 1994; Delany & Bresler, 1995) that using wavelets which have several zero moments, the wavelet transformed filtered functions will have *essential* compact support.

## 2.2 Wavelets

**2.2a Continuous wavelet transform of 1-D signals:** The continuous wavelet transform  $W_\psi(f)(a, b)$  of a signal  $f(t)$  is defined as (Chui 1992):

$$W_\psi(f)(a, b) = \int_{-\infty}^{\infty} |a|^{-1/2} f(t) \overline{\psi\left(\frac{t-b}{a}\right)} dt, \quad (7)$$

where  $a \in \mathbb{R}^+$ ,  $b \in \mathbb{R}^3$  are the dilation and translation, respectively, of a single wavelet function  $\psi(t)$  called the *mother wavelet*.  $\overline{\psi}$  denotes complex conjugation. A very important property for wavelets is the regularity, which means the smoothness of the wavelet function. Regularity  $R$  of the mother wavelet  $\psi(t)$  is defined as (Aldroubi, 1996):

$$\int_{-\infty}^{+\infty} t^r \psi(t) dt = 0, \quad (8)$$

where  $r$  is an integer such that  $0 < r < R$ .

Thus a mother wavelet with regularity  $R$  has  $R - 1$  vanishing moments or  $\Psi(\omega)$  (Fourier transform of  $\psi(t)$ ) has a zero of order  $R$  at origin, because (Chui 1992):

Given a function  $f$ , it is possible to obtain the low resolution signal scale  $j$  in the following manner (Daubechies 1992):

$$f^{(j)}(k) = (h(\cdot) * f^{(j+1)})(2k)$$

and

$$d^{(j)}(k) = (g(\cdot) * d^{(j+1)})(2k),$$

where  $*$  represents 1-D convolution.  $h$  and  $g$  are two filters associated with the filters  $\tilde{h}$  and  $\tilde{g}$ . The finer scale approximation coefficients  $f^{j+1}(l)$  can be synthesized from the low resolution signal scale approximation and detail coefficients,  $f^{(j)}$  and  $d^{(j)}$ , as

$$f^{(j+1)}(k) = \sum_n \tilde{h}(2n - k) f^{(j)}(n) + \sum_n \tilde{g}(2n - k) d^{(j)}(n)$$

where  $\tilde{h}$  and  $\tilde{g}$  are defined as  $\tilde{h}(n) = h(-n)$  and  $\tilde{g}(n) = g(-n)$ .

## 2.4 $1/f$ processes

A  $1/f$  process is a nonstationary random process with a power spectrum

$$S(f) = \frac{\sigma^2}{|f|^\gamma},$$

where  $\sigma$  is a constant and  $\gamma$  is known as the spectral exponent.

It can be shown that (Wornell & Oppenheim 1992)

$$D = 2.5 - \frac{\gamma}{2},$$

where  $D$  is known as the fractal dimension. If we choose  $\gamma = 1$ , then  $1 < D < 2$ . Hence fractal dimension of the signal is not an integer, which lies in  $(1, 2)$  and the signal is self-similar. This type of signals are known as *fractal signals*. Here we concentrate on fractal signals.

## 2.5 Statistical properties of discrete wavelet transform coefficients

From the regularity condition of the mother wavelet,  $\Psi(\omega)$ , the Fourier transform of the signal has a zero of order  $R$  at the origin of the frequency plane. It ensures that processing with mother wavelet essentially removes the low frequency components. These detail coefficients are wide-sense stationary even when the signal is non-stationary (Masry 1993). This shows that the energy of the signal is concentrated around zero frequency. In our analysis, we have assumed the signal to be stationary. However, in case of any non-stationarity present in the signal, processing with only detail coefficients will effectively remove it. Consequently, processing with only detail coefficients will be simpler than processing the original signal itself. We have also

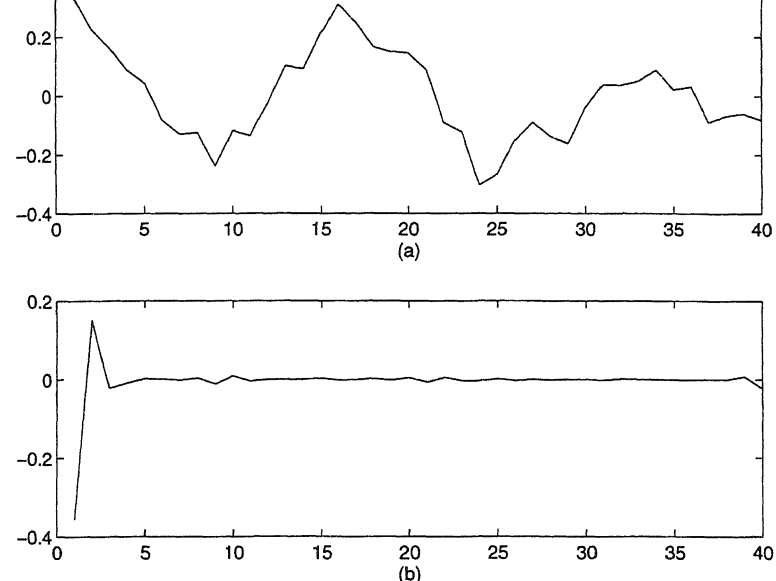


Figure 1. ACF of highest level detail coefficients with (a) Haar wavelet, (b) with Daubechies' wavelet.

not only makes detail signals WSS but almost decorrelates them also. Correlation of detail coefficients can be obtained by calculating autocorrelation at a given over scale to scale. Denoting detail coefficients at scale  $m$  (resolution level  $2^m$ ) where  $m$  and  $n$  are the dilation and translation indices respectively, it can be shown (van 1997)

$$E[d_m^k d_n^l] \sim \mathcal{O}(|2^m k - 2^n l|^{(\gamma-R-1)}). \quad (15)$$

This gives the correlation across scales, as well as at a particular scale. Consequently with higher regularity mother wavelets it is possible to achieve fast decay of correlation coefficients. This property is illustrated in figure 2.5. Furthermore, it can be shown that detail coefficients are mutually uncorrelated and their variance decreases geometrically with scale  $m$  and at each scale the variance,  $\sigma_{2^m}$ , can be expressed as (Wornell 1993)

$$\sigma_{2^m}^2 = \sigma^2 2^{-\gamma m}. \quad (16)$$

## Wiener filtering

We assume that the original signal itself is a Gaussian process and corrupted by independent additive white Gaussian noise (WGN). Clearly Wiener filtering gives an unbiased estimate of the uncorrupted signal since it minimises the mean square error in the case. Instead of doing Wiener filtering directly on the signal itself, we decompose

that wavelet decomposition whitens the  $1/f$  process. Complexity is greatly reduced by adopting this technique (Wornell & Oppenheim 1990).

Let  $r_n^m$ ,  $w_n^m$  and  $x_n^m$  be the detail coefficients of the corrupt signal, the original uncorrupt signal at a scale  $m$  (level  $2^m$ ). Hence,  $r_n^m$  is obtained by doing Wiener filtering at each scale and the problem is to find the optimal filter impulse response  $h_n^m$  so that for the input  $r_n^m$  the output will be an optimal estimate  $\hat{x}_n^m$  of  $x_n^m$ . We have,

$$\hat{x}_n^m = r_n^m \star h_n^m = \sum_{k=-\infty}^{+\infty} r_{n-k}^m h_k^m = \sum_{k=-\infty}^{+\infty} r_k^m h_{n-k}^m,$$

where  $\star$  denotes linear convolution.

The optimal filter impulse response  $h_n^m$  at a given scale  $m$  is given by

$$h_n^m = \frac{\sigma^2 \beta^{-m}}{\sigma^2 \beta^{-m} + \sigma_w^2} \delta[n],$$

where  $\sigma$  and  $\beta$  are signal parameters,  $\sigma_w^2$  is the variance of the noise defined by the equation  $\sigma_{2^m}^2 = \sigma^2 2^{-\gamma m}$ , where  $\sigma_{2^m}^2$  is the variance of the signal at resolution  $m$ .

From the above equation we see that Wiener filter reduces the variance of the noise. Here Wiener filtering is done only on detail coefficients because the energy of the signal is concentrated at low frequencies and consequently the noise is additive white Gaussian noise.

#### 4. ROI reconstruction

We now consider the problem of ROI reconstruction when the image is reconstructed from projections taken at different angles. It is shown that projections at a different angles can be considered to reconstruct the image for different values of  $\gamma$ .

*Data Collection:* The non-locality property of Radon transform makes it possible to reconstruct from projections only over that region. It requires projections taken for the entire object (with a large number of projections at a coarse resolution) at a low number of angles and the values of the projections at the missing angles interpolated suitably (Olsen & DeStefano 1990). If the projections are taken at a fine resolution, then the projections at an increased number of angles are taken. A comprehensive data collection strategy can be found in (Delany & Bresler 1988, Delany & Bresler 1994).

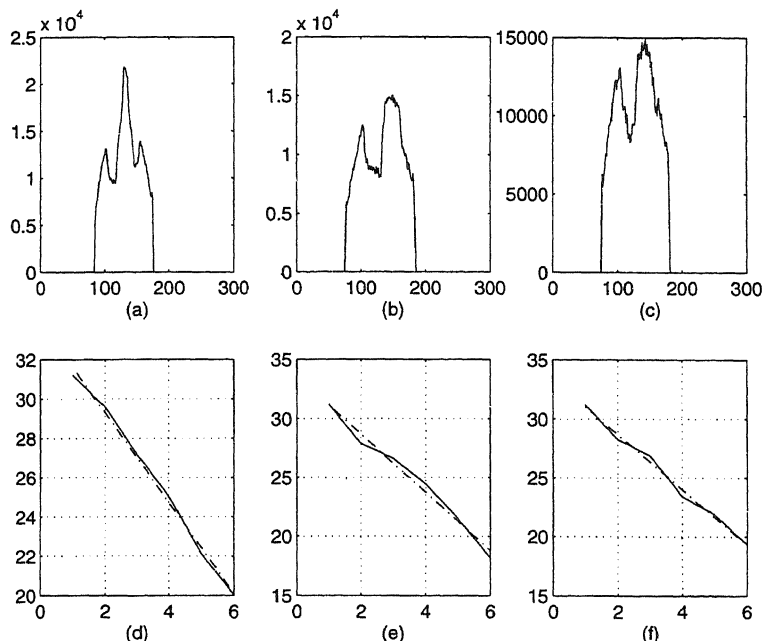
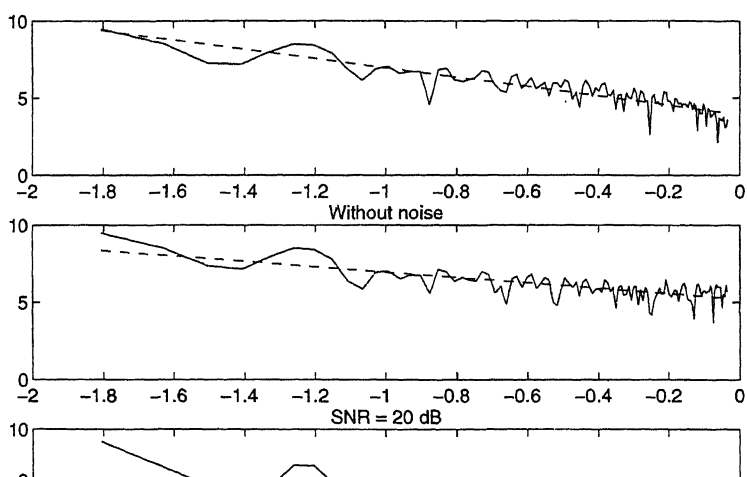


**Figure 2.** A few typical projection data and their approximation to the fractal model; — actual variance of detail coefficients. against scale; --- straight-line fit.



typical projections against the resolution on a log-log graph. This is self-evident.

The Wiener filtering process involves decomposition of the signal. The length of the signal corresponds to the filter length. As an example, Daubechies filter is used the signal length at the lowest level will be padding the signal with suitable number of zeros so that the signal length is  $\times 2^k$  where  $k$  is an integer, denoting the resolution level. For a signal of length 256, we zero-pad it upto 320. At level 5, the filter length is 32. The reconstructed signal, after an inverse wavelet transform, is an estimate of the original signal.

*Estimating fractal signal parameters:* Maximum likelihood (ML) estimation of fractal signals was introduced by Wornell & Oppenheim (1992). Wavelet decomposition technique is used as a tool and wavelet filter bank can decorrelate the  $1/f$  signal but provide a power law variance spectrum also (figure 3). Here it is assumed that the original  $1/f$  signal contains additive white Gaussian noise and we estimate fractal dimension using Wornell–Oppenheim ML estimation algorithm (Wornell &

#### 4.1 Algorithm for ROI reconstruction

Figure 4 outlines the entire filtering and reconstruction process. It should be noted that the diagram is simply for the purpose of illustration and the values shown do not reflect the values we used in our simulation. Note that the projections are sparsely sampled in the angular variable. In the diagram,  $N/2$  full exposure projections and  $N/2$  reduced exposure projections means that there are  $N$  projections over the ROI and  $N/2$  away from the ROI explained in the steps below.

- (1) A wavelet decomposition is done on each full exposure projection. The filter length is equal to filter length. The detail coefficients are estimated using the Daubechies filter bank. We add only the detail coefficients corresponding to the projections over the ROI and obtain the estimate of the projections over the entire object.
- (2) A wavelet decomposition is done on the reduced exposure projections. The filter length is equal to the filter length. The low resolution coefficients are not processed as they are not localised. Thus before doing a wavelet transform on the reduced exposure detail coefficients, we must obtain the low resolution coefficients.

full exposure projections of length 40

reduced exposure projections of length 20

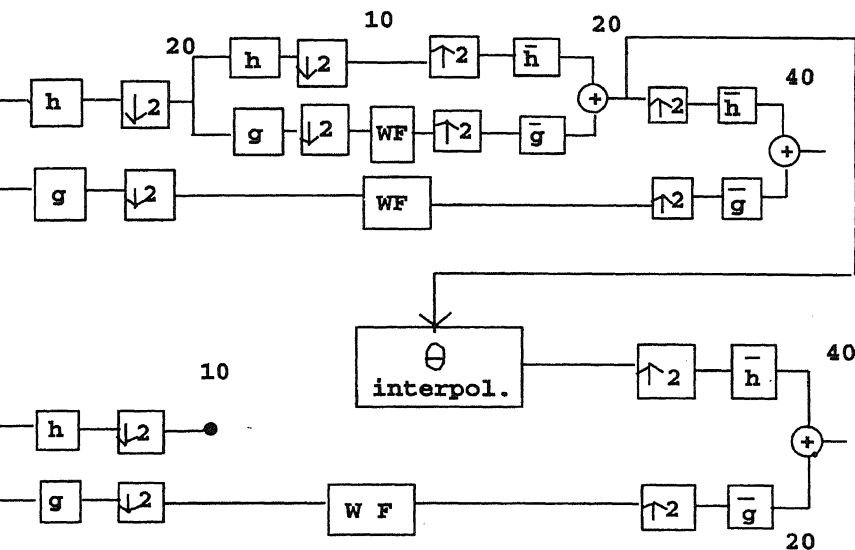


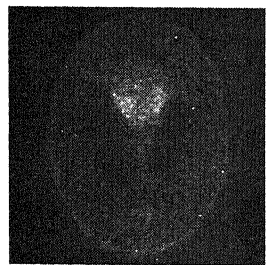
Figure 4. Simple schematic of the algorithm (the values are simply for the purpose of illustration; they do not reflect the values used in simulations), showing the wavelet decomposition, Wiener filtering and wavelet synthesis. Numerals denote signal lengths at various stages.  $h$  and  $g$  are of length 10.

using the detail coefficients available for the ROI. Note that the detail coefficients at a particular resolution will be smaller in length than the low resolution coefficients, the former is obtained only for the ROI. Thus the addition of the detail coefficients can be only over the ROI.

projection data for all the angles is now obtained, with the detail information restricted only to the ROI.

of the result obtained in step (4) results in an object reconstruction which has a high resolution over the ROI and a low resolution elsewhere.

By performing the synthesis of wavelet coefficients at a particular scale, we can obtain various resolutions. This can also be done sequentially, and the radiologist can view the image at finer and finer resolutions.



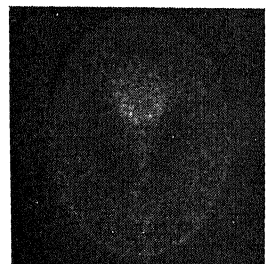
(a)



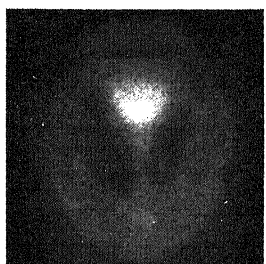
(b)



(c)



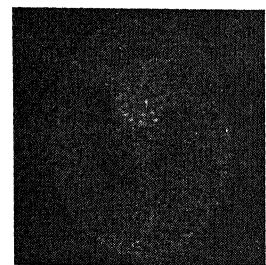
(d)



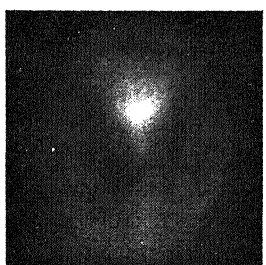
(e)



(f)



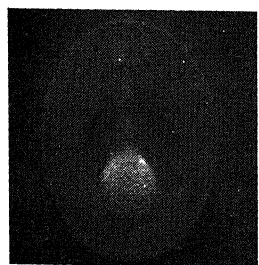
(g)



(h)



(i)



(j)

**Figure 5.** Noisy and estimated images: (a), (d), (g) – noisy images at

of the phantom image consists of 128 parallel rays while each projection of the images consist of 193 (approx.  $128\sqrt{2}$ ) rays. The ROI is defined to lie at the approximately covers 1/4th of the image. The ROI can be shifted to some other change of co-ordinates. We have used Daubechies' wavelets of length 10 ( $h$  is of (Daubechies 1992).

In figure 5j, the image is reconstructed from the full projection data at 128 angles without noise. The effect of noise on the data when no estimation techniques are used is shown in figure 5a, d and g, for 15, 10 and 5 dB. The result of using the filter with Daubechies wavelet is shown in figure 5b, e and h. It is apparent that noise has been removed. The smoothing of the edges can be explained by looking at the corresponding back-projection. A typical projection and the output after filtering is shown in figure 6. The high frequency details of the projections are removed as the filtering is unable to estimate the high frequency signal from the noise. For purposes of comparison, we constructed using the Haar basis. The presence of circular rings can be accounted for by comparing the corresponding reconstructed projection. The estimated projection contains sharp edges. On back-projection, the sharp edges lead to rings in the image. The error in the estimation using the Haar wavelet is because of several factors. The estimation process assumes that the wavelet coefficients are decorrelated from scale to scale. Figure 1 shows the autocorrelation function with both the Haar and Daubechies' wavelets. The decorrelation in the second case is greater than in the first. Thus our assumption is more correctly adhered to in the second case. As has been shown before, the

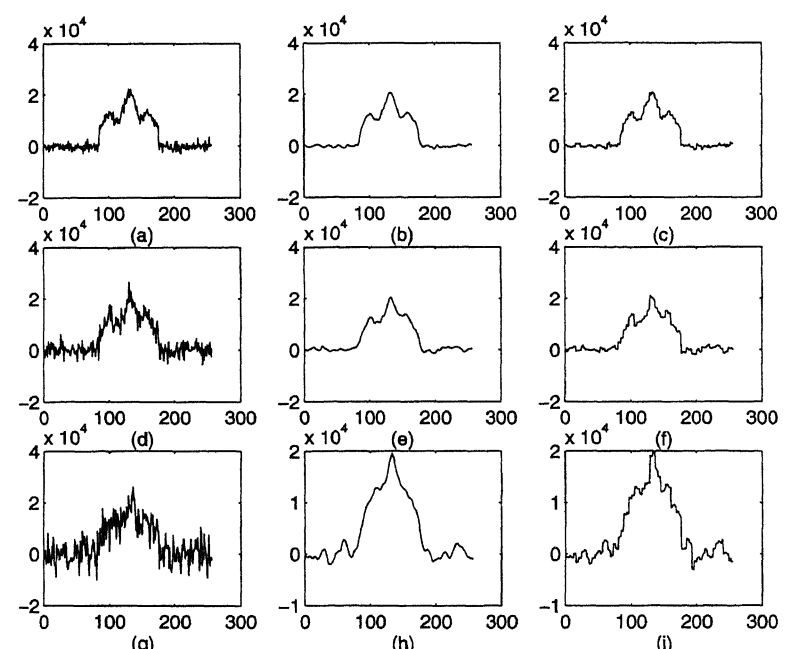
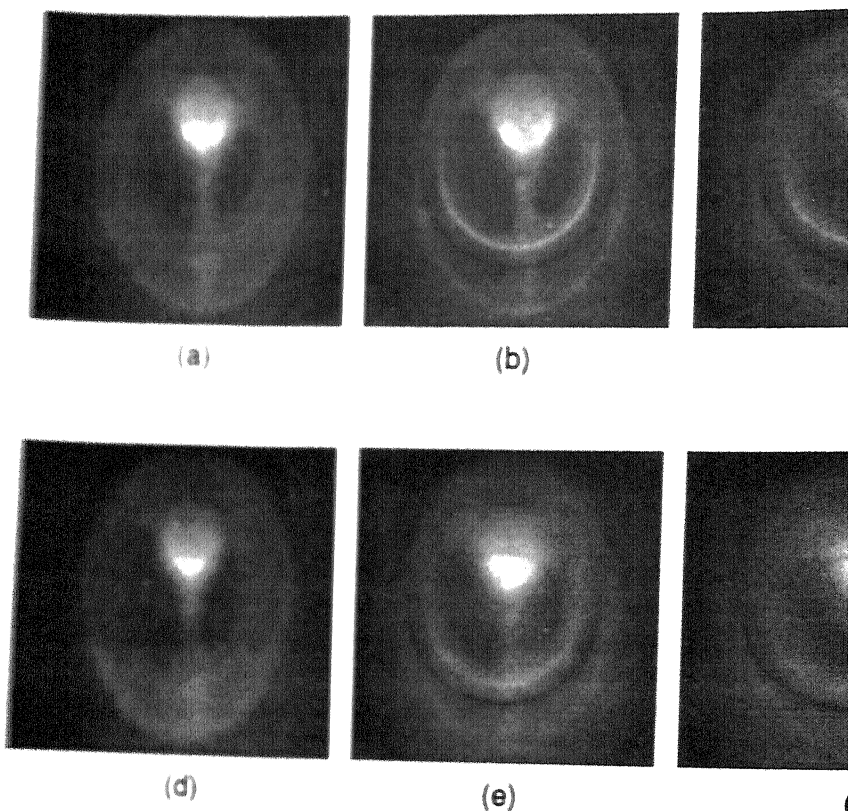


Figure 6. Noisy and estimated signals: (a), (d), (g) = noisy signals at 15, 10 and 5 dB.

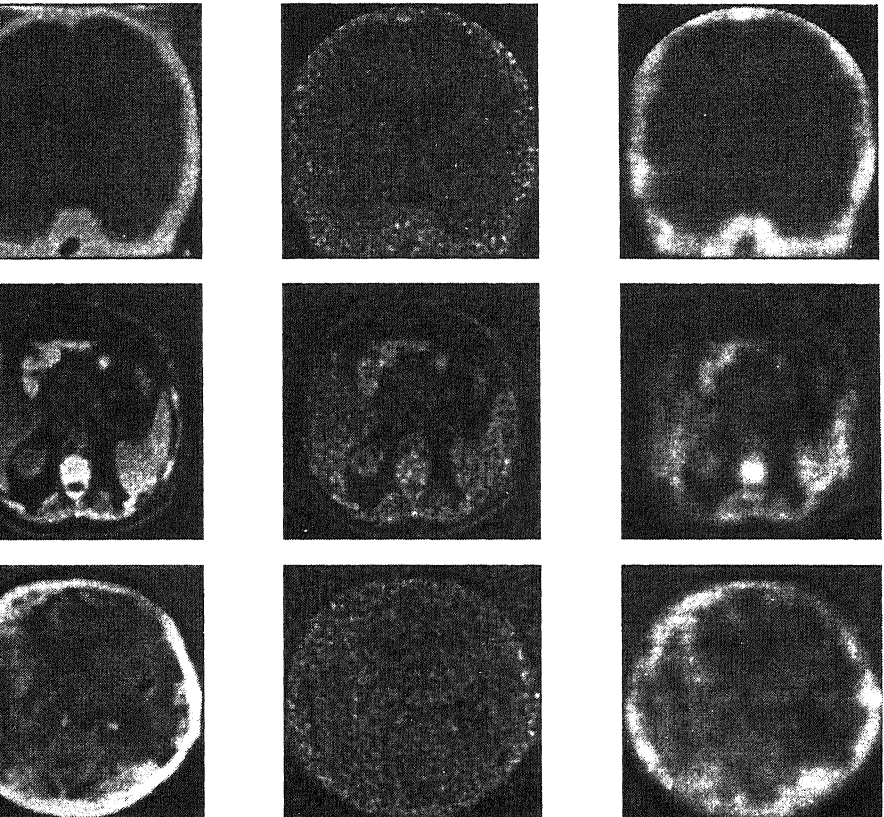


**Figure 7.** (a), (b) – ROI reconstruction at two consecutive resolutions below the original, works at 15 dB SNR. (c), (d), (e) – ROI reconstruction at high resolution with SNR = 20, 15, 10.5 dB respectively.

clique's correlation increases with the regularity of the wavelet. For the Haar,  $R = 1$ ; Daubechies' wavelet in our example,  $R = 5$ . Figure 7 shows the result of SNR reduction.

In figure 7a and d, we show the multiresolution reconstruction at two different SNR of 15dB. Wiener filtering is easily applicable to multiresolution of a signal as it works directly in the scale space domain. Comparing with new construction from noiseless projections, we find the absence of fine scale edges from the low-resolution reconstruction.

Figure 8b, c, e and f show the results for the DCT.



ure 8. Reconstruction of the images from noisy projections at 15 dB SNR. The columns b, c) show the original image, noisy image and noise removed image respectively. The s correspond to images A, B, C respectively.

ow good is the  $1/f$  model?

re algorithm described thus far hinges on the assumption that the projection of image at each angle is a fractal signal. To test our assumption, we considered a few medical images obtained from medical texts. Here we show the results on three of images we collected (figure 8). We refer to the images as A, B and C.

scan of the large frontal lobe.

frontal CT scan in the investigation of the cortical areas (frontal, temporal, parietal), car, parasellar and third ventricle region.

ominal scan.

e 9 shows the linear trend in the detail coefficients across scales. The next two show the noise removal and reconstruction using this fractal model. The results

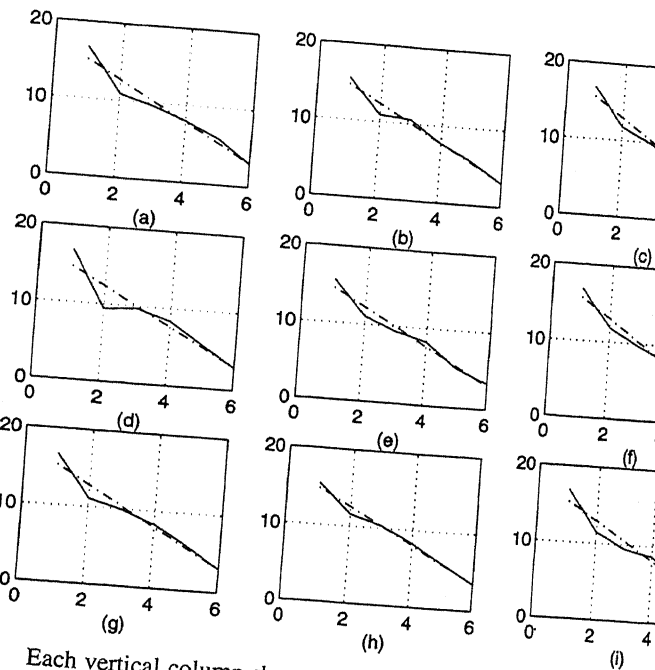


**Figure 9.** Each vertical column shows the straight line fit on three typical images A, B, C. Column 1 corresponds to image A and so on. (— actual v. detail coefficients against scale; --- straight line fit.)

## 6. Conclusion

In this paper, we have shown how multiresolution and ROI reconstruction when projections are noisy. For this purpose, we have assumed a fractal projections and filtered the noise by using a Wiener filter. This filtering gives output as it is done on the detailed coefficients obtained on performing a position on the projections. These detailed coefficients are localised and used this property for ROI reconstruction.

## References

- Aldroubi A 1996 The wavelet transform: a surfing guide. In *Wavelets in medicine* (Boca Raton, FL: CRC Press)
- Bhatia M, Willsky A S 1996 A wavelet based method for multiscale tomographic *IEEE Trans. Med. Imaging* 15: 92–101
- Barman K 1997 *Multiscale processing of 1/f signals*. M E thesis, Electrical Engineering, Indian Institute of Science, Bangalore

Roberts B A 1986 Reconstruction from projections. In *Handbook of pattern recognition and image processing* (Orlando, FL: Academic Press)

1993 The wavelet transform of stochastic processes with stationary increments and its relations to fractional Brownian motion. *IEEE Trans. Inf. Theory* 39: 260–265

1986 *The mathematics of computerized tomography* (New York: John Wiley and Sons)

1996 Optimal time-frequency projection for localised tomography. In *Wavelets in medicine and biology* (Boca Raton, FL: CRC Press)

DeStefano J 1994 Wavelet localisation of the radon transform. *IEEE Trans. Signal Processing* 42: 2055–2067

W 1993 Wavelet-based representation of  $1/f$  family of fractal processes. *Proc. IEEE* 81: 1448–1450

W, Oppenheim A V 1992 Estimation of fractal signals from noisy measurements using wavelets. *IEEE Trans. Signal Process.* 40: 611–625



## onal invariance of two-level group codes over dihedral cyclic groups

JYOTI BALI<sup>1</sup> and B SUNDAR RAJAN<sup>2</sup>

<sup>1</sup> Department of Electrical Engineering, Indian Institute of Technology, Hauz Khas, New Delhi 110 016, India

<sup>2</sup> Department of Electrical Communication Engineering, Indian Institute of Science, Bangalore 560 012, India  
e-mail: jbali@ee.iitd.ernet.in; bsrajan@ece.iisc.ernet.in

**Abstract.** Phase-rotational invariance properties for two-level constructed, (using a binary code and a code over a residue class integer ring as component codes) Euclidean space codes (signal sets) in two and four dimensions are discussed. The label codes are group codes over dihedral and dicyclic groups respectively. A set of necessary and sufficient conditions on the component codes is obtained for the resulting signal sets to be rotationally invariant to several phase angles.

**Keywords.** Multilevel codes; group codes; dihedral groups; coded modulation.

### duction

known (Viterbi & Omura 1979; Bendetto *et al* 1987) that digital communication in White Gaussian Noise (AWGN) channel can be modelled as transmission from a finite set of points, called signal set, of a finite dimensional vector space. Maximum Likelihood soft decoding then becomes choosing the closest point in the set, in the sense of Euclidean distance, from the received point in the space. Ability of error performance to a large extent is dominated by the minimum of these distances of the signal points. The problem of signal set design for AWGN then is choosing a specified number of points in a space of specified dimensions in such way that the minimum distance is the maximum possible.

where,  $d_E(a, b)$  denotes the squared Euclidean distance between  $a$  and  $b$ . The identity element of  $G$  is denoted by  $e$ . If  $G$  and  $S$  have the same number of elements, then each element of  $S$  can be labelled with the elements of  $G$ , and such a labelling satisfying condition (1) is referred as a matched labelling (Loeliger 1991, 1992). A signal space code is said to have the property that the Euclidean distance distribution of the points in the signal set from any point is same, known as Uniform Error property (UEP). If a signal space code of dimension  $N$  is matched to a group  $G$  and  $\mu$  is a matched labelling, then  $\mu$  is called a mapping.

$\mu^n: G^n \rightarrow S^n$  given by  $\mu^n(g_0, g_1, \dots, g_{n-1}) = (\mu(g_0), \mu(g_1), \dots, \mu(g_{n-1}))$  gives a signal set in  $Nn$  dimensions, called the signal space code and it is matched to a group  $C$ . Forney (1991) has shown that such signal space codes are special cases of a class of codes known as geometrically uniform codes which have been called as the label code of the signal space code.

Recently ‘multilevel constructions’ have been reported using binary linear block codes and suitable mapping of coded bits onto a signal set of small dimension (Barg & Zeng 1991; Kschischang *et al* 1989; Kasami *et al* 1991; Calderbank & Seshadri 1991; Caire 1994; Garello & Bendetto 1995; Imai & Hirakawa 1997). Multilevel signal sets have attracted wide spread research because of their amenability for multistage decoding (Calderbank 1989; Takata *et al* 1993; Kofman *et al* 1993). A multilevel signal set, or multilevel block code of  $L$  levels uses  $L$  block codes, called component codes, over finite alphabets of possibly different sizes. A signal set  $S$ , called a multilevel signal set of dimension  $N$ , has  $\prod_{i=1}^L m_i$  points, where  $m_i, i = 1, 2, \dots, L$ , are the sizes of the component codes with each point labelled by an ordered  $L$ -tuple with one entry from each component code. With this labelling, a set of  $L$  codewords, one from each code, corresponds to a point in  $S$  in  $N$  dimensions, with each coordinate of  $L$  codewords choosing a point in the component codes. All such points corresponding to all possible combinations of codewords of the component codes is the multilevel constructed signal space code or Euclidean space code.

This paper reports rotational invariance properties of coded signal sets. We present a two-level ( $L = 2$ ) construction for a class of two-dimensional ( $N = 2$ ) and four-dimensional ( $N = 4$ ) signal sets. Four-dimensional signal sets have been studied by several authors (Welti & Lee 1974; Zetterberg & Brancik 1975; Gersho & Lawrence 1984; Birdsall 1989; Visintin *et al* 1992). Gersho & Lawrence (1984) describe the design and implementation for a particular 2-bits per dimension four-dimensional signal set which readily lends itself to simple encoding and decoding. For this encoding and decoding, there is a gain in noise margin over conventional 16-point(two-dimensional) quadrature amplitude modulation (QAM) signalling. In our two-level construction the component codes are a binary code and a linear code over a residue class integer ring. The two-level construction is based on the well known Welch bound for linear codes (Welch 1974).

The class of dihedral groups is defined by

$D_M = \{r^i s^j | r^M = s^2 = e, r^i s = sr^{-i}, 0 \leq i < M, j = 0, 1\}$  where  $e$  is the identity of  $D_M$ . The group operation can be expressed as

$$(r^{i_1} s^{j_1})(r^{i_2} s^{j_2}) = r^{i_1+i_2(1-2j_1)} s^{j_1+j_2},$$

and the inverse of an element is given by

$$(r^i s^j)^{-1} = r^{i(2j-1)} s^j.$$

This group has  $2M$  elements, where  $M$  is an arbitrary integer and  $r$  and  $s$  are called the generators of  $D_M$ .

### DEFINITION 1

Let  $S$  denote a unit circle in 2-dimensions. A matched labelling  $\mu : D_M \rightarrow S$ , for a  $2M$ -asymmetric PSK signal set matched to  $D_M$  is said to be an  $m$ -labelling,  $0 \leq m \leq M - 1$ , with angle of asymmetry  $\phi$ ,  $-\pi/2M < \phi < \pi/2M$ , and denoted by  $ml\phi$ , if

$$\mu(r^i s^j) = \exp\{\sqrt{-1}[j((2m+1)(\pi/M)+\phi)+il2\pi/M]\},$$

$$i = 0, 1, \dots, M - 1, \quad j = 0, 1, (l, M) = 1$$

Definition 1 is general and includes Asymmetric PSK(APSK) signal sets. It is shown (Bali & Rajan 1997b) that for a given group code APSK performs better than SPSK under certain conditions. In this paper, however, we will be considering only SPSK signal sets, i.e.,  $\phi = 0$  throughout. Observe that various values of the parameter  $m$  gives different labellings of the SPSK signal set with  $m = 0$  corresponding to labelling the signal points in natural order in the anticlockwise direction. Our results in this paper hold even if  $m \neq 0$ .

The class of dicyclic groups is defined by

$$DC_{2M} = \{r^i s^j | r^M = s^2 = (rs)^2, 0 \leq i < 2M, j = 0, 1\}.$$

This group has  $4M$  elements,  $M$  being any positive integer and is generated by  $r$  and where,  $r^{2M} = e$ , the identity element. The group operation can be expressed as

$$(r^{i_1} s^{j_1})(r^{i_2} s^{j_2}) = r^{(i_1+i_2+j_1(Mj_2-2i_2)) \text{modulo } 2M} s^{(j_1+j_2) \text{modulo } 2}$$

and the inverse of an element is given by

$$(r^i s^j)^{-1} = r^{-i+j(M+2i)} s^j$$

### DEFINITION 2 (Bali & Rajan 1997b)

Let  $S$  denote the unit sphere in 4 dimensions. The matched labelling we consider is the subset of  $S$  (shown in figure 1 – the  $x_1 - x_2$  plane constitutes the first two dimensions and the  $x_3 - x_4$  plane constitutes the remaining two).

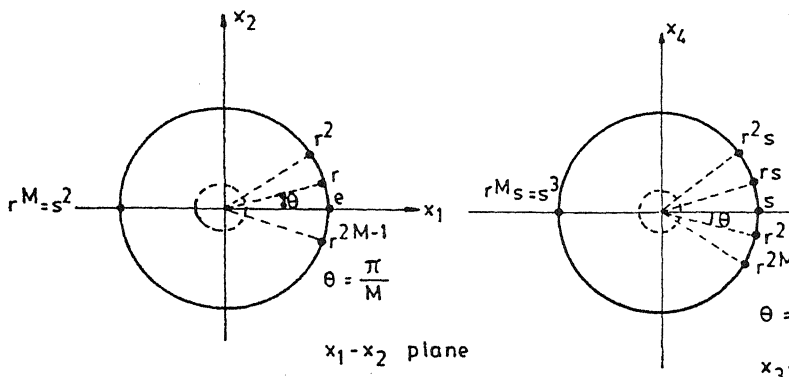


Figure 1. A signal set matched to  $DC_{2M}$ .

consisting of  $4M$  points and the matched labelling  $\mu : DC_{2M} \rightarrow S$ , is

$$\begin{aligned}\mu(r^k s^l) = & (1 - l) \cos(k\pi/M), (1 - l) \sin(k\pi/M), \\ & l \cos(k\pi/M), -1 \sin(k\pi/M).\end{aligned}$$

It is routine calculation to check that the mappings of definitions 1 and 2 satisfy the conditions for matched labelling given in (1).

### 3. Two-level group codes and their characterization

The block diagram of a two-level block-coded modulation is shown in figure 2a. Let  $X$  and  $Y$  be length  $n$  codes over alphabets  $X = \{x_1, x_2, x_3, x_4\}$ , ( $m_1 = 4$ ) and  $Y = \{y_1, y_2, \dots, y_{2M}\}$ , ( $m_2 = 2M$ ). Figure 2b shows a labelling of  $S$  consisting of eight points on the circles of  $X$  and  $Y$ . For codewords  $a = (a_0, \dots, a_{n-1}) \in C_1$  and  $b = (b_0, \dots, b_{n-1}) \in C_2$ , each pair  $(a_i, b_i)$ ,  $i = 0, 1, \dots, n-1$ , selects a point in  $S$ , and the pair  $(a, b)$  selects a point in  $2n$  dimensions. The collection of all such points in  $2n$  dimensions, corresponding to all possible pairs of codewords constitute the two-level block coded modulation (signal set) or signal space code. This paper deals with  $X$  and  $Y$  being  $Z_2$  class integers modulo 2 and modulo  $\lambda$  respectively, where  $\lambda = M$  for codes over  $DC_{2M}$  and  $\lambda = 2M$  for codes over  $DC_{2M}$ .

#### DEFINITION 3

Let  $C_s$  and  $C_r$  be length  $n$  codes over respectively,  $Z_2 = \{0, 1\}$  and  $Z_\lambda = \{0, 1, \dots, \lambda - 1\}$  and  $a = (a_0, \dots, a_{n-1}) \in C_s$ ,  $b = (b_0, \dots, b_{n-1}) \in C_r$ . Let  $c_{a,b}$  denote

$$(b_0 a_0, b_1 a_1, \dots, b_{n-1} a_{n-1}) \in Z_2^n \times Z_\lambda^n$$

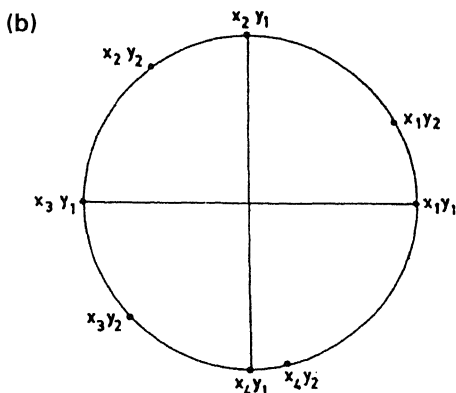
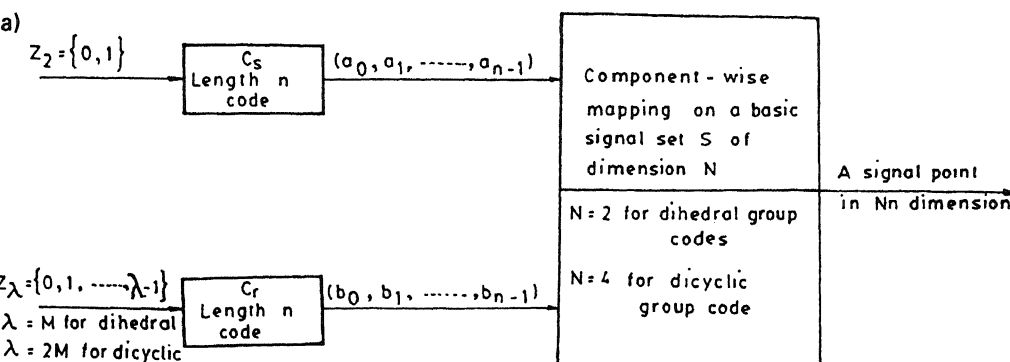


**Figure 2.** (a) Block diagram of a two-level block coded modulation. (b) Labelling of an 8-PSK signal set with  $X$  and  $Y$ .

Bigleiri & Caire (1994) have studied the Geometrical Uniformity properties of signal space codes obtained by  $L$ -level construction. The component codes used are  $L$  linear binary codes with the  $2^L$ -ary SPSK as the basic signal set. The points of the PSK signal set can be designated with either the cyclic group with  $2^L$  elements or with the dihedral group with  $2^L$  elements. They derive conditions under which the resulting multilevel code is a group code over the cyclic or dihedral group.

In the rest of the section we give the necessary and sufficient conditions on the component codes of the two-level construction shown in figure 2a to result in a group code over  $D_M$  and  $DC_{2M}$ .

**Theorem 1** (Bali & Rajan 1997a, 1998). *The two-level code  $C = r^{C_r} s^{C_s}$  is a group code over  $D_M$  if and only if*

obtained as

$$C_r = C_1 + 2C_2 + \cdots + 2^{L-2}C_{L-1},$$

then theorem 1 coincides with theorem 1 of Bigleiri & Caire (1994).

Proof of theorem 1 and the Euclidean distance properties of the resulting asymmetric PSK signal space codes can be seen in Bali & Rajan (1998).

*Example 1.* If  $C_r = Z_M^n$ , i.e., if  $C_r$  is the trivial code consisting of all over  $Z_M$ , then for any binary linear code  $C_s$ , conditions of theorem 1 hence the resulting code is a group code over  $D_M$ .

*Example 2.* If  $C_s$  is a repetition code consisting of all zero and all one  $C_r$  is any linear code over  $Z_M$ , then conditions of theorem 1 are satisfied code is a group over  $D_M$ .

*Example 3.* Let  $C_s = \{000, 111\}$  and  $C_r = \{000, 220, 132, 312, 200, 0Z_4$ . Then the resulting two-level code is a group code over  $D_4$  and has codewords

$$\begin{aligned} &\{(r^0, r^0, r^0), (r^2, r^2, r^0), (r^1, r^3, r^2), (r^3, r^1, r^2), \\ &(r^2, r^0, r^0), (r^0, r^2, r^0), (r^3, r^3, r^2), (r^1, r^1, r^2), \\ &(s, s, s), (r^2s, r^2s, s), (r^1s, r^3s, r^2s), (r^3s, r^1s, r^2s), \\ &(r^2, s, s), (s, r^2s, s), (r^3s, r^3s, r^2s), (r^1s, r^1s, r^2s)\}. \end{aligned}$$

Observe that in this example,  $M$  is a power of 2, but  $C_r$  is a non-deco-

*Example 4.* Let  $C_r = \{0000, 1233, 3211, 0222, 1011, 2022, 3033, 2210\}$   $C_s = \{0000, 1111\}$ . For these codes  $C_s \odot 2C_r = \{0000, 2022\} \subseteq C$  two-level code  $r^{C_r}s^{C_s}$  is a group code over  $D_4$  and the codewords are:

$$\begin{aligned} &(1111), (1, r^2, r^2, r^2), (r^3, r^2, r, r), (r, r^2, r^3, r^3), \\ &(r, 1, r, r), (r^2, r^2, 1, 1), (r^3, 1, r^3, r^3), (r^2, 1, r^2, r^2), \\ &(s, s, s, s), (s, r^2s, r^2s, r^2s), (r^3s, r^2s, rs, rs), \\ &(rs, r^2s, r^3s, r^3s), (rs, s, rs, rs), (r^2s, r^2s, s, s), \\ &(r^3s, s, r^3s, r^3s), (r^2, 1, r^2, r^2), \end{aligned}$$

The following theorem gives the necessary and sufficient conditions codes of the two-level construction shown in figure 2a to result in a group

### Rotational invariance of two-level group codes

The proof is similar to that of theorem 1 and is omitted. We list below a few classes of group codes over  $DC_\lambda$ .

**Example 5.** If  $C_r = Z_{2\lambda}^n$ , i.e., if  $C_r$  is the trivial code consisting of all possible  $n$ -tuples over  $Z_{2\lambda}$ , then for any binary linear code  $C_s$ , conditions of theorem 1 are satisfied hence the resulting code is a group code over  $DC_\lambda$ .

**Example 6.** If  $C_s$  is a repetition code consisting of all zero and all one vectors only, conditions of theorem 1 are satisfied for any linear code over  $Z_{2\lambda}$  containing all codewords, as  $C_r$  code.

**Example 7.** Let  $C_s$  be any binary code with the property  $C_s \odot C_s \subseteq C_s$  and  $C_r$  is a parity check code over  $Z_{2\lambda}$ . Then the resulting two-level code is a group code over  $DC_\lambda$ .

Notice that when all the three conditions of theorem 1 are satisfied for a set of component codes then these can be used to construct both group codes over the dihedral group as well as group codes over the dicyclic group. The resulting coding gain when used as dihedral group code is given by

$$G_D = d_D/4 \sin^2(\pi/2^R),$$

and when used as dicyclic group code is given by

$$G_\lambda = d_{DC}/4 \sin^2(\pi/2^{R/2})$$

where  $d_D$  and  $d_{DC}$  denote the MSED of the signal space codes of dihedral and dicyclic group codes respectively and  $R$  denotes the rate of the code in bits per channel (Kschischang *et al* 1989).

Theorems 3 and 4 below identify two situations for component codes satisfying conditions of both theorems 1 and 2; labelling with dicyclic groups gives better performance compared to labelling with dihedral groups.

**Theorem 3.** If  $C_s$  is a  $(n, k, d_s)$  binary linear code with  $C_s \odot C_s \subseteq C_s$  and  $C_r = Z_{2M}$  then, the two-level code construction will give group code over both  $D_M$  and  $DC_{2M}$  such a pair of component codes

(i)                  If  $2 \cos(\pi/4M) > \Gamma(R)$ ,

where  $\Gamma(R) = \sin(\pi/2^{R/2})/\sin(\pi/2^R)$  then,  $G_\lambda > G_D$ .

(ii)                If  $R > 2.68$  then,  $G_D > G_\lambda$ .

**Theorem 4.** If  $C_s$  is a  $(n, n/2, 2)$  binary code ( $n$  even) with generator matrix

$$\begin{bmatrix} 1 & 1 & 0 & 0 & 0 & 0 & \dots & 0 & 0 \\ 0 & 0 & 1 & 1 & 0 & 0 & \dots & 0 & 0 \\ \dots & \dots \\ 0 & 0 & 0 & 0 & 0 & 0 & \dots & 1 & 1 \end{bmatrix}$$

and  $C_r$  is  $(n, n - 1, 2)$   $2M$ -ary parity check code then,  $G_\lambda > \sin(\pi/2^{R/2})/\sin(\pi/2^R)$ .

*Proof.* It is easy to verify that the component codes in the statement satisfy the conditions of both theorems 1 and 2. The rest of the proof is similar to theorem 3.

*Example 8.* Consider the case  $n = 8$ ,  $M = 2$  in theorem 4. The bits per symbol,  $\log_2 M = 1$ .

$$\frac{G_D}{2} = \frac{2 \sin^2(\pi/8)}{\sin^2(\pi/2^{2.25})} = 0.7782735 \quad (-1.02 \text{ dB})$$

$$2 \sin^2(\pi/4) / \sin^2(\pi/2^{2.25/2}) = 1.0171907 \quad (0.0740239 \text{ dB}) > G_D$$

#### 4. Phase rotational invariance

For L-level codes with binary component codes phase invariance has been reported (Kasami *et al* 1994a). In this section we discuss phase invariance properties of two-level group codes over  $D_M$  and  $DC_{2M}$ .

For  $mL$  of a  $2M$ -SPSK signal set, a codeword

$$(r^{y_0}s^{x_0}, r^{y_1}s^{x_1}, \dots, r^{y_i}s^{x_i}, \dots, r^{y_{n-1}}s^{x_{n-1}}) \in C,$$

is mapped onto the point

$$\exp\{\sqrt{-1}[x_0((2m+1)\pi/M) + y_02\pi/M]\}, \dots,$$

$$\exp\{\sqrt{-1}[x_i((2m+1)\pi/M) + y_i2\pi/M]\}, \dots,$$

$$\exp\{\sqrt{-1}[x_{n-1}((2m+1)\pi/M) + y_{n-1}2\pi/M]\},$$

in  $2n$ -dimensional space. There is a one-one correspondence between the  $2n$ -dimensional points given by (3) and (4). The code is said to be phase invariant under rotation by angle  $\theta$ , if whenever (4) is a signal point for a codeword in  $C$ , then so is

$$\exp\{\sqrt{-1}[x_0((2m+1)\frac{\pi}{M}) + y_02\pi/M + \theta]\}$$

$(2\pi/M)$ , rotations where  $k$  divides  $M$ , iff the all  $k$  vector  $(k, k, \dots, k) \in C_r$ ,  
 $(2\pi/M)$ , rotations where  $k$  and  $M$  are relatively prime, iff the all-1 vector  $(1, 1, \dots,$   
 $\in C_r$ ,  
 $/M$  rotations iff all-1 vector is present in  $C_r$  and  $C_s$ .

Let  $M/k = \lambda$ . Then replacing  $y_i$  by  $y_i + \lambda$ ,  $i = 0, 1, \dots, n - 1$ , in (3) corresponds  
 $\theta$  in (4) getting replaced by  $\lambda 2\pi/M$ , and the converse.

If  $k$  and  $M$  are relatively prime, then  $k 2\pi/M$  rotations can be obtained by  $k$  successive  
 $\pi/M$  rotations and  $2\pi/M$  rotations can be obtained by  $u$  successive  $k 2\pi/M$  rotations  
where  $u$  is given by  $uk + vM = 1$  (Bezout's Theorem). Hence it is sufficient to  
consider  $2\pi/M$  rotations only for which all-1 vector  $(1, 1, \dots, 1)$  should be in  $C_r$ ,  
which follows from (i) with  $\lambda = M$ .

Suppose all-1 vectors are present in both  $C_r$  and  $C_s$ . Presence of all-1 vector in  $C_s$   
guarantees rotational invariance by  $(2m+1)\pi/M = m2\pi/M + \pi/M$ . The presence of  
all-1 vector in  $C_r$  guarantees rotational invariance by all multiples of  $2\pi/M$ , including  
 $m2\pi/M$ . Clearly, rotational invariance for both  $m2\pi/M + \pi/M$  and  $-m2\pi/M$   
implies rotational invariance for  $\pi/M$ . The converse is straightforward.  $\square$

a  $4n$ -dimensional signal set obtained using a two level group code over  $DC_{2M}$ , a  
word

$$r^{y_0} s^{x_0}, r^{y_1} s^{x_1}, \dots, r^{y_i} s^{x_i}, r^{y_{n-1}} s^{x_{n-1}} \in C \quad (5)$$

mapped onto the point

$$\begin{aligned} & (1 - x_0) \exp^{\{\sqrt{-1}[y_0\pi/M]\}}, x_0 \exp^{\{\sqrt{-1}[-y_0\pi/M]\}}, \dots \\ & (1 - x_i) \exp^{\{\sqrt{-1}[y_i\pi/M]\}}, x_i \exp^{\{\sqrt{-1}[-y_i\pi/M]\}}, \dots \\ & (1 - x_{n-1}) \exp^{\{\sqrt{-1}[y_{n-1}\pi/M]\}}, x_{n-1} \exp^{\{\sqrt{-1}[-y_{n-1}\pi/M]\}} \end{aligned} \quad (6)$$

dimensional space. There is a one-one correspondence between codewords of the  
code given by (5) and  $4n$ -dimensional points given by (6). The code is said to be  
rotationally invariant to an angle  $\theta$ , if whenever (6) is a signal point for a codeword in  $C$ ,  
the codeword corresponding to

$$\begin{aligned} & (1 - x_0) \exp^{\{\sqrt{-1}[y_0\pi/M+\theta]\}}, x_0 \exp^{\{\sqrt{-1}[-y_0\pi/M+\theta]\}}, \dots \\ & (1 - x_i) \exp^{\{\sqrt{-1}[y_i\pi/M+\theta]\}}, x_i \exp^{\{\sqrt{-1}[-y_i\pi/M+\theta]\}}, \dots \\ & (1 - x_{n-1}) \exp^{\{\sqrt{-1}[y_{n-1}\pi/M+\theta]\}}, x_{n-1} \exp^{\{\sqrt{-1}[-y_{n-1}\pi/M+\theta]\}} \end{aligned}$$

codeword in  $C$ . The following theorem give the conditions on the component codes for

**Theorem 6.** A two-level group code,  $\mathbf{C} = r^{C_r} s^{C_s}$  over  $DC_{2M}$  is invariant to

- (i)  $k(\pi/M)$ , rotations where  $k$  divides  $M$ , iff the all  $k$  vector  $(k, k, \dots, k)$  is in  $C_r$ ,
- (ii)  $k(\pi/M)$ , rotations where  $k$  and  $M$  are relatively prime, iff the all-1 vector  $(1, 1, \dots, 1)$  is in  $C_r$ ,

Notice that the minimum angle of rotational invariance in this case is  $\pi/180^\circ$ . In 2M-SPSK it is  $2\pi/M$ . Moreover, the  $C_s$  code plays no role in the condition of rotational invariance, i.e., the minimal angle of rotational invariance is completely determined by the  $C_r$  code.

## 5. Conclusion

Rotational invariance properties of signal space codes obtained by group codes over dihedral groups and dicyclic groups are discussed. The group codes are obtained by two-level construction from a binary code and a code over residue class ring. The signal space codes obtained from group codes over dihedral group codes are in  $2n$  dimensions and those obtained from dicyclic group codes are in  $4n$  dimensions, where  $n$  is the length of the code. Theorem 3 includes conditions under which the code is invariant to the minimum angle for dihedral group codes. If the component codes satisfy the conditions of the theorem then the effect of phase ambiguity in carrier recovery in multiples of  $2\pi/M$  can be nullified by two-stage differential encoding as follows: before the encoder (and before the modulator) the sequence of symbols to be transmitted is  $(\dots, y_{i-1}x_{i-1}, y_i x_i, y_{i+1}x_{i+1}, \dots)$  where  $(\dots, x_{i-1}, x_i, x_{i+1}, \dots)$  is the binary sequence and  $(\dots, y_{i-1}, y_i, y_{i+1}, \dots)$  is the corresponding sequence of phases. First differentially encode the binary sequence  $\{x_i\}$  resulting in the sequence  $\{x'_i\}$ . After this the original sequence becomes  $(\dots, y_{i-1}x'_{i-1}, y_i x'_i, y_{i+1}x'_{i+1}, \dots)$ . This above sequence can be seen as the interleaved version of two subsequences. The first subsequence, say  $S_0 = \{y_j x'_j\}$ , consists of those symbols with  $x'_j = 0$  and the second subsequence, say  $S_1 = \{y_j x'_j\}$ , consists of those symbols with  $x'_j = 1$ . Now differentially encode each of the  $M$ , the  $\{y_j\}$  parts of the each subsequence.

It is straightforward to verify that by two stage differential decoding process in reverse order of encoding, the effects of phase rotations by multiple of  $2\pi/M$  can be removed.

Theorem 4 includes conditions under which the codes are invariant to the minimum angle for dicyclic group codes. If the component codes satisfy the conditions of the theorem then the effect of phase ambiguity in carrier recovery in multiples of  $\pi/M$  can be nullified by two-stage differential encoding as in the dihedral group code case without the first stage. i.e., differential encoding of binary symbols is not needed for due to rotation invariance the two binary components do not get affected.

Bali J, Rajan B S 1997a Block coded asymmetric PSK modulation using two-level group codes over dihedral groups. *IEEE International Symposium on Information Theory*, Ulm, Germany

Bali J, Rajan B S 1997b Two-level group codes over four dimensional signal sets. *Proc. 1997 National Conf. on Communications*, pp 101–105

Bali J, Rajan B S 1998 Block coded PSK modulation using two-level group codes over dihedral groups. *IEEE Trans. Info. Theory* 44: (in press)

Bendetto S, Biglieri E, Castellani V 1987 *Digital transmission theory* (Englewood Cliffs, NJ: Prentice-Hall)

Biglieri E, Caire G 1994 Symmetry properties of multilevel coded modulation. *IEEE Trans. Info. Theory* 40: 1630–1632

Calderbank A R 1989 Multilevel codes and multistage decoding. *IEEE Trans. Commun.* 37: 222–229

Calderbank A R, Seshadri N 1993 Multilevel codes for unequal error protection. *IEEE Trans. Info. Theory* 39: 1234–1248

Cusack E L 1984 Error control coding for QAM signalling. *Electron. Lett.* 20: 62–63

Forney G D 1991 Geometrically uniform codes. *IEEE Trans. Info. Theory* 37: 1241–1260

Garello R, Bendetto S 1995 Multilevel construction of block and trellis group codes. *IEEE Trans. Info. Theory* 41: 1257–1264

Gershko A, Lawrence V B 1984 Multidimensional signal constellations for voiceband data transmission. *IEEE J. Selected Areas in Commun.* 2: 687–702

mai H, Hirakawa S 1977 A new multilevel coding method using error correcting codes. *IEEE Trans. Info. Theory* 23: 371–377

Kasami T, Takata T, Fujiwara T, Lin S 1991a On linear structure and phase rotation invariant properties of block M-PSK modulation codes. *IEEE Trans. Info. Theory* 37: 164–167

Kasami T, Takata T, Fujiwara T, Lin S 1991b On multilevel block modulation codes. *IEEE Trans. Info. Theory* 37: 965–975

Kofman Y, Zehavi E, Shamai S 1994 Performance analysis of a multilevel coded modulation system. *IEEE Trans. Commun.* 42: 299–312

Kschischang F R, de Buda P G, Pasupathy S 1989 Block codes for M-ary phase shift keying. *IEEE J. Selected Areas in Commun.* 7: 900–913

Loeliger H A 1991 Signal sets matched to groups. *IEEE Trans. Info. Theory* 37: 1675–1682

Loeliger H A 1992 *On Euclidean space group codes*. Ph D thesis, Swiss Federal Institute of Technology, Zurich

Pottie G J, Taylor D P 1989 Multilevel codes based on partitioning. *IEEE Trans. Info. Theory* 35: 87–98

Saha D, Birdsall T 1989 Quadrature-quadrature phase-shift keying. *IEEE Trans. Commun.* 37: 437–448

Sayegh S I 1986 A class of optimum block codes in signal space. *IEEE Trans. Commun.* 34: 1043–1045

Takata T, Ujita S, Kasami T, Lin S 1993 Multistage decoding of multilevel block M-PSK modulation codes and its performance analysis. *IEEE Trans. Info. Theory* 39: 1204–1218

Visintin M, Biglieri E, Castellani V 1992 Four-dimensional signalling for bandlimited channels. *IEEE Trans. Commun.* 40: 21–34

Welti G R, Lee J S 1974 Digital transmission with coherent four-dimensional codes. *Trans. Info. Theory* 20: 497-502

Zetterberg L H, Brandstrom H 1977 Codes for combined phase and amplitude in a four-dimensional space. *IEEE Trans. Commun.* 25: 943-950

# Power spectrum estimation of complex signals and its application to Wigner–Ville distribution: A group delay approach

S V NARASIMHAN \*, E I PLOTKIN and M N S SWAMY

Centre for Communication and Signal Processing, Department of Electrical and Computer Engineering, Concordia University, 1455, De Maisonneuve Blvd. West, Montreal, H3G 1M8, Canada

\*Present address: Aerospace Electronics Division, National Aerospace Labs, Bangalore, 560 017, India

e-mail: svnarsim@nalsic.ernet.in

**Abstract.** In this paper, a method of estimating the power spectrum of a complex signal based on the Group Delay function (GD) is proposed and also applied to the Wigner–Ville Distribution (WVD) to reduce the ripple effect due to the truncation of the autocorrelation sequence. The proposed method is realised by the GD for a complex signal and the modified GD concept. This extends the performance advantages of the modified GD applicable to a real signal, to a complex one. Further, its application to WVD, reduces the truncation/ripple effect without sacrificing any frequency resolution, as no *common window function* is used. Significant improvement in performance, in terms of reduction in variance without any compromise on resolution and higher noise immunity, has been found over those of the periodogram and windowed WVD.

**Keywords.** Complex signals; power spectrum estimation; group delay approach; Wigner–Ville distribution; Gibb's ripple effect.

## 1. Introduction

Generally, spectral estimation aims at extracting information about the system, from its observed output (in the absence of the input), and a signal, when it is associated with noise. A good spectral estimator, for a given length of data, provides an estimate which has as high a resolution and as low a bias and variance as possible. These factors depend on the signal scenario (data length, window and the associated noise). The variance of the basic periodogram is large, though it has good resolution, low bias and good signa-

lobe of the spectrum of the window and this results in a poor resolution. At the cost of resolution, the averaged PSE provides a lower variance, due to the number of segments averaged and the window used, for a given length. In parametric methods (Kay 1988), even for a relatively short data set, a high resolution and low variance. But this is valid only when the signal satisfies the assumed model and the signal to noise ratio is high.

Though the power spectral density (PSD) based on the Fourier transform provides spectral information, it does not explicitly provide a time reckoning. To alleviate this, the spectral content is the same for ever. To analyse nonstationary signals, the time FT, which gives spectral information about the data within a window, was introduced and this involves a tradeoff between the time localization and frequency resolution. To alleviate this, the Wigner–Ville distribution (WVD), a time–frequency representation (TFR) was introduced (Cohen 1989). The WVD, at any rate, is the FT of the instantaneous autocorrelation (IACR) sequence of infinite lags. Theoretically, it has infinite resolution both in time and frequency. However, it is the Pseudo WVD (PWVD) that is computed which considers IACR over a finite number of lags. In PWVD, in order to overcome the abrupt truncation of the IACR, ripples (Gibb's effect) in the TFR along the frequency axis, the IACR is multiplied by a *common window function* and for a given lag length, this deteriorates the resolution.

The group delay function (GD), the negative derivative of phase, provides improved resolution over that of the PSE and facilitates the estimation of parameters (Yegnanarayana *et al* 1984). However, spectral estimation based on the GD, also suffers from *smearing* and the reduction in variance is only at the cost of resolution. Recently, a modification for the GD, which not only preserves the good resolution of the PSE, in particular, the good frequency resolution, but also reduces the variance of the estimate, has been proposed (Murthy & Yegnanarayana 1991; Yegnanarayana 1992). This basically removes the zeros close to the unit circle, without affecting the poles and zeros of the system or the signal (assuming the zeros if any are outside the unit circle). White noise or spectral ripples introduce zeros close to the unit circle. In the case of a system, the output of a system driven by a white noise or a signal with its associated poles and zeros, the signal spectrum associated with ripples due to signal truncation, the variance of the estimated zeros close to the unit circle, irrespective of their origin. Consequently, the reduction in variance effect of only these zeros results in reduced variance without compromising the frequency resolution.

In this paper, modification for the GD has been applied to a complex signal, achieved by considering the GD for a complex signal (Reddy & Rao 1992). In the case of the WVD, the IACR being an analytic complex signal, the modified group delay function (GD) approach has been *tailored* to remove the ripples in the WVD by applying any *common window*, to achieve preservation of the frequency resolution and better noise immunity.

## 2.1 Group delay function for a complex signal

If  $x(n)$  is a minimum phase signal, then (Reddy & Rao 1987)

$$\ln |X(\omega)| = \sum_{n=0}^{\infty} [c_R(n) \cos \omega n + c_I(n) \sin \omega n], \quad (1)$$

$$\theta(\omega) = \sum_{n=0}^{\infty} [-c_R(n) \sin \omega n + c_I(n) \cos \omega n], \quad (2)$$

where  $\theta(\omega) = \theta_v(\omega) + 2\pi I(\omega)$ ,  $\theta_v(\omega)$  is the principal value of the phase,  $\theta(\omega)$  is the unwrapped phase and  $c(n) = c_R(n) + jc_I(n)$  are the complex cepstral coefficients.  $R$  and  $I$  refer to the real and imaginary parts. For a minimum phase signal, the logmagnitude spectrum and the phase are related by a single set of complex cepstral coefficients. The GD  $\tau_m(\omega)$  is given by

$$\begin{aligned} \tau_m(\omega) &= -\partial\theta(\omega)/\partial\omega \\ &= \sum_{n=0}^{\infty} [nc_R(n) \cos \omega n + nc_I(n) \sin \omega n]. \end{aligned} \quad (3)$$

$c_R(n)$  and  $c_I(n)$  are derived from the magnitude and hence  $\tau_m(\omega)$  is called the magnitude GD for a complex signal (MGDC). Also, (3) is

$$\tau_m(\omega) = (1/2)FT[(nc(n) - nc^*(-n))], \quad (4)$$

where  $*$  indicates conjugate operation. If  $nc(n)$  is conjugate symmetric, then

$$\tau_m(\omega) = FT[nc(n)]. \quad (5)$$

For a mixed phase signal, the logmagnitude and phase are not related by a single set of cepstral coefficients and two different cepstral sequences  $c_1(n) = c_{1R}(n) + jc_{1I}(n)$  and  $c_2(n) = c_{2R}(n) + jc_{2I}(n)$ , for magnitude and phase respectively, are defined.  $c_1(n)$  and  $c_2(n)$  are the complex cepstral coefficients of minimum phase signals derived from magnitude and phase respectively. For this case, the magnitude group delay (MGDC) is the same as given by (3) (using  $c_1(n)$  instead of  $c(n)$ ); however, the Phase group delay (PGDC) is different and is given by

$$\tau_p(\omega) = \sum_{n=0}^{\infty} [nc_{2R}(n) \cos \omega n + nc_{2I}(n) \sin \omega n]. \quad (6)$$

To compute,  $\tau_p(\omega)$ , from (6),  $c_2(n)$  has to be derived from the phase function  $\theta(\omega)$  which is an unwrapped one. But  $\tau_p(\omega)$  can be directly computed from the FTs  $X(\omega)$  and  $Y(\omega)$  of the signals  $x(n)$  and  $y(n) = nx(n)$ , respectively, by

$$\tau_p(\omega) = -[X_R(\omega)Y_R(\omega) + X_I(\omega)Y_I(\omega)]/|X(\omega)|^2 \quad (7)$$

a minimum phase signal, as the MGDC is the ratio of the signal spectrum to the PGDC can be used for computing the MGDC.

## 2.2 The modified group delay for a complex signal

The variance of a spectral estimate is due to the undesired fine structure which capture the spectral envelope and discard the fine structure without affecting the zeros close to the unit circle manifest as spikes in the GD. Further, the spikes depend upon whether the zero is inside or outside the unit circle. Spikes which contribute significantly to the fine structure of the spectrum cannot be removed by normal smoothing without the loss of resolution. A method suggested by Murthy & Yegnanarayana (Murthy & Yegnanarayana 1988 & Murthy 1992) removes these spikes effectively. Presently, it is proposed a modification to the MGD for complex signals (MGDC).

Assuming that the signal under consideration  $x(n)$  is generated by a linear system, driven by a complex white noise or has complex sinusoids with complex noise and, further, that its spectrum  $X(\omega)$  can be put in a rational form where the denominator corresponds to the system or sinusoids and the numerator corresponds to the excitation or the associated noise, respectively. For this case, the MGD

$$\tau_m(\omega) = \tau_{mN}(\omega) - \tau_{mD}(\omega),$$

where  $\tau_{mN}(\omega)$ , and  $\tau_{mD}(\omega)$ , are the MGDCs for  $N(\omega)$  and  $D(\omega)$ . The MGDC  $\tau_m(\omega)$  is given by (7), where  $x(n) = x_m(n)$  and  $y(n) = y_m(n) = nx_m(n)$  is the minimum phase equivalent of  $x(n)$ . It can be shown that

$$\tau_m(\omega) = \frac{\alpha_N(\omega)}{|N(\omega)|^2} - \frac{\alpha_D(\omega)}{|D(\omega)|^2}.$$

$\alpha_N(\omega)$  and  $\alpha_D(\omega)$  are the numerators of (7) for  $\tau_{mN}(\omega)$  and  $\tau_{mD}(\omega)$  respectively. The MGDC  $\tau_{mN}(\omega)$  will have large amplitude spikes due to the very small values of  $|N(\omega)|^2$  which are close to the unit circle, while this is not so with  $\tau_{mD}(\omega)$ , as the zeros of  $D(\omega)$  are well within the unit circle. Hence, in  $\tau_m(\omega)$ , the effect of excitation or the noise (both have zeros near the unit circle) masks the system or the signal component assumed to be an all-pole one. The effect of these zeros could be reduced in the MGDC  $\tau_m(\omega)$ , (9), by  $|N(\omega)|^2$ . Further, as the envelope of  $|N(\omega)|^2$  is nearly constant, the features of  $\tau_{mD}(\omega)$  continue to exist, with  $|N(\omega)|^2$  fluctuations superimposed on the modified MGDC (MGDCM)  $\tau_{mo}(\omega)$ , is

$$\tau_{mo}(\omega) = \tau_m(\omega)|N(\omega)|^2.$$

For the computation of MGDCM, an estimate of  $|N|(\omega)|^2$ ,  $|\hat{N}(\omega)|^2$  is required to the MGDC. This is achieved by computing the ratio of the signal spectrum,  $|X(\omega)|^2$ , to the smoothed power spectrum of the signal,  $|\bar{X}(\omega)|^2$ , obtained from the cepstral coefficient sequence. The values of  $|N(\omega)|^2$  around the zeros have been set to zero so that it cancels small values in the denominator of the first term of the MGDC estimate. The estimate  $|\hat{N}(\omega)|^2$  should retain all the sharp fluctuations of the logmagnitude spectrum and should have a flat spectral envelope.

of GD from the magnitude spectrum is different from that for a real signal. Further, for a minimum phase signal, as the MGDC and PGDC are same, the above expression for PGDC can be used for computing the MGDC.

## 2.2 The modified group delay for a complex signal

The variance of a spectral estimate is due to the undesired fine structure. It is of interest to capture the spectral envelope and discard the fine structure without affecting the former. The zeros close to the unit circle manifest as spikes in the GD. Further, the polarity of the spikes depend upon whether the zero is inside or outside the unit circle. It is these spikes which contribute significantly to the fine structure of the spectrum and their effect cannot be removed by normal smoothing without the loss of resolution. The modification suggested by Murthy & Yegnanarayana (Murthy & Yegnanarayana 1991; Yegnanarayana & Murthy 1992) removes these spikes effectively. Presently, it is proposed to apply this modification to the MGD for complex signals (MGDC).

Assuming that the signal under consideration  $x(n)$  is generated by a complex all-pole system, driven by a complex white noise or has complex sinusoids with complex white noise and, further, that its spectrum  $X(\omega)$  can be put in a rational form  $N(\omega)/D(\omega)$ , the denominator corresponds to the system or sinusoids and the numerator corresponds to the excitation or the associated noise, respectively. For this case, the MGDC is given by

$$\tau_m(\omega) = \tau_{mN}(\omega) - \tau_{mD}(\omega), \quad (8)$$

where  $\tau_{mN}(\omega)$ , and  $\tau_{mD}(\omega)$ , are the MGDCs for  $N(\omega)$  and  $D(\omega)$  respectively. Also  $\tau_m(\omega)$  is given by (7), where  $x(n) = x_m(n)$  and  $y(n) = y_m(n) = nx_m(n)$ ,  $x_m(n)$  being the minimum phase equivalent of  $x(n)$ . It can be shown that

$$\tau_m(\omega) = \frac{\alpha_N(\omega)}{|N(\omega)|^2} - \frac{\alpha_D(\omega)}{|D(\omega)|^2}. \quad (9)$$

$\alpha_N(\omega)$  and  $\alpha_D(\omega)$  are the numerators of (7) for  $\tau_{mN}(\omega)$  and  $\tau_{mD}(\omega)$  respectively.  $\tau_{mN}(\omega)$  will have large amplitude spikes due to the very small values of  $|N(\omega)|^2$ , near the zeros which are close to the unit circle, while this is not so with  $\tau_{mD}(\omega)$ , as the roots of  $D(\omega)$  are well within the unit circle. Hence, in  $\tau_m(\omega)$ , the effect of excitation or the associated noise (both have zeros near the unit circle) masks the system or the signal component which is assumed to be an all-pole one. The effect of these zeros could be reduced by multiplying  $\tau_m(\omega)$ , (9), by  $|N(\omega)|^2$ . Further, as the envelope of  $|N(\omega)|^2$  is nearly flat, the significant features of  $\tau_{mD}(\omega)$  continue to exist, with  $|N(\omega)|^2$  fluctuations superimposed on it. Hence the modified MGDC (MGDCM)  $\tau_{mo}(\omega)$ , is

$$\tau_{mo}(\omega) = \tau_m(\omega)|N(\omega)|^2. \quad (10)$$

For the computation of MGDCM, an estimate of  $N(\omega)|^2$ ,  $|\hat{N}(\omega)|^2$  is required in addition to the MGDC. This is achieved by computing the ratio of the signal power spectrum,  $|X(\omega)|^2$ , to the smoothed power spectrum of the signal,  $|\tilde{X}(\omega)|^2$ , obtained by the truncated cepstral coefficient sequence. The values of  $|N(\omega)|^2$  around the zeros have to be preserved so that it conceals small changes in the envelope of the spectrum.

## complex signal

For a signal  $x(t)$ , WVD is defined as

$$W_x(t, \omega) = \int_{-\infty}^{\infty} x(t + \tau/2)x^*(t - \tau/2)e^{-j\omega\tau} d\tau, \quad (11)$$

where  $r(\tau) = [x(t + \tau/2)x^*(t - \tau/2)]$  is the instantaneous autocorrelation function and  $*$  indicates conjugate operation. For computational purposes, it is necessary to weigh the signal by a window before evaluating the WVD and this window slides along the time axis.

For a window function,  $h(t)$ ,  $h(t) = 0$  for  $|t| > T/2$ , the WVD of the windowed signal is

$$W_{xh}(t, \omega) = \int_{-\infty}^{\infty} W_x(t, \xi) W_h(t - \xi) d\xi, \quad (12)$$

where  $W_h(t, \omega)$  is the WVD of the window function. This WVD of the windowed signal is called *Pseudo Wigner–Ville Distribution (PWVD)*,  $PW_x(t, \omega)$ . The effect of the window is to *smear* the WVD along the frequency axis. For a real symmetrical window, the PWVD is the FT of the windowed function  $[x(t + \tau/2)x^*(t - \tau/2)]$ , the window being  $h^2(\tau/2)$ .

The window eats away the correlation function at higher lags which results in poor spectral resolution.

The quadratic operation on the signal, causes the WVD to be bilinear and this introduces crossterms for multicomponent signals (Flandrin 1984; Velez & Absher 1990). The crossterm appears midway between every two components of the signal. Its amplitude is proportional to the product of the two components' amplitudes and it oscillates in time at a frequency equal to the frequency separation between them. The crossterm effect, which makes the interpretation of the WVD difficult, can be reduced by smoothing the WVD along the time axis. The smoothing process, in time for crossterms and in frequency for the lag window, can be considered a two-dimensional convolution of the WVD of the signal with that of the smoothing kernel,  $\Phi(t, \omega)$  (Flandrin 1984). Using different smoothing kernels, a class of distributions known as *Cohen's class* (Cohen 1989) can be realized. The kernel determines the properties of the distribution (Jeong & Williams 1992). The properties, viz. marginality in frequency, instantaneous frequency and frequency support are not satisfied for common windows due to smearing.

The very definition of the WVD demands the signal to be sampled at twice the Nyquist sampling rate, otherwise it introduces aliasing in the frequency domain as the periodicity is  $\pi$  instead of  $2\pi$ . This is overcome by using an analytic signal (Picone 1988) which necessitates further processing techniques to handle complex signals.

In the computation of PWVD, for a given lag length, the lag windowing used to take care of the truncation effects eats away the higher IACR lags and reduces the frequency resolution relative to that of no windowing. Further, the very definition of the WVD, which results in an aliasing in the frequency domain, demands the conversion of a real signal to a complex analytic signal. With the MGDCM, as the zeros close to the unit circle are removed without applying any window, the loss in the frequency resolution which would

the zeros due to the associated white noise, the proposed WVD indirect noise immunity.

For the MGDC computation, the starting point is the signal under mentioned in § 2.1. However, to apply the MGDC to the present TFR, the along the time axis (SIACR) is the beginning point and the magnitude (1), at a particular time instant is obtained from the FT of the SIACR WVD slice estimate. This estimate, at a frequency, is supposed to be a power represents the power spectral density (PSD). However, due to the inevitable rectangular window, the values may become negative. This is due to the convolved with the FT of the rectangular window. Presently, as the computation MGDC  $\tau_m(\omega)$ , involves logarithmic operation, ((1) and (3)), it is necessary that the FT of the SIACR is positive. This is achieved by raising the floor level scaling up the SIACR at zeroth lag. Further, in computing  $\tau_m(\omega)$  the equal spectrum is computed from the PSD and the linearly weighted cepstral coefficient is made conjugate symmetric.

According to (10), the MGDCM,  $\tau_{mo}(\omega)$ , is computed by using an estimate of the spectrum and this estimate is  $[X(\omega)/\bar{X}(\omega)]^2$ ,  $\bar{X}(\omega)$  being the cepstrally smoothed version of the spectrum by the truncated cepstral sequence of  $x(n)$ . That is,

$$\hat{N}(\omega) = X(\omega)/\bar{X}(\omega) = 1 + [\Delta(\omega)/\bar{X}(\omega)].$$

Here,  $\Delta(\omega)$  represents the fluctuating part of  $X(\omega)$ . By multiplying  $\tau_m(\omega)$  with the spectrum which is free from contribution due to input or the associated noise, an improved resolution is obtained and this is different from  $\bar{X}(\omega)$ . For a specific spectral characteristic, in the GD  $\tau_m(\omega)$ , the contribution is only due to the noise to get a  $\tau_{mo}(\omega)$ , which is free from fluctuations,  $\tau_m(\omega)$  has to be multiplied by

$$\tau_{mo}(\omega) = \tau_m(\omega)|\Delta(\omega)|^2.$$

Presently, it is required to remove the ripple on the floor, which is due to the spectral characteristic and the pedestal height is immaterial as it is not relevant to the WVD. The PSD which is free from the ringing/ripple effect and has better resolution is obtained from  $\tau_{mo}(\omega)$ , using (14) and by retracing the MGDC computation procedure in the order ((3) and (1)). It is important to note that in obtaining the processed cepstral coefficient sequence has to be made conjugate symmetric. If only the positive importance, then only the positive values of the  $\tau_{mo}(\omega)$  above a certain threshold are considered. To achieve the improved WVD, these operations have to be carried out for each sample. It is important to note that since no window is applied, the proposed WVD has frequency domain properties better than the PWVD.

sinusoids in complex white Gaussian noise. The AR process and the complex s are the same as those considered by (Yegnanarayana & Murthy 1992), except former is a complex version.

AR system considered has roots at  $(0.6321 + j0.7593)$  and  $(0.7569 + j0.6204)$ . the same AR process which is associated with complex white Gaussian noise signal-to-noise ratio (SNR) equal to 0 dB is considered. For sinusoids plus white

$$x(n) = \sqrt{10}e^{j2\pi(0.10)n} + \sqrt{20}e^{j2\pi(0.15)n} + u(n), \quad (15)$$

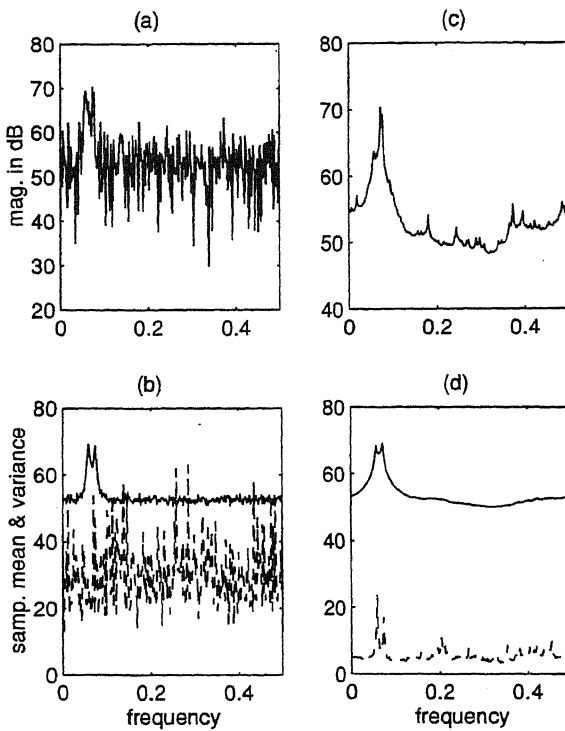
ered the signal.  $u(n)$  is the additive complex white Gaussian noise, and its variance ed to get SNRs equal to 20 dB and 0 dB. For the AR process and for the sinusoids e, the data lengths used are 256 and 100 points respectively. For both the cases, ntting the  $|N(\omega)|^2$  estimate, the smoothed spectrum is obtained by considering the cepstral coefficients.

erformance of the MGDCM for the AR signal and for the sinusoids considered, = 0 dB, are shown in figures 1 and 2 respectively. Further, these results are compared with those of the PSE. In figures 1 and 2, (a) and (c) correspond to individual s; (b) and (d) show the mean and variance of the estimate obtained by 50 realizations. The individual estimate obtained by MGDCM is free from the fine structure due put and the associated noise. The variance plots shown also support this as the ance is very high compared to those of MGDCM. Further, the reduction in variance achieved by the proposed method over the PSE is quantified by computing the Sum Variance Ratio (SSVR) given by  $SSVR = \sum V_\tau(\omega) / \sum V_P(\omega)$ , where  $V_\tau(\omega)$  or the variance computed by the GD approach and  $V_P(\omega)$  for that by PSE. For process and for sinusoids, the SSVR has values of 0.1783 and 0.0438 respectively. The mean plots are similar, except that the mean obtained by the PSE has still e fluctuations, even after averaging 50 estimates. For the clean AR process and sinusoids with noise (SNR = 20 dB), the SSVR values are 0.7471 and 0.0126 respectively. The reduction in variance achieved is more significant for sinusoids than for process.

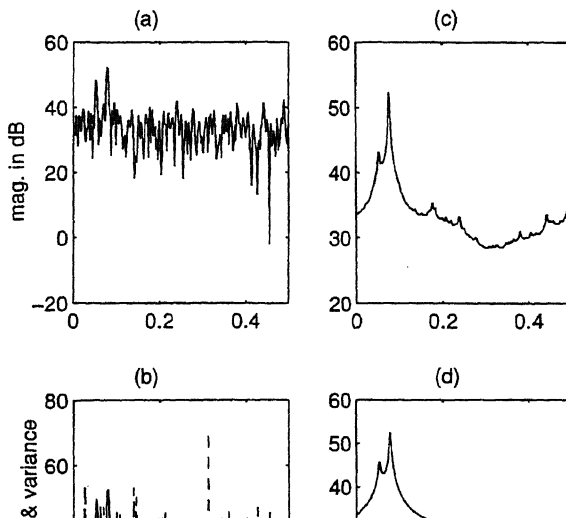
smoothing parameter, the number of cepstral coefficients used, determines the of the proposed estimators and to get a good variance reduction, this number e kept as small as possible. Compared to the PSE, the proposed estimator has a ntly low variance. Further, depending upon the signal and its associated noise, its ranges only from 70% to 2% of that of the PSE and the reduction seems to be ective when the SNR is low.

### *Performance of the improved WVD*

ormance of the proposed method is illustrated for both FSK and chirp signals. red by the WVD, the signals are converted to analytic signals by computing the transform of the original real signal. The Hilbert transform has been realised by



**Figure 1.** Performance for the AR process (SNR = 0 dB). Individual periodogram (a) and MGDCM (c) and variance (---) by MGDCM (d).



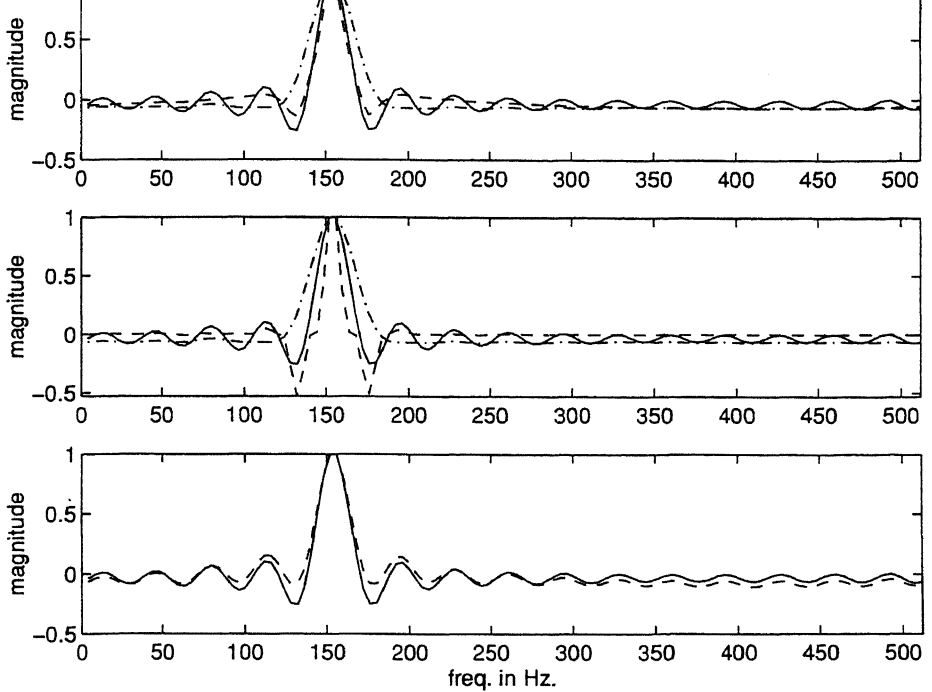
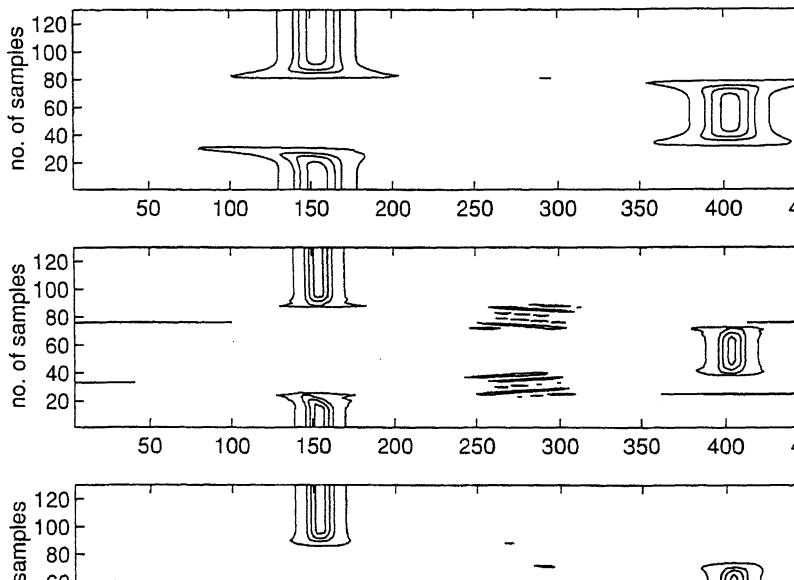
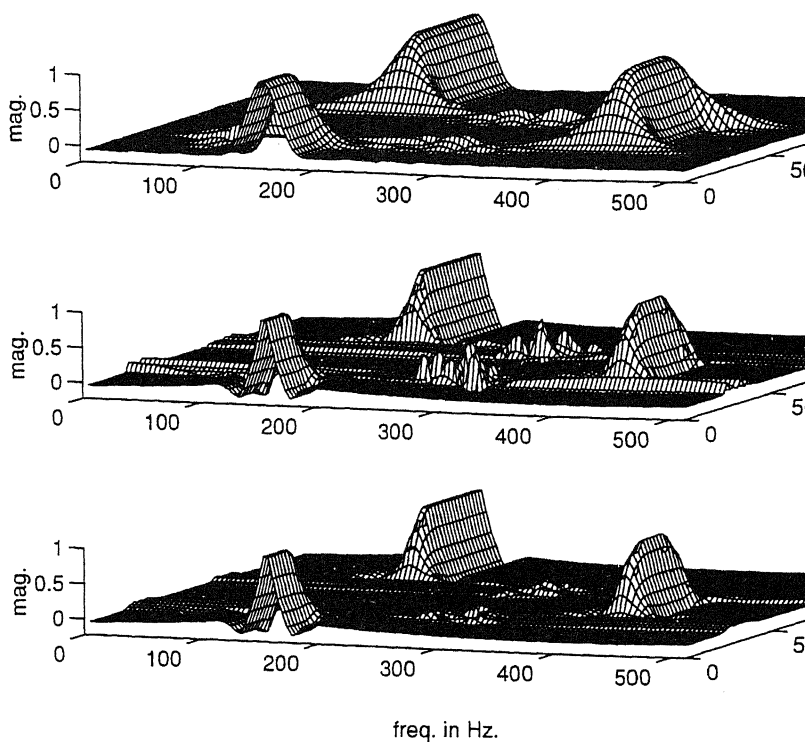


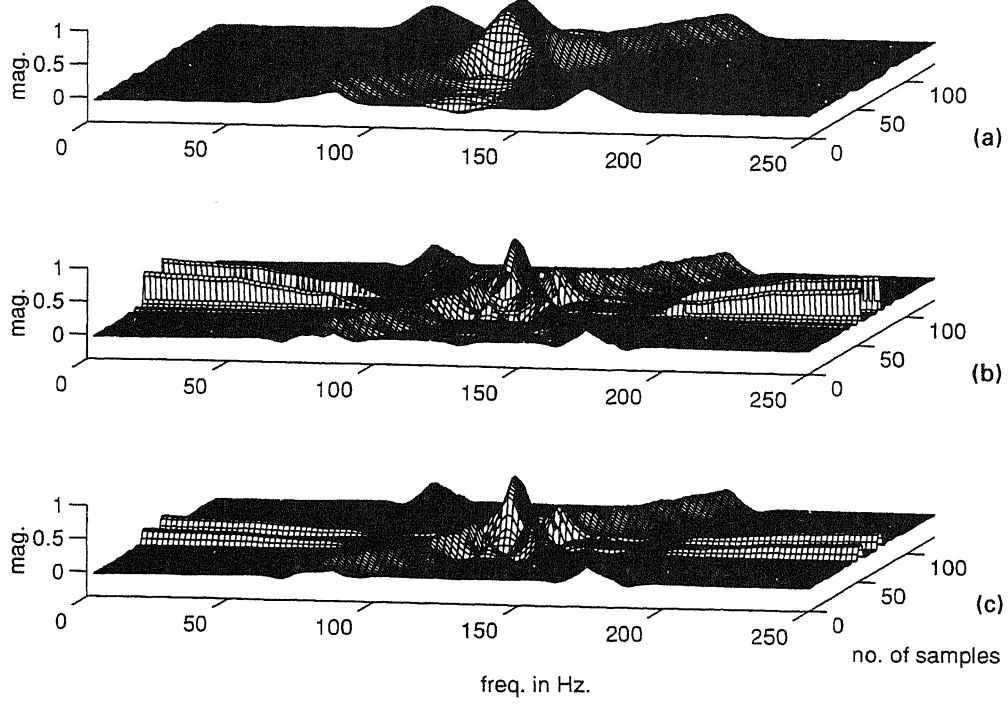
**Figure 3.** Comparison of the resolution and ripple reduction by PWVD and MGDCM. **(a)** WVD slice by: - rectangular window (RW), --- Hamming, - - MGDCM, **(b)** WVD slice by: - RW, --- Hamming, -- MGDCM, **(c)** WVD slice by: - RW and -- MGDCM, using  $|\hat{N}(\omega)|^2$ .

For the FSK signal, the number of lags considered is 31. To reduce the crossterms, 5-point boxcar smoothing is applied along the time axis, for the autocorrelation function at each lag. Further, a discrete FT of length 128 points is used. For the PWVD, the SIACR is weighted by a Hamming window. For the proposed method, to avoid the negative spectral values in the PSD, SIACR at zeroth lag has been lifted by a factor of 100. The  $|\Delta(\omega)|$  estimate is obtained by considering the initial 8 cepstral coefficients in computing the smoothed PSD.

To get a comparative performance view, a section of the TFR obtained by the proposed method and by the PWVD, corresponding to the same instant of time, are shown in figure 3. This brings out the ripple reduction ability and the frequency resolution preserving ability of the proposed method (figure 3a). Further, in the MGDCM domain, a better improvement in frequency resolution is observed (figure 3b) and this is due to the very nature of the GDC. The use of the  $|\hat{N}(\omega)|^2$  estimate is unable to remove the ripple (figure 3c) and this is due to the fact that the fluctuations in it are different from what is required to be canceled in the MGDC (for the ripple on the floor).

The TFR obtained by the proposed method removes ripples/ringing due to abrupt truncation and at the same time preserves the resolution of the rectangular window (figure 4b).





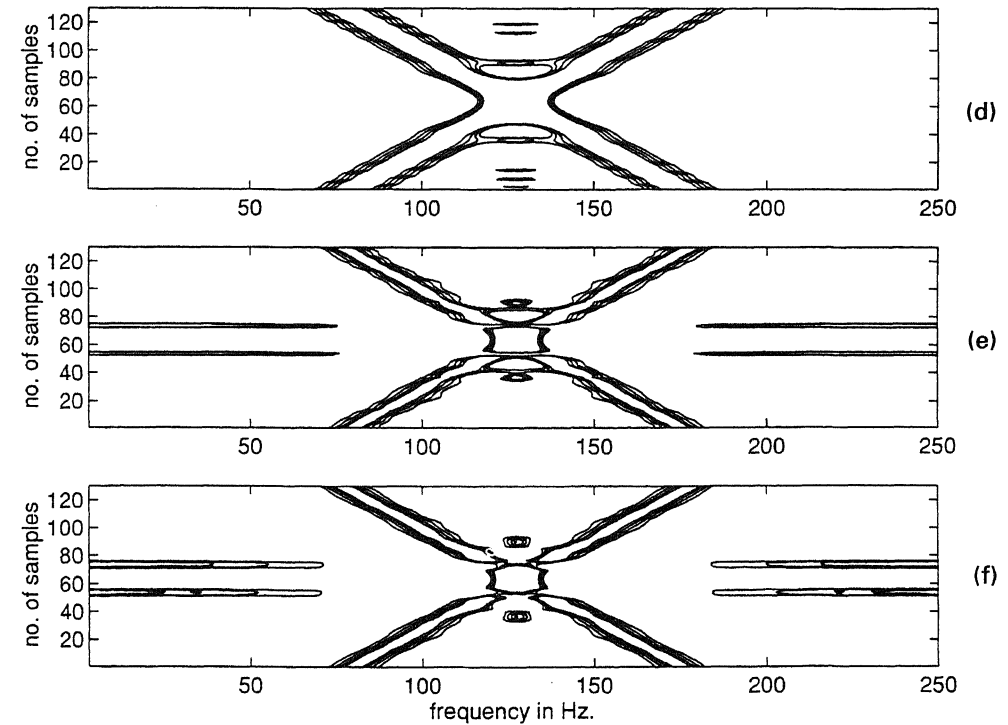
(b)

(c)

(d)

(e)

(f)



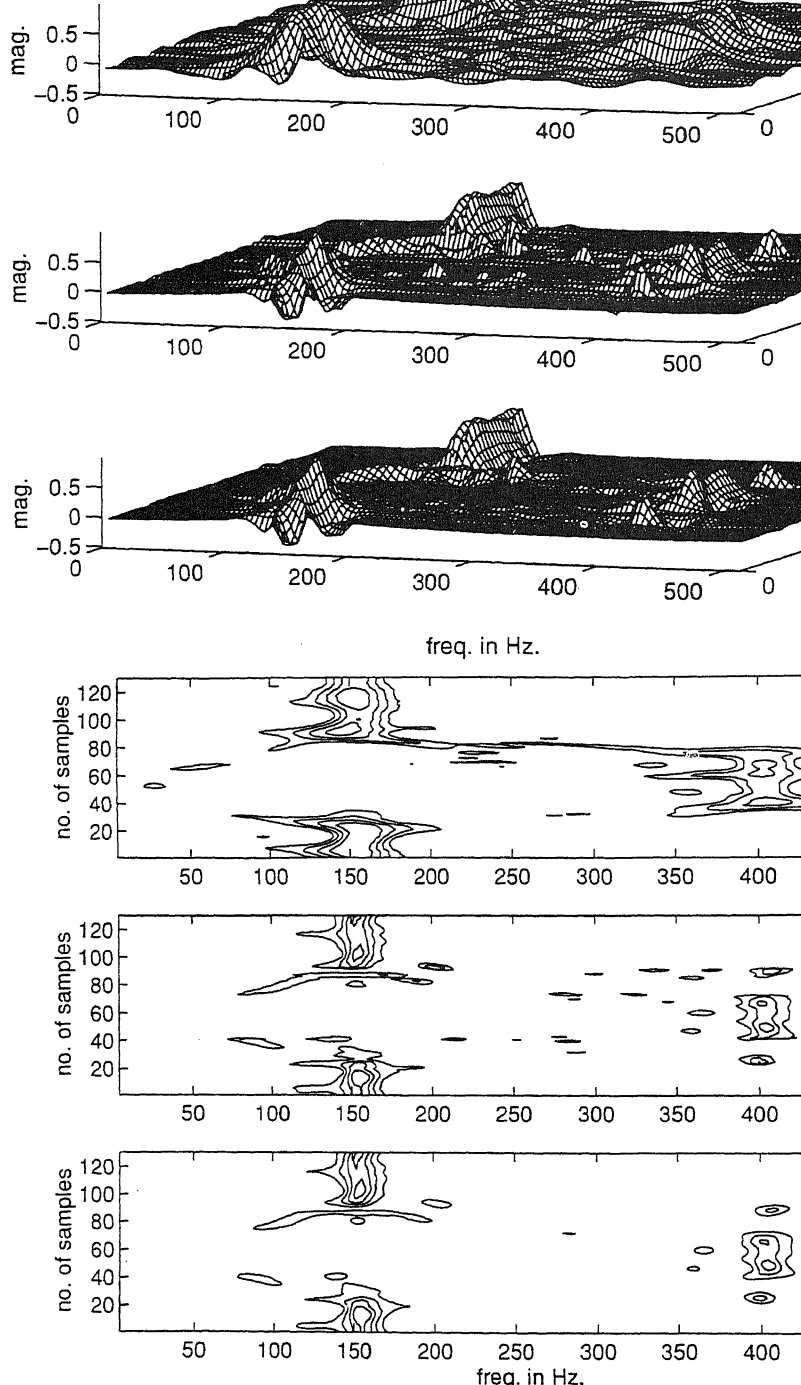
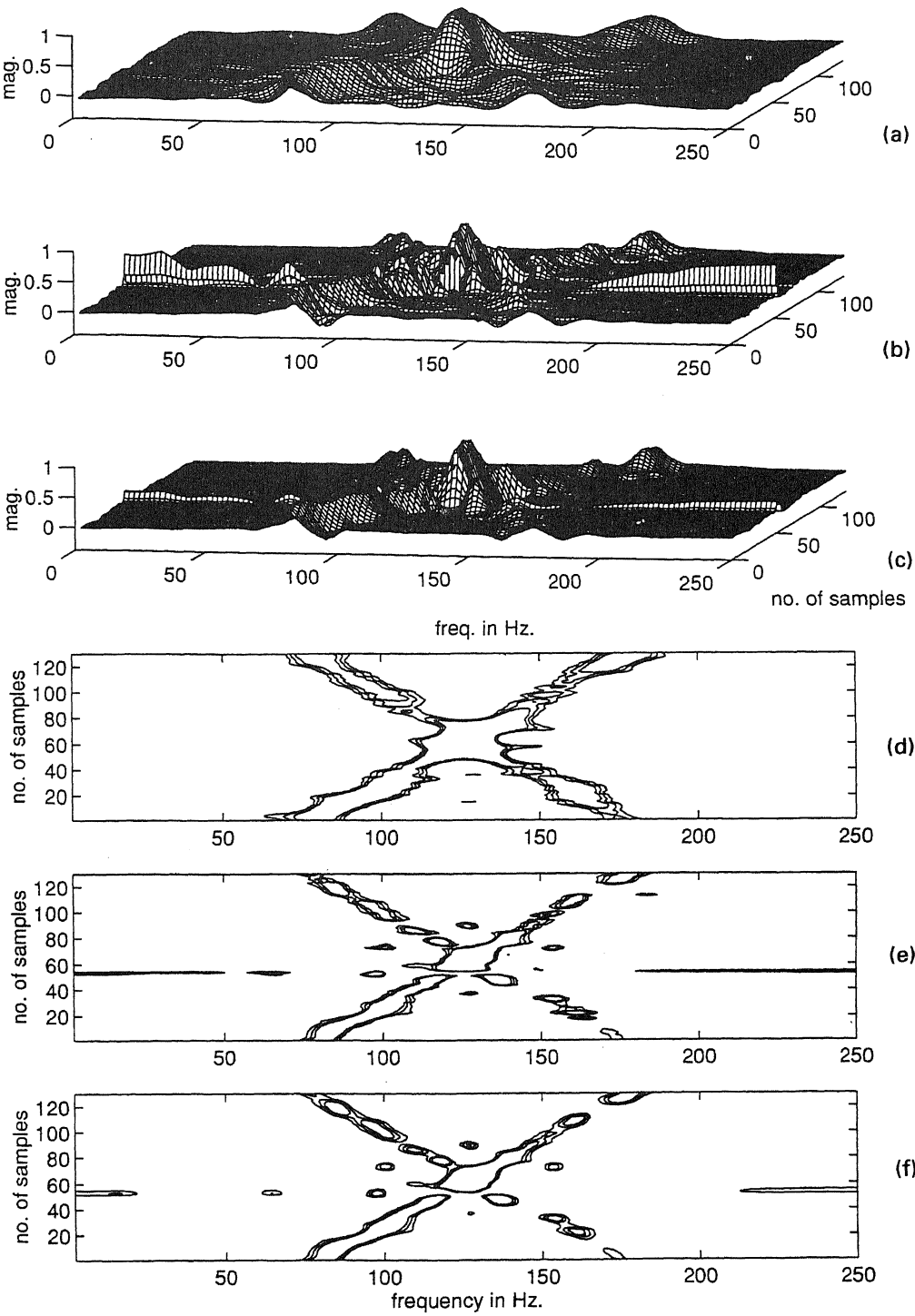


**Figure 6.** TFR representation for FSK signal with white noise by (a) PWV and (c) MGDCM after second smoothing. (d), (e) and (f) Contour plots for



The contour plots corresponding to figure 4a-c are shown in figure 4d-f. They support the fact that the resolution is improved over the PWVD. If peak location is of interest, then the GDMCM, above a certain thresholded in the TF plane rather than the PSD. This provides additional freedom (figure 3b).

For the linear chirp signal, the results obtained are shown in figure 5a. It is smoothed along the time axis by a 9-point boxcar window. For this case, the lag is increased by a factor 100. A floor level above a minimum value improves the performance. However, increasing the floor level by a very large amount does not affect the TFR estimation. For the estimation of  $|\Delta(\omega)|^2$ , the first 8 cepstral coefficients are used in computing the smoothed PSD. Figure 5c shows the TFR obtained by the proposed method with a second time smoothing (box car of 5 points). The ripple effect was less when compared to that of PWVD even prior to the second smoothing (figure 5b). However, the second smoothing helped in reducing the ridge effect which occurs at the region of crossing of the two chirps (figure 5c). The crossterms may be due to their nature and as they are similar to ripples on the frequency axis, they are flattened. In this case also, the frequency resolution is improved and the ripple effect is reduced. The contour plots shown in figure 5d-f are the results.

The performance of the proposed method, for the above signals in the presence of noise at SNR = 5 dB, is shown in figures 6 and 7 respectively. In both cases, the proposed method, the spectral peaks due to noise are reduced relatively to those of the periodogram. This is expected as the MGDCM not only removes the zeros due to the ripple effect but also the zeros due to noise and it does not distinguish between the two.

## 5. Conclusions

A method was proposed for estimating the power spectrum for a complex signal. The proposed method combines the concepts of the GD for a complex signal and the modified GDMCM. In this approach, the WVD is applied to the WVD to remove the ripple effect, due to the truncation of the autocorrelation sequence, by tailoring the modified GDMCM for a complex signal, MGDCM.

The proposed MGDCM method provides a spectral estimate which has a lower variance than that of the periodogram, without compromising on spectral resolution. Depending upon the signal scenario, the proposed estimator has a variance which is about 70% to 2% of that of the periodogram. Further, as the variance of the MGDCM is effective when the SNR is low, its immunity to noise is very significant.

The improved WVD based on the MGDCM was found to be very effective in removing the ripple effect due to truncation and in preserving the resolution of a real signal as no *common window function* is used. Further, since in addition to removing the ripples due to the spectral ripple the zeros due to white noise are also removed, it is

## References

Cohen L 1989 Time-frequency distribution – A review. *Proc. IEEE*. 77: 941–981

Flandrin P 1984 Some features of time-frequency representation of multicomponent signals. In: *Conf. on Acoustics, Speech and Signal Processing*, pp 41B.4.1–41B.4.4

Jeong J, Williams W J 1992 Kernel design with reduced interference distributions. *IEEE Trans. Signal Process.* 38: 402–412

Kay S M 1988 *Modern spectral estimation: Theory and application* (Englewood Cliffs, NJ: Prentice Hall)

Murthy H A, Yegnanarayana B 1991 Speech processing using group delay function. *Signal Process.* 22: 259–267

Picone J 1988 Spectrum estimation using an analytic signal representation. *Signal Process.* 15: 169–182

Reddy G R, Rao V V 1987 Group delay functions for complex signals. *Signal Process.* 12: 5–14

Velez E F, Absher R G 1990 Spectral estimation based on the Wigner–Ville representation. *Signal Process.* 20: 325–346

Yegnanarayana B, Murthy H A 1992 Significance of group delay functions in spectrum estimation. *IEEE Trans. Signal Process.* 40: 2281–2289

Yegnanarayana B, Saikia D K, Krishnan T R 1984 Significance of group delay functions in signal reconstruction from spectral magnitude or phase. *IEEE Trans. Acoustics, Speech Signal Process.* ASSP-32: 610–623



# Asymptotic equivalence of some adaptive biquad notch filters

V V KRISHNA<sup>1</sup> and C G HIREMATH

Signion Systems Pvt. Ltd., 6-3-569/1/2, Rockdale Compound, Somajiguda  
Hyderabad 500 082, India

<sup>1</sup> Present address: ZSP Corporations, 2855, Kifer Road, Suite 200, Santa Clara  
CA, 95051, USA  
e-mail: vvkris@zsp.com; signion@hotmail.com

**Abstract.** A diverse choice of biquad designs is available for adaptive notch filtering or line enhancement (ANF/ALE) applications. We consider one such biquad proposed over a decade ago by David and coworkers and show its equivalence to two other formulations in terms of their pole-zero pair locations in the  $z$ -plane. By equivalence, we imply that all these adaptive IIR filters possess comparable asymptotic performance. Further, a simple modification involving only a normalizing factor, is seen to enhance the performance of this filter. This modified ANF/ALE design is then shown to be equivalent to two other recently proposed adaptive biquads.

**Keywords.** Adaptive IIR filters; adaptive line enhancement; adaptive signal detection; adaptive signal processing; IIR digital filters; poles and zeros.

## 1. Introduction

Adaptive IIR notch filters (ANFs) provide superior performance at a lower computational cost relative to their FIR counterparts in suppressing tonal interference in wideband signals. This advantage holds equally well for adaptive line enhancers (ALEs) as well, where a sinusoid immersed in white noise needs to be extracted. As demonstrated in figure 1, the twin tasks of notch filtering and line enhancement may be viewed as complementary operations using a common framework. Further details of the topic can be had from overviews by Regalia (1995) and others Krishna & Hiremath (1995).

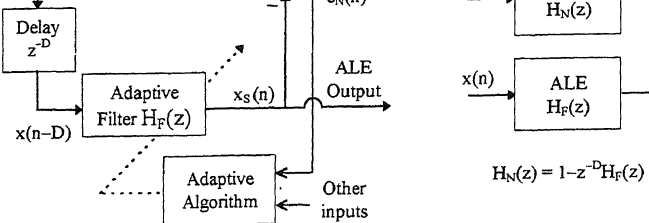


**Figure 1.** Adaptive notch filter (ANF) block diagram. The structure can be used as an ANF or as an adaptive line enhancer (ALE), depending on the actual output. For sinusoids in white noise, a delay  $D = 1$  is sufficient.

different IIR adaptive filters have identical pole-zero pair locations in the z-plane to yield comparable asymptotic (infinite data) performance. However, tracking and tracking properties can differ depending on the specific parameter bisection, adaptation as well as on the adaptation algorithm employed.

As a reference design, we consider the biquad proposed by David and co-workers (*et al* 1983; Hush *et al* 1986), hereafter referred to as the DEESHA filter (under the leadership of one of the members in the team). This design is discussed briefly in the following section, and then show its equivalence with other filters developed by Cho *et al* (1989) and Cho & Martin (1991). In the fourth section, we consider a modified DEESHA filter to improve performance and examine its relation to two other biquads proposed by Cho & Martin (1989) and Regalia (1990).

## 2. “DEESHA” ANF/ALE

The DEESHA notch filter is given by

$$H_{N,1}(z) = \left[ 1 - \left( \frac{2}{1+r^2} \right) \rho z^{-1} + z^{-2} \right] / [1 - \rho z^{-1} + r^2 z^{-2}]$$

where  $0 \ll r < 1$ , and  $-2r < \rho < 2r$ . The factor  $\rho = (1+r^2) \cos(\omega_N)$  allows the filter to acquire the notch frequency  $\omega_N$  while “ $r$ ” controls the notch bandwidth. The placement of poles inside the unit circle guarantees the stability of the filter. The bounds on  $\rho$  given above may be violated to handle very low (near d.c.) or very high frequency (near Nyquist sampling rate) sinusoids without any penalty (Krishna & Hiremath 1995). The design of DEESHA filter suggested by Farhang-Boroujeny (1994) is

$$H_{N,1}(z) = \frac{1 - 2\rho_0 z^{-1} + z^{-2}}{1 - (1+r_0)\rho_0 z^{-1} + r_0 z^{-2}},$$

where  $\rho_0 = \rho/(1+r^2) = \cos(\omega_N)$  and  $r_0 = r^2$ . For a fixed  $r_0$ , DEESHA is a narrowband notch filter. That is, its bandwidth is independent of the notch frequency. As a result,  $\omega_N$  converges to the unknown frequency of the sinusoid with time scaling (Krishna & Hiremath 1995). The

# Asymptotic equivalence of some adaptive biquad notch filters

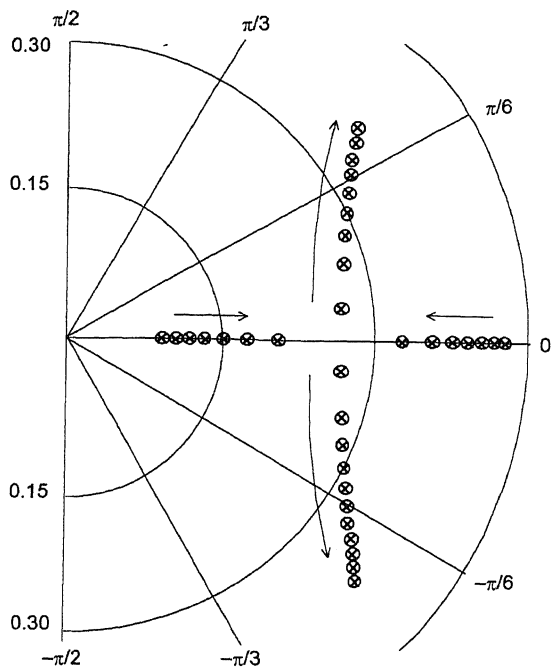
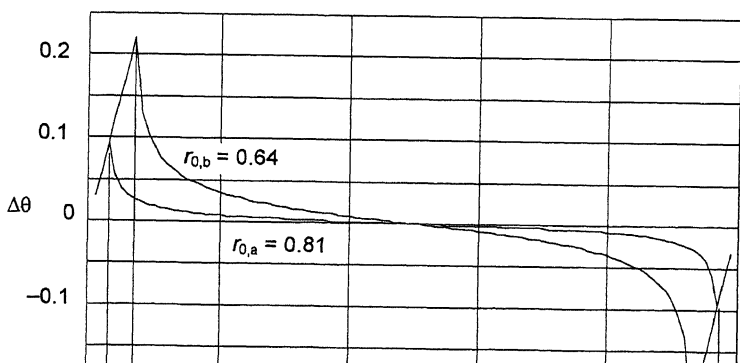


**Figure 2.** The dependence of pole location on  $r_0$  for DEESHA ANF. The notch frequency is at  $\omega_N = \pi/4$  and the arrows indicate increasing  $r_0$ .



as a larger value of  $r_0$  is selected within its upper limit, but at the same time filter convergence and tracking rates will also decrease.

The notch filter requires its zeros to be located on the unit circle at an angle to the frequency of input sinusoid. The position of its poles is however determined by the notch frequency as well as by the choice of  $r_0$ . Figure 2 shows some poles when  $r_0$  is varied for notching at frequency 0.25 (normalized). In figure 3, the angle between a zero and its neighbouring pole is illustrated. Except for the case with a normalized frequency 0.5, the poles lie at an angle closer to the real axis than the zeros. At very low or very high frequencies (depending on  $r_0$ ), the poles may lie on the real axis itself. This characteristic ensures that the biquad provides a constant notch irrespective of the input sinusoid frequency and thereby, a bias-free estimate in the presence of background white "noise".

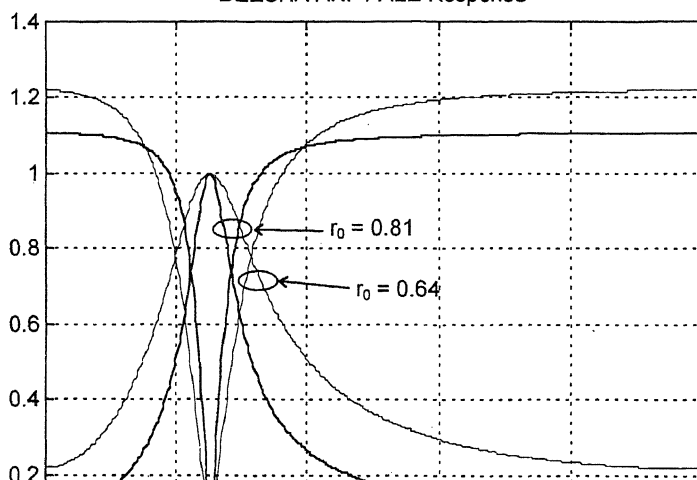
The band pass filter (BPF)  $H_{F,1}(z)$  of the ALE corresponding to DEESHA ANF  $H_{N,1}(z)$  is given by

$$H_{N,1}(z) = \frac{(1 - r_0)(\rho_0 - z^{-1})}{1 - (1 + r_0)\rho_0 z^{-1} + r_0 z^{-2}}.$$

Note that the ANF and ALE are related by  $H_{N,1}(z) = 1 - z^{-1} H_{F,1}(z)$ . The ALE has poles at the same location inside the unit circle as ANF, but has only a single zero lying outside the unit circle. The zero can lie on the unit circle itself, if  $\omega_N = 0$ . The SNR enhancement factor for DEESHA ALE is given by  $(1 + r_0)/(1 - r_0)$ .

Figure 4 illustrates the magnitude response of the notch filter and line enhancement filter based on DEESHA biquad for some values of  $r_0$ .

DEESHA ANF / ALE Response



### 3. DEESHA filter's relatives

We shall now examine the relation between DEESHA and Cho-Choi-Lee notch filters (Cho *et al* 1990). This latter design was derived from Rao-Kung filter (Rao & Kung 1984) using simple approximations and its performance was demonstrated (Cho & Lee 1993) to be superior to the original Rao-Kung design in terms of reduced frequency bias. The Rao-Kung ANF is given by

$$H_{N,2}(z) = \frac{1 + a_1 z^{-1} + a_2 z^{-2}}{1 + \alpha a_1 z^{-1} + \alpha^2 a_2 z^{-2}}, \quad (4)$$

where  $-2 < a_1 < +2$  and  $0 < a_2 < 1$  control the notch frequency  $\omega_N = \cos^{-1}(-a_1/(2\sqrt{a_2}))$ , while  $\alpha$  called pole contraction factor, places poles inside the unit circle *on a radial line below the zeros for all notch frequencies*. Note that the zeros will lie on unit circle only for  $a_2 = 1$ , when this ANF becomes identical to yet another notch filter proposed by Nehorai (1985). Unlike the DEESHA filter, both these ANFs are not constant bandwidth filters (i.e. bandwidth now depends on notch frequency) and thus suffer convergence bias induced by white noise component of the input (Krishna & Hiremath 1995; Regalia 1995). Bias can be a debilitating factor in applications such as phase jitter cancellation in carrier recovery phase lock loops (PLLs) used in high speed modems (Cupo & Gittin 1989). Cho *et al* (1990) considered the lattice equivalent of (4) given as

$$H_{N,2}(z) = \frac{1 + k_0(1 + k_1)z^{-1} + k_1 z^{-2}}{1 + q_0(1 + q_1)z^{-1} + q_1 z^{-2}}, \quad (5)$$

where  $q_0(1+q_1) = \alpha k_0(1+k_1)$ ,  $q_1 = \alpha^2 k_1$ ,  $k_0 = a_1/(1+a_2)$  and  $k_1 = a_2$ . Then, assuming a pole contraction factor  $\alpha \approx 1.0$ , they used the approximations  $q_0(1+q_1) \approx k_0(1+\alpha k_1)$  and  $q_1 \approx \alpha k_1$ , and substituted  $q_0 = k_0$  and  $q_1 = \alpha k_1$  in (5) to obtain

$$H_{N,3}(z) = \frac{1 + k_0(1 + k_1)z^{-1} + k_1 z^{-2}}{1 + k_0(1 + \alpha k_1)z^{-1} + \alpha k_1 z^{-2}}. \quad (6)$$

For  $k_1 = 1$ , (which leads to zeros on the unit circle as does the Nehorai filter), this system function finally simplifies to the Cho-Choi-Lee notch filter,

$$H_{N,4}(z) = \frac{1 + 2k_0 z^{-1} + z^{-2}}{1 + k_0(1 + \alpha)z^{-1} + \alpha z^{-2}}, \quad (7)$$

where  $0 < \alpha < 1$ , and  $-1 \leq k_0 \leq 1$ .

Cho & Lee (1993) termed the design in (7) as a "lattice ANF" and compared its performance with the Rao-Kung and Nehorai filters which were designated as "direct form". This loose choice of terminology creates an impression that the Cho-Lee filter performs better (in terms of bias) somehow because it is a "lattice ANF". Comparing (7) with the DEESHA system function given by Fasheng Boroujeny in (2) earlier, it is immediately

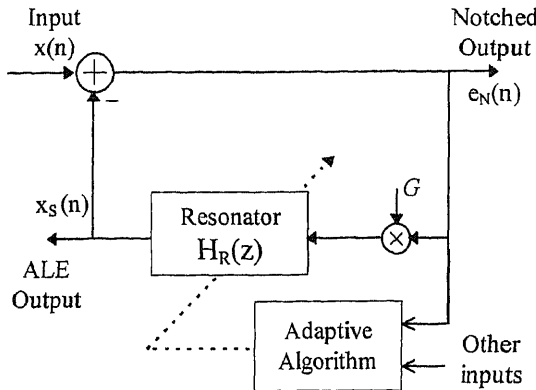


**Figure 5.** ANF/ALE based on Mukund–Martin’s Resonator in a loop (RIL) structure.

inside a stable feedback loop having a loop gain (or, damping factor) ‘ $G$ ’. Mukund & Martin explored its use mainly for line enhancement and for estimating the unknown frequency  $\omega_S$  of a sinusoid but it can be used for notch filtering as well. The resonator, which is a BPF with infinite  $Q$ -factor is given by

$$H_R(z) = \frac{z_R}{z - z_R} + \frac{z_R^*}{z - z_R^*} = \frac{2a_R z^{-1} - 2z^{-2}}{1 - 2a_R z^{-1} + z^{-2}}, \quad (8)$$

where  $z_R = \exp(j\omega_R)$  or  $a_R = \cos(\omega_R)$  determines the resonant frequency  $\omega_R$ . The filter parameter  $a_R$  is adapted (Mukund & Martin 1991) to obtain  $\omega_R = \omega_S$  upon convergence.

To ensure loop stability, we require  $0 < G < 1/2$ . Using straightforward algebra we can derive the system function between the input  $x(n)$  and notched output  $e_N(n)$  as

$$H_{N,5}(z) = \frac{1 - 2a_R z^{-1} + z^{-2}}{1 - 2(1 - G)a_R z^{-1} + (1 - 2G)z^{-2}}. \quad (9)$$

Comparing with (2), this is identical to DEESHA ANF for  $G = (1 - r_0)/2$  and  $a_R = \rho_0$ ! In fact, the performance of Mukund & Martin’s “resonator in a loop” design depends on the selectable value of loop gain, ‘ $G$ ’, to the same extent as DEESHA ANF depends on  $r_0$ . Note, however that the notch filter bandwidth reduces as  $G$  approaches zero.

Similarly, we can also see that the input  $x(n)$  and resonator output  $x_S(n)$  are related by a system function,  $z^{-1}H_{F,5}(z)$  where  $H_{F,5}(z)$  is identical to the BPF of DEESHA ALE given in (3). This equivalence between DEESHA filter and the more recent Mukund–Martin’s (1993) design may appear surprising or even disappointing, if it were to be naively expected that the infinite- $Q$  resonator in the loop would offer arbitrarily high frequency selectivity. Mukund & Martin (1991) further showed that their ALE provides an SNR improvement factor of  $(1 - G)/G$ , which exactly corresponds to  $(1 + r_0)/(1 - r_0)$  given by DEESHA.

#### 4. Enhanced “DEESHA” ANF/ALE

For moderate values of  $r_0$  (usually required during initial convergence or tracking time varying frequencies), the DEESHA filter performance is not satisfactory. The SNR improvement

tor for ALE  $(1 + r_0)/(1 - r_0)$ , remains small. Also, the magnitude response of the ANF may from its notch frequency exceeds unity (figure 4). In fact, the response at d.c. and normalized folding frequency,  $f = 1$ , equals  $2/(1 + r_0)$ . Both these problems can be simply solved using the structure shown in figure 6. Here, the new notch filter output  $e_N(n)$  is only a scaled version of the original output (the notch filter pole-zero locations in the z-plane remain undisturbed). The scale factor 'S' is selected such that the magnitude response at  $f = 0$  or 1, equals unity. That is, we require  $S = (1 + r_0)/2$ . The modified magnitude response is plotted (figure 7) for two different values of  $r_0$  and may be compared with the earlier responses.

The scaled output  $e_{NE}(n)$  of the notch filter is then used to derive an enhanced ALE signal  $x_{SE}(n)$ . The enhanced ALE system function  $H_{FE}(z)$  given by

$$H_{FE}(z) = 1 - H_{NE}(z) = \frac{(1 - r_0)}{2} \frac{1 - z^{-2}}{1 - (1 - r_0)\rho_0 z^{-1} + r_0 z^{-2}} \quad (10)$$

has its poles at the same location as  $H_F(z)$  in (3), but has *two real zeros*, that remain fixed at  $z = +1$  and  $z = -1$  on the unit circle. In particular, these fixed zeros are of great help when  $r_0$  is small (i.e. the filter bandwidth is large). This is brought out in figure 7 where the magnitude response of the enhanced DEESHA filter is plotted. It can be easily shown that the SNR enhancement obtained using (10) equals  $2/(1 - r_0)$ . Depending on the value of  $r_0$  selected, the improvement over DEESHA ALE can range from 1 to 2 dB or more. We shall now consider two more ANF/ALE designs and draw a relationship with the enhanced DEESHA filter. Both these designs also satisfy the relation  $H_F(z) = 1 - H_N(z)$  between their BPF and notch filter as in (10) above. That is, there is no *explicit* delay ahead of the BPF here, unlike the general framework of figure 1 (the "missing" delay, which is essential, is actually incorporated within the notch filter transfer function). Finally, the ALE components of these two designs offer an SNR improvement factor identical to that of the enhanced DEESHA.

The first of the two designs was proposed by Kwan & Martin (1989). To conserve space, we look only at the BPF (in ALE) here, as the corresponding notch filter can be easily

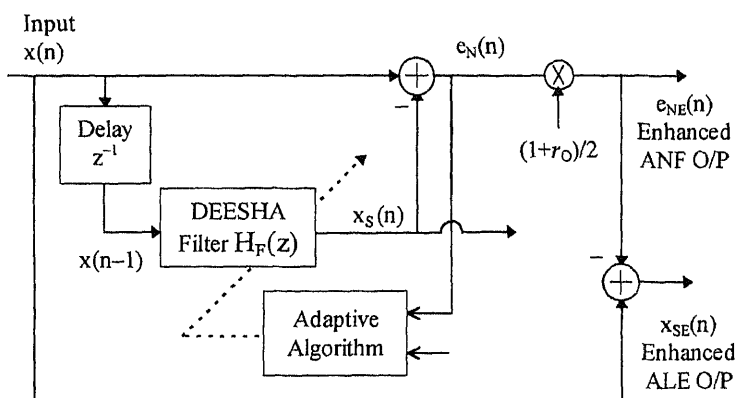
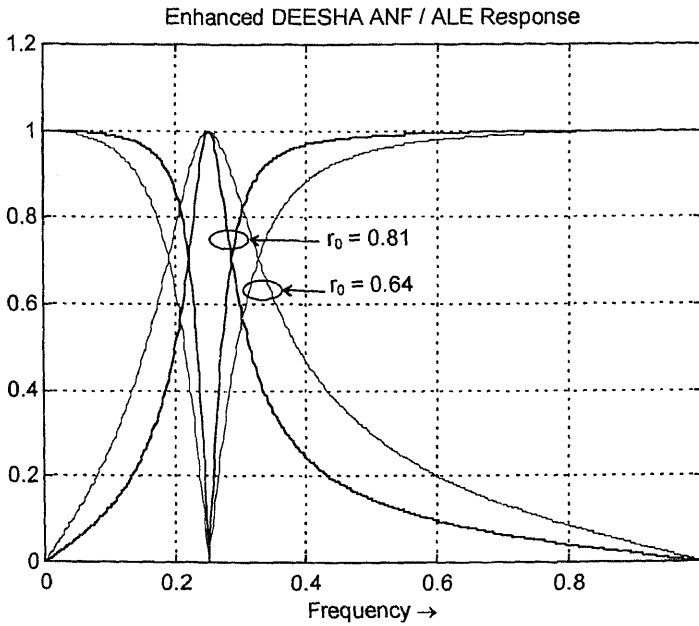


Figure 6. Modification to enhance DEESHA ANF/ALE performance.



**Figure 7.** Magnitude response of enhanced DEESHA ANF/ALE. The notch is at  $f_N = 0.25$ , and  $r_0 = 0.81$  and  $0.64$ . These characteristics may be compared with those in figure 4.

derived:

$$H_{F,6}(z) = \frac{c_2}{2} \frac{(1 - z^{-2})}{[1 - (2 - c_2 - c_1^2)z^{-1} + (1 - c_2)z^{-2}]} \quad (11)$$

Here,  $c_1$  tracks the frequency of input sinusoid and has to be adapted, while  $c_2$  controls the filter bandwidth. A simple eyeballing of (10) and (11) suffices to bring out the relations  $r_0 = 1 - c_2$  and  $r_0 = (2 - c_2 - c_1^2)/(2 - c_2)$ .

The other filter we consider here was proposed by Regalia (1990). Looking once again at only its BPF, we have

$$H_{F,7}(z) = \frac{1 - \sin(\theta_2)}{2} \frac{(1 - z^{-2})}{1 - \sin(\theta_1)[1 + \sin(\theta_2)]z^{-1} + \sin(\theta_2)z^{-2}}, \quad (12)$$

with obvious relations to enhanced DEESHA given by  $\rho_0 = \sin(\theta_1)$  and  $r_0 = \sin(\theta_2)$ .  $\theta_1$  controls the resonant frequency of ALE (same as notch frequency  $\omega_N$  of ANF) and can be adapted using any appropriate algorithm to acquire and track the input sinusoid.  $\theta_2$  determines the filter bandwidth similar to the factor,  $r_0$  in case of enhanced DEESHA filter.

## 5. Conclusions

In this correspondence, we have established some relationships between different ANF/ALE designs. Looking back, while some of these inter-relationships seem obvious (in particular, between DEESHA and the “lattice filter” of Cho, Choi and Lee), surprisingly this

spect has not been highlighted elsewhere. Even in certain instances where two different notch filters have been examined, invariably the comparison is between a so called "lattice filter" and an inherently biased design such as that of Nehorai's (Cho & Lee 1993; Regalia 1995).

Our curiosity to explore these relations was aroused by the pole-zero plots of these various designs. We were assisted in this exploration by Farhang-Boroujeny's (1994) recasting of the DEESHA filter function. As the links between the DEESHA filter and others became clear, this naturally led to the simple modification of figure 6 which improves its performance both in notch filtering and in line enhancement.

What is the implication of these relations that have been shown between various biquads or ANF/ALE applications? Mainly we have the assurance that equivalent designs will offer similar asymptotic performance, in terms of bias-free convergence or for ALE, the NR improvement factor. Also, we hope that the confusion compounded by the wide variety of design choices is reduced by the equivalences discussed here. However, the convergence and tracking behaviour can significantly differ depending on the adaptation technique employed and on the specific parameter being updated. For example, Regalia's design given by Mukund & Martin (1993) where  $\theta_1$  is adapted, is quite suited to handle very low or very high frequencies. As for the enhanced DEESHA biquad, either  $\rho_0$  or  $\omega_N$  can be adapted. Its acquisition and tracking behaviour for very low or high frequencies will be superior for the latter choice (Farhang-Boroujeny 1994; Krishna & Hiremath 1995) and will be on par with that of Regalia's. All these issues require careful consideration while selecting a particular biquad design and adaptation approach for a given application.

## References

Cho N I, Lee S U 1993 On adaptive lattice notch filter for the detection of sinusoids. *IEEE Trans. Circuits Syst.* 40: 405–415

Cho N I, Choi C-H, Lee S U 1990 Adaptive line enhancer using IIR notch filter. *IEEE Trans. Acoust. Speech Signal Process.* 37: 585–589

Cupo R L, Gitlin R D 1989 Adaptive carrier recovery systems for digital data communications receivers. *IEEE J. Selected Areas Commun.* JSAC-7: 1328–1339

David R A, Stearns S D, Elliot G R, Etter D M 1983 IIR algorithm for adaptive line enhancement. *Proc. IEEE Int. Conf. Acoustics Speech Signal Processing* pp 17–20

Farhang-Boroujeny B 1994 An IIR adaptive line enhancer with controlled bandwidth. *Proc. Singapore Int. Conf. Circuits and Systems '94* pp 835–839

Hush D R, Ahmed N, David R, Stearns S D 1986 An adaptive IIR structure for sinusoidal enhancement, frequency estimation and detection. *IEEE Trans. Acoust. Speech Signal Process.* 34: 1380–1389

Krishna V V, Hiremath C G 1995 Adaptive IIR Notch Filters. Technical Report No. 95-4/BRC, Signion Systems Pvt. Ltd.

Kwan T, Martin K 1989 Adaptive detection and enhancement of multiple sinusoids using a cascade IIR filter. *IEEE Trans. Circuits Syst.* 36: 937–947

Mukund P, Martin K 1991 Resonator based filter-banks for frequency-domain applications. *IEEE Trans. Circuits Syst.* 38: 1145–1159

Mukund P, Martin K 1993 A second order hyperstable adaptive filter with no post-error filtering. *Proc. IEEE Int. Symp. Circuits and Systems* pp 447–450

Nehorai A 1985 A minimal parameter adaptive notch filter with constrained poles and zeros. *IEEE Trans. Acoust. Speech Signal Process.* 33: 983–996

Rao D V B, Kung S Y 1984 Adaptive notch filtering for the removal of sinusoids in noise. *IEEE Trans. Acoust. Speech Signal Process.* 32: 791–802

Regalia P A 1990 A novel lattice based adaptive IIR notch filter. In *Signal Processing V: Theories and Applications* (eds.) L Torres, E Masgrau, M A Lagunas (Amsterdam: Elsevier) pp 261–264

Regalia P A 1995 *Adaptive IIR filtering in signal processing and control* (New York: Marcel Dekker)

# convergence and bias in the LSG algorithm for adaptive lattice filters

ROHIT NEGI<sup>1</sup> and P G POONACHA<sup>2</sup>

Department of Electrical Communication Engineering, Indian Institute of Technology, Powai, Bombay 400 076, India

Present address: <sup>1</sup>Information Systems Laboratory, Durand 112, Stanford University, Stanford, CA 94305-9510, USA

<sup>2</sup>Silicon Automation Systems, # 3008, 12th B Main, 8th Cross, HAL II Stage, Bangalore 560 008, India

e-mail: negi@isl.stanford.edu; poonacha@sasi.com

**Abstract.** The lattice filter has several desirable characteristics that make it attractive in adaptive applications. The Lattice Stochastic Gradient (also called Gradient Adaptive Lattice algorithm) is popularly used to adapt the lattice filter. However, a theoretical study of the bias in the reflection coefficient and the convergence of the LSG algorithm have not been studied extensively yet. This paper presents some theoretical results on these issues. It is hoped that the results will also present some insights into the factors affecting the convergence of the filter.

**Keywords.** Adaptive filters; lattice filters; convergence analysis; adaptive algorithms.

## Introduction

The lattice filter is useful in adaptive applications because it possesses several desirable characteristics such as orthogonalization of the input, faster convergence, simple stability checking criteria etc. The Lattice Stochastic Gradient (LSG), also called Gradient Adaptive lattice (GAL) algorithm, is popularly used to adapt the (FIR) lattice filter as it is fast and has a reasonably low computation.

In adaptive filtering literature, there is a lack of rigorous theoretical analysis on the issues of bias in filter coefficient and the convergence of the algorithms. The analysis of the convergence of the LMS algorithm for the transversal filter is handled by making the 'independence assumption', which though handy, seems somewhat artificial. An analysis which does not use this assumption is detailed by Douglas & Meng (1992) for a restricted kind of input.

Such rigorous analysis is absent in the case of the lattice filter. Honig & Messerschmitt have proposed convergence models by Honig & Messerschmitt (1981) for analysis of speed of convergence that are partly analytic.

This paper attempts to prove absence of bias in reflection coefficient and the convergence of the LSG algorithm using more rigorous arguments. The notation used is that followed by Honig & Messerschmitt (1984).

The order update equations of the lattice filter are:

$$\begin{aligned} e_f(T/n) &= e_f(T/n - 1) - k_n^b \cdot e_b(T - 1/n - 1), \\ e_b(T/n) &= e_b(T - 1/n - 1) - k_n^f \cdot e_f(T/n - 1), \end{aligned} \quad (1)$$

where  $e_f$  and  $e_b$  represent the forward and backward errors respectively,  $T$  is the time index,  $k_n^f$  and  $k_n^b$  are forward and backward reflection coefficients of the  $n$ th stage. In the LSG algorithm,  $k_n^f = k_n^b$ .

The lattice stochastic gradient algorithms is:

$$\begin{aligned} k_n(T + 1) &= k_n(T) + \frac{1}{E(T/n - 1)} \\ &\quad [e_f(T/n - 1) \cdot e_b(T/n) + e_b(T - 1/n - 1) \cdot e_f(T/n)], \\ E(T/n - 1) &= \lambda \cdot E(T - 1/n - 1) + e_f^2(T/n - 1) + e_b^2(T - 1/n - 1), \end{aligned} \quad (2)$$

with  $e_f(T/0) = e_b(T/0) = u(T)$  and  $E(0/n - 1) = +ve$  constant  $\forall n = 1, \dots, N$ .

## 2. Theoretical results on the LSG algorithm

Both the results presented below require assumption of ergodic input  $u(T)$  to the lattice filter Middleton (1960) for the definition of ergodic process used). The proof on convergence of the LSG algorithm requires, in addition, the assumption of ‘independent enough’ input (defined later).

### 2.1 Absence of bias in $k_n(T)$ in the LSG algorithm

**Theorem 1.** *The lattice filter coefficients  $k_n(T)$  are asymptotically unbiased when the LSG adaptive algorithm is used, assuming an ergodic input. ie.*

$$\lim_{T \rightarrow \infty} E[k_{n+1}(T + 1)] = k_{n+1}^{opt}.$$

*Proof.* The LSG algorithm implements the following expression recursively

$$k_{n+1}(T + 1) = \frac{\sum_{i=0}^T 2 \cdot e_f(i/n) \cdot e_b(i - 1/n)}{\sum_{i=0}^T \{e_f^2(i/n) + e_b^2(i - 1/n)\}}. \quad (3)$$

Denote the numerator and denominator of the above fraction as NUM and DEN respectively, for convenience.

Here, we have considered the case  $\lambda = 1$  only, which is usually taken for stationary input. Now define

$$N_0 = E[2 \cdot e_f(T/n) \cdot e_b(T - 1/n)],$$

$$D_0 = E[e_f^2(T/n) + e_b^2(T - 1/n)]. \quad (4)$$

We can write  $\frac{1}{T} \text{NUM} = N_0 + n(T)$  and  $\frac{1}{T} \text{DEN} = D_0 + d(T)$ .

If  $u(T)$  is assumed to be ergodic, and we assume that the coefficients  $k_j$ ,  $j = 1, \dots, n$  have converged (to constant values), then  $e_f(T/n) \cdot e_b(T - 1/n)$  and  $e_f^2(T/n) + e_b^2(T - 1/n)$  can be shown to be ergodic processes. Then  $\lim_{T \rightarrow \infty} \frac{1}{T} \text{NUM} = N_0$  with probability 1, and  $\lim_{T \rightarrow \infty} \frac{1}{T} \text{DEN} = D_0$  with probability 1,

which means

$$\lim_{T \rightarrow \infty} n(T) = 0, \text{ with probability 1, and}$$

$$\lim_{T \rightarrow \infty} d(T) = 0, \text{ with probability 1,}$$

where ‘probablity 1’ means that the probability of the event that  $\lim_{T \rightarrow \infty} n(\Omega_j, T) \neq 0$  is zero ( $n(\Omega_j, T)$  denotes the  $j$ th sample function of the process  $n(T)$ ). Now

$$k_{n+1}(T + 1) = \frac{\text{NUM}/T}{\text{DEN}/T} = \frac{N_0}{D_0} \cdot \left[ \frac{1 + \frac{n(T)}{N_0}}{1 + \frac{d(T)}{D_0}} \right], \quad (5)$$

$$E[k_{n+1}(T + 1)] = k_{n+1}^{opt} \cdot E \left[ \frac{1 + \frac{n(T)}{N_0}}{1 + \frac{d(T)}{D_0}} \right], \quad (6)$$

where  $k_{n+1}^{opt}$  is the optimum Wiener solution in the MMSE sense.

Now, we prove that for the expectation on the RHS, denoted by  $E[(\cdot)]$  for convenience,  $\lim_{T \rightarrow \infty} E[(\cdot)] = 1$  under the ergodicity assumptions made above.

$$E[(\cdot)] = E \left[ \frac{1 + \frac{n(T)}{N_0}}{1 + \frac{d(T)}{D_0}} \right] = \sum_{j \in S} \left[ \frac{1 + \frac{n(\Omega_j, T)}{N_0}}{1 + \frac{d(\Omega_j, T)}{D_0}} \right] \cdot P(\Omega_j), \quad (7)$$

$$\begin{aligned} |E[(\cdot)] - 1| &= \left| \sum_{j \in S_c} \left[ \frac{\frac{n(\Omega_j, T)}{N_0} - \frac{d(\Omega_j, T)}{D_0}}{1 + \frac{d(\Omega_j, T)}{D_0}} \right] \cdot P(\Omega_j) \right. \\ &\quad \left. + \sum_{j \in \bar{S}_c} \left[ \frac{\frac{n(\Omega_j, T)}{N_0} - \frac{d(\Omega_j, T)}{D_0}}{1 + \frac{d(\Omega_j, T)}{D_0}} \right] \cdot P(\Omega_j) \right| \\ &\leq \sum_{j \in S_c} \left| \frac{\frac{n(\Omega_j, T)}{N_0} - \frac{d(\Omega_j, T)}{D_0}}{1 + \frac{d(\Omega_j, T)}{D_0}} \right| \cdot P(\Omega_j) \\ &\quad + \sum_{j \in \bar{S}_c} \left| \frac{\frac{n(\Omega_j, T)}{N_0} - \frac{d(\Omega_j, T)}{D_0}}{1 + \frac{d(\Omega_j, T)}{D_0}} \right| \cdot P(\Omega_j) \end{aligned}$$

where  $S$  denotes the joint sample space of the random processes  $n(T)$  and  $d(T)$ ,  $S_c$  denotes the subset comprising all sample functions  $n(\Omega_j, T)$  and  $d(\Omega_j, T)$  which converge to zero as  $T \rightarrow \infty$ , and  $\bar{S}_c$  denotes the complement of  $S_c$ .

Considering the second summation in above inequality, we see that since  $[1 + d(\Omega_j, T) / D_0] = \text{DEN} / D_0 T$ , and DEN is always positive non-zero, hence we can bound the absolute value of the fraction by an upper bound  $M$ . Then,

$$\left| \sum_{j \in \bar{\mathcal{S}}_c} [(\cdot)] \cdot P(\Omega_j) \right| \leq M \cdot \sum_{j \in \bar{\mathcal{S}}_c} P(\Omega_j),$$

which is zero under the ergodicity assumptions and above.

Considering the first summation in same inequality, we see that since all  $n(\Omega_j, T)$  and all  $d(\Omega_j, T) \in \mathcal{S}_c$  converge to zero as  $T \rightarrow \infty$ , hence, given a  $\delta > 0$ , we can find a  $T_0$  such that  $|n(\Omega_j, T)|$  and  $|d(\Omega_j, T)|$  are both  $\leq \delta$  for  $T \geq T_0$ .

Therefore, for  $T \geq T_0$ , the absolute value of the fraction in the summation  $\leq k \cdot \delta$ , where  $k$  has a finite value. Hence,

$$\left| \sum_{j \in \mathcal{S}_c} [(\cdot)] \cdot P(\Omega_j) \right| \leq k \cdot \delta \cdot \underbrace{\sum_{j \in \mathcal{S}_c} P(\Omega_j)}_{\text{1 by ergodicity}},$$

which implies that

$$|E[(\cdot)] - 1| \leq k \cdot \delta, \quad \text{for } T \geq T_0. \quad (8)$$

Hence,  $\lim_{T \rightarrow \infty} E[(\cdot)] = 1$  which implies that

$$\lim_{T \rightarrow \infty} E[k_{n+1}(T+1)] = k_{n+1}^{\text{opt}}. \quad (9)$$

By following a method similar to the one used above, if we consider

$$\begin{aligned} & E[\{k_{n+1}(T+1) - k_{n+1}^{\text{opt}}\}^l] \\ &= (k_{n+1}^{\text{opt}})^l \cdot E \left[ \left\{ \left( \frac{n(T)}{N_0} - \frac{d(T)}{D_0} \right) / \left( 1 + \frac{d(T)}{D_0} \right) \right\}^l \right] \quad l = 2, 3, \dots, \end{aligned}$$

then, it can be shown that the term  $E[(\cdot)]$  on the RHS converges to zero as  $T \rightarrow \infty$ .

Thus, all central moments of  $k_n(T) \rightarrow 0$  as  $T \rightarrow \infty$ , which means that  $k_n(T)$  converges to a constant value.

Thus, under the assumption of ergodic  $u(T)$ , it is proved that  $k_1(T)$  converges to a fixed value which is also the optimum value i.e.  $k_1$  obtained has no bias.

Now, ergodic  $u(T)$  and convergence of  $k_1(T)$  to optimum value is sufficient to prove the convergence of  $k_2(T)$  to its optimum value, and so on.

Thus, all  $k_n(T)$  converge to their respective optimum values.  $\square$

## 2.2 Proof of convergence of $k_n(T)$ to a stable stationary point when the LSG algorithm is used

**Theorem 2.** Assuming an ergodic and ‘independent enough’ input (defined below), the lattice filter coefficients  $k_n(T)$  converge to stable stationary points, when the LSG adaptive algorithm is used.

*proof.* This proof uses the method of conversion of a recursive difference equation to an ordinary differential equation (see Goodwin & Payne 1977, pp 192–196).

Consider the LSG algorithm (2). It can be rewritten as

$$\begin{aligned} k_n(T+1) = & k_n(T) + \frac{1}{E(T/n-1)} \cdot [2 \cdot e_f(T/n-1) \\ & \cdot e_b(T-1/n-1) - k_n(T) \\ & \cdot \{e_f^2(T/n-1) + e_b^2(T-1/n-1)\}]. \end{aligned} \quad (10)$$

$$E(T/n-1) = \sum_{j=0}^T \lambda^{T-j} \cdot \{e_f^2(j/n-1) + e_b^2(j-1/n-1)\}. \quad (11)$$

Assume ergodic input  $u(T)$ . Also, assume that the stages  $1, \dots, n-1$  have ‘adapted’; by which we mean that  $\{k_i(T)\}$ ,  $i = 1, \dots, n-1$  have each converged to a stable stationary point.

We prove that in such a case  $k_n(T)$  will also converge to a stationary point

For convenience, denote expectation operator  $E[(\cdot)]$  as  $(\cdot)$ .

From (10), we can write

$$\begin{aligned} k_n(T+M) = & k_n(T) + \sum_{j=0}^{M-1} \left[ \frac{1}{E(T+j/n-1)} \right] \\ & \cdot [2 \cdot e_f(T+j/n-1) \cdot e_b(T+j-1/n-1) - k_n(T+j) \\ & \cdot \{e_f^2(T+j/n-1) + e_b^2(T+j-1/n-1)\}]. \end{aligned} \quad (12)$$

Let  $T = 0$  denote the time when all the first  $(n-1)$  stages have ‘adapted’. Then from (11), we get

$$\bar{E}(T/n-1) = \sum_{j=0}^T \lambda^{T-j} \cdot \{2 \cdot P_{n-1}\},$$

where

$$P_{n-1} = \bar{e}_f^2(j/n-1) = \bar{e}_b^2(j-1/n-1), \text{ and } P_{n-1}$$

independent of time by the assumption that  $k_i(j)$ ,  $i = 0, \dots, n-1$  have converged to a stable stationary solution.

$$\begin{aligned} \Rightarrow \bar{E}(T/n-1) &= \left[ \frac{1 - \lambda^{T+1}}{1 - \lambda} \right] 2 \cdot P_{n-1} \\ \Rightarrow \bar{E}(T/n-1) &\approx \underbrace{\left[ \frac{\ln(1/\lambda)}{1 - \lambda} \cdot 2 \cdot P_{n-1} \right]}_{\text{constant}=\beta} T. \end{aligned} \quad (13)$$

The approximation holds when  $T \ll |1/\ln(\lambda)|$ .

Now, since  $\bar{E}(T/n-1) = \beta \cdot T$ , we use the heuristic that for large  $T$ ,  $E(T/n-1) = \beta \cdot T$  also. Then, since increment in  $k_n(T)$  is inversely proportional to  $(T+j)$ , for  $T \gg M$ , we

can replace  $k_n(T + j)$  in (12) by  $k_n(T)$ , which gives

$$\begin{aligned}
 k_n(T + M) &= k_n(T) + \sum_{j=0}^{M-1} \left[ \frac{1}{E(T + j/n - 1)} \right] \\
 &\quad \cdot \overbrace{\left[ 2 \cdot e_f(T + j/n - 1) \cdot e_b(T + j - 1/n - 1) \right.}^{\text{denote by PRO}(T+j)} \\
 &\quad \left. - k_n(T) \cdot \underbrace{\{e_f^2(T + j/n - 1) + e_b^2(T + j - 1/n - 1)\}}_{\text{denote by SUM}(T+j)} \right] \\
 \bar{k}_n(T + M) &= \bar{k}_n(T) + \sum_{j=0}^{M-1} \left[ \frac{1}{E(T + j/n - 1)} \right] \\
 &\quad \cdot [\text{PRO}(T + j) - k_n(T) \cdot \text{SUM}(T + j)]. \tag{14}
 \end{aligned}$$

Now, let us assume that the input  $u(T)$  is, in addition to being ergodic, also an ‘independent enough’ process, by which we mean that  $\exists$  a finite ‘ $l$ ’ such that  $u(T)$  and  $u(T - j)$  are independent  $\forall j \geq l$ . We shall call this the assumption of ‘independent-enoughness’.

Next, we note the input samples that appear in the various terms of the summation in (14)

$E(T + j/n - 1)$  has samples  $u(T + j), u(T + j - 1), \dots, u(0)$ .

$\text{PRO}(T + j)$  has samples  $u(T + j), \dots, u(T + j - n)$  and  $k_i, i \leq n - 1$ .

$\text{SUM}(T + j)$  has samples  $u(T + j), \dots, u(T + j - n)$  and  $k_i, i \leq n - 1$ .

$k_n(T)$  has samples  $u(0), u(1), \dots, u(T - 1)$ . However, by the heuristic that  $E(T/n - 1) \propto T$ , it seems reasonable to believe that the dependence of  $k_n(T)$  on  $u(\tau)$  will ‘decrease’ as  $\tau$  increases. At this stage, we cannot rigorously justify this, and hence, this decreasing dependence can be considered an assumption. We call this the assumption of “decreasing dependence”.

Since we are considering large  $T$ , we can write  $E(T + j/n - 1) \approx \sum_{r=0}^{T+j-n-l} [e_f^2(\tau/n - 1) + e_b^2(\tau - 1/n - 1)]$ , so that  $E(T + j/n - 1)$  now has samples  $u(T + j - n - l), u(T + j - n - l - 1), \dots, u(0)$ .

Comparing the samples  $u(\tau)$  in  $E(T + j/n - 1)$ ,  $\text{PRO}(T + j)$  and  $\text{SUM}(T + j)$ , and noting that  $k_i, i \leq n - 1$  have already ‘adapted’ before  $T = 0$ , we conclude that by the assumption of ‘independent-enoughness’,  $E(T + j/n - 1)$  is independent of  $\text{PRO}(T + j)$  and of  $\text{SUM}(T + j)$ .

Again, comparing the samples  $u(\tau)$  in  $k_n(T)$  and  $\text{PRO}(T + j)$ ,  $\text{SUM}(T + j)$ , we can say that for  $j \geq (l + n - 1)$ ,  $k_n(T)$  is independent of both  $\text{PRO}(T + j)$ , and of  $\text{SUM}(T + j)$ . Choose  $M$  large enough (but  $\ll T$ ), such that  $\sum_{j=0}^{M-1} (\cdot) \approx \sum_{j=l+n-1}^{M-1} (\cdot)$ . Therefore, for all terms in the summation,  $k_n(T)$  is independent of  $\text{PRO}$  and  $\text{SUM}$ .

Finally, if  $E(T + j/n - 1) \approx \sum_{\tau=p}^{T+j-n} [e_f^2(\tau/n - 1) + e_b^2(\tau - 1/n - 1)]$  where  $p$  is large enough so that the assumption of “decreasing dependence” of  $k_n(T)$  is valid for terms of  $E(T + j/n - 1)$ , then  $k_n(T)$  will also be independent of  $E(T + j/n - 1)$ . Under these

conditions, we can write (14) as

$$\bar{k}_n(T+M) = \bar{k}_n(T) + \sum_{j=0}^{M-1} \frac{1}{T+j} \cdot \left[ \frac{1}{E(T+j/n-1)/(T+j)} \right] \cdot [\overline{\text{PRO}}(T+j) - \bar{k}_n(T) \cdot \overline{\text{SUM}}(T+j)].$$

Since  $u(T)$  is assumed to be ergodic, hence  $e_f^2(T/n-1) + e_b^2(T-1/n-1)$  is also ergodic. Therefore, according to lemma 1 (see appendix A), we see that for  $\lambda = 1$ ,  $[E(\cdot)/(T+j)] \rightarrow 1/[\overline{E}(\cdot)/(T+j)]$  as  $T \rightarrow \infty$ . We assume that for large  $T$  (but  $|1/\ln(\lambda)|$ ), we can replace  $1/[E(\cdot)/(T+j)]$  by  $1/[\overline{E}(\cdot)/(T+j)]$  even for  $\lambda \neq$

Finally, noting that  $\overline{\text{PRO}}(T+j) = r_{fb}$ ,  $\overline{\text{SUM}}(T+j) = 2 \cdot P_{n-1}$  and  $\overline{E}(\cdot)/T = \beta$ , where  $r_{fb}$ ,  $P_{n-1}$  and  $\beta$  are independent of time for the conditions of ergodicity of  $u(\tau)$ , and 'adaptation' of the lower  $n-1$  stages, we can write the above equation as

$$\bar{k}_n(T+M) = \bar{k}_n(T) + \frac{1}{\beta} \cdot [r_{fb} - \bar{k}_n(T) \cdot 2 \cdot P_{n-1}] \cdot \underbrace{\sum_{j=0}^{M-1} \left[ \frac{1}{T+j} \right]}_{\text{small}}.$$

Converting this difference equation to an ODE

$$\frac{d}{dt}(\bar{k}_n(t)) = \frac{1}{\beta} \cdot [r_{fb} - \bar{k}_n(t) \cdot 2 \cdot P_{n-1}]. \quad (15)$$

The ODE gives us the stationary point

$$\begin{aligned} \bar{k}_n(t) &= r_{fb}/[2 \cdot P_{n-1}] \\ &= \frac{E[2 \cdot e_f(T/n-1) \cdot e_b(T-1/n-1)]}{E[e_f^2(T/n-1) + e_b^2(T-1/n-1)]}, \end{aligned}$$

which is also the optimum Wiener solution in the MMSE sense.

To check for stability of the stationary point, we write

$$\frac{d}{dt}(\Delta \bar{k}_n(t)) = - \left[ \frac{1}{\beta} \cdot 2 \cdot P_{n-1} \right] \Delta \bar{k}_n(t).$$

Hence stability is guaranteed iff  $2 \cdot P_{n-1}/\beta > 0$ , i.e.  $\left[ \frac{1-\lambda}{\ln(1/\lambda)} \right] > 0$ , which is true.

Hence, we conclude that under the assumptions made, when the lower  $n-1$  stages of the lattice filter have converged to stable stationary points, then the  $n$ th stage will also do so. The first stage does not require convergence of any other stage.

Thus, the first stage 'adapts' the earliest. Next, the second stage 'adapts' (since the first stage has already adapted), and so on for higher stages.

This completes the proof.  $\square$

## Results and discussion

While the two results presented above can both be regarded as proving absence of bias in reflection coefficient as well as convergence of the LSG algorithm, yet they are not quite

identical. The first result holds only for the case  $\lambda = 1$  (which of course should be used for truly stationary input).

The second result holds for other values of  $\lambda$  also. The price to be paid is less rigour in the proof as several heuristics have to be introduced. However, we feel that the second result provides insight into the working of the filter in the way that the first result does not. For, example, a look at the ODE obtained shows that the speed of convergence depends on  $(1 - \lambda)/\ln(1/\lambda)$ , which is independent of the MSE  $P_{n-1}$  and is very nearly independent of  $\lambda$  for values close to 1.

#### 4. Conclusion

The paper has attempted to approach the issues of convergence of the LSG algorithm and the absence of bias in the reflection coefficient in a somewhat more rigorous manner than is available in literature at present. The conditions imposed on the input are admittedly very strict, but they would be satisfied by Gaussian processes, which are used in simulation studies. However, it is clear that mere wide-sense stationarity is not enough for convergence. It is to be seen whether the conditions imposed on the input can be weakened.

The authors would like to thank one of our reviewers for bringing to our attention a recent paper by Fan & Liu (1993), which proves the convergence of the LSG algorithm under more general conditions.

#### Appendix A

In this appendix, we state and prove lemma 1.

*Lemma 1.* If  $w(T)$  is a stationary, ergodic random process with  $\overline{w(T)} = w_0$ , and  $E(T) = \frac{1}{T} \cdot \sum_{j=0}^T w(j)$ , then

$$\lim_{T \rightarrow \infty} \left[ \overline{\frac{1}{E(T)}} \right] = \frac{1}{w_0}.$$

*Proof.* The proof uses arguments similar to those in the proof given in 2.1

Since  $w(T)$  is stationary ergodic, hence we can write,

$$E(T) = w_0 + n(T),$$

where  $n(T) \rightarrow 0$  with probability 1 as  $T \rightarrow \infty$ .

Hence, we can write

$$\left[ \overline{\frac{1}{E(T)}} \right] = \frac{1}{w_0} \cdot \left[ \overline{\frac{1}{1 + n(T)/w_0}} \right]. \quad (16)$$

Next, we show that the expectation on the RHS  $\rightarrow 1$  as  $T \rightarrow \infty$ . Write

$$1 - \left[ \overline{\frac{1}{1 + n(T)/w_0}} \right] = \left[ \overline{\frac{n(T)/w_0}{1 + n(T)/w_0}} \right].$$

then, by writing the expectation as two summations, in a manner similar to that used in 2.1, we get

$$\left| 1 - \overline{\left[ \frac{1}{1 + n(T)/w_0} \right]} \right| \leq \sum_{k \in S_c} \left| \frac{n(\Omega_k, T)/w_0}{1 + n(\Omega_k, T)/w_0} \right| \cdot P(\Omega_k) \\ + \sum_{k \in \bar{S}_c} \left| \frac{n(\Omega_k, T)/w_0}{1 + n(\Omega_k, T)/w_0} \right| \cdot P(\Omega_k),$$

here  $S_c$  consists of all sample functions  $n(\Omega_k T)$  of  $n(T)$  which converge to zero as  $\rightarrow \infty$ , and  $\bar{S}_c$  is the complement of  $S_c$ .

Now, the second summation on the RHS is zero since the denominator of the fraction always positive and  $\sum_{k \in \bar{S}_c} P(\Omega_k) = 0$ .

As for the first summation on the RHS, given any  $\delta$ , we can find a  $T_0$  such that for  $\geq T_0$

$$\sum_{k \in S_c} \left| \frac{n(\Omega_k, T)/w_0}{1 + n(\Omega_k, T)/w_0} \right| \cdot P(\Omega_k) \leq p \cdot \underbrace{\delta \sum_{k \in S_c} P(\Omega_k)}_1,$$

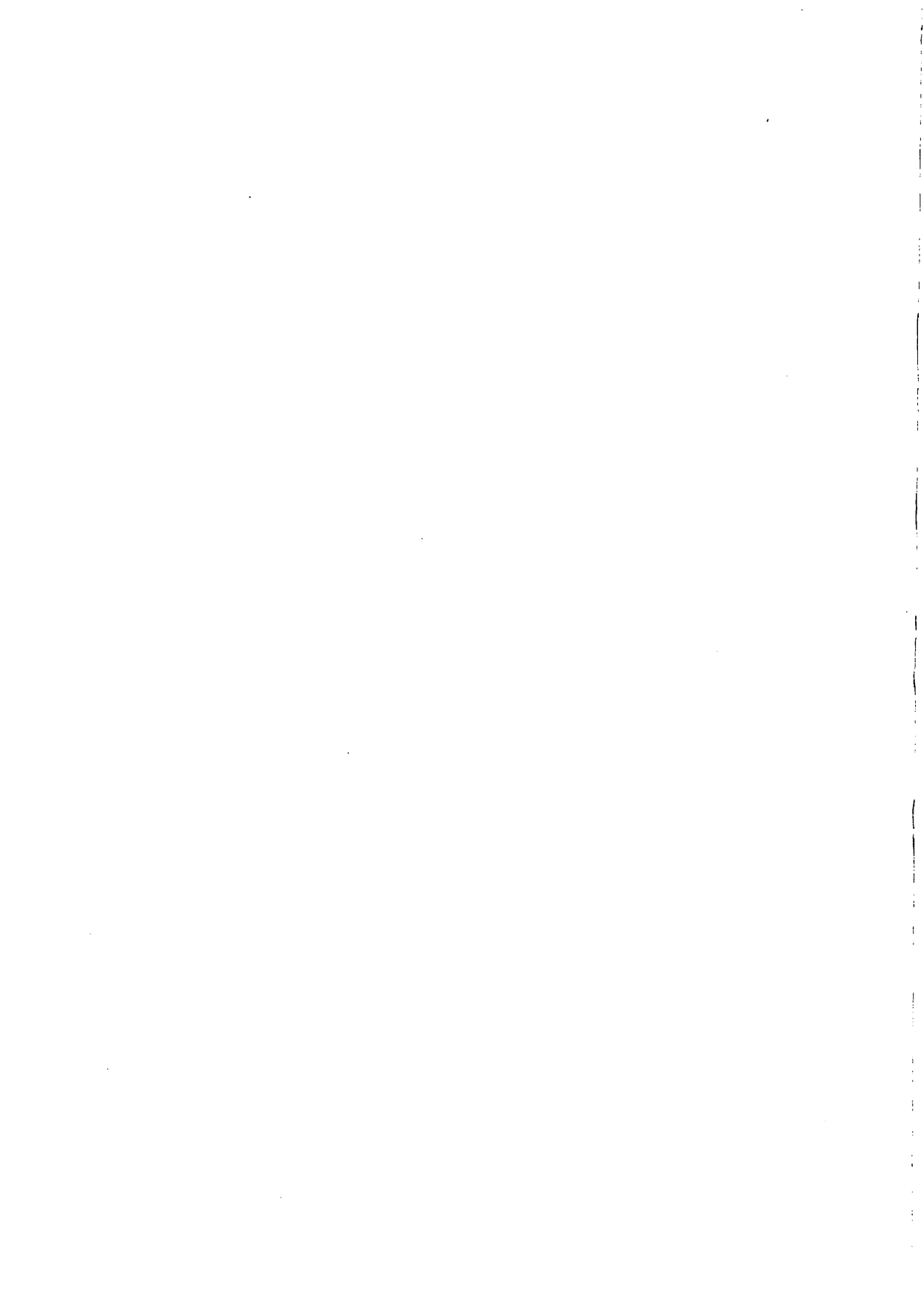
here  $p$  is a finite number.

Thus, we have shown that as  $T \rightarrow \infty$ , the expectation on the RHS of (16)  $\rightarrow 1$ .

This therefore proves the lemma.  $\square$

## References

- Douglas S, Meng T H Y 1991 Exact expectation analysis of the LMS adaptive filter without the independence assumption. *Proc. IEEE Int. Conf. on Acoustics, Speech and Signal Processing*, pp 61–64
- Han H, Liu X 1993 GAL and LSL revisited: new convergence results. *IEEE Trans. Signal Process.* 41: 55–66
- Goodwin G C, Payne R L 1977 *Dynamic system identification experimentation, design, and data analysis* (New York: Academic Press)
- Konig M L, Messerchmitt D G 1981 Convergence properties of an adaptive digital lattice filter. *IEEE Trans. Acoust., Speech Signal Processing* 29: 642–653
- Oppenheim K L, Messerchmitt D G 1984 *Adaptive filters – Structures, algorithms and applications* (Boston: Kluwer Academic)
- Shannon D 1960 *Introduction to statistical communication theory* (New York: McGraw-Hill)



# **Q imbalance correction in time and frequency domains with application to pulse doppler radar**

N SIVANNARAYANA and K VEERABHADRA RAO

SHL, Research Centre Imarat, Vignyanakancha, Hyderabad 69, India  
e-mail: siva@rci.ernet.in

**Abstract.** Digital In-phase(I) and Quadrature phase(Q) imbalance correction schemes are presented for improving the balance between I & Q signals by rejecting the image frequencies due to imbalance. The imbalance errors in the analog and digital demodulation schemes are highlighted. Simplified correction schemes are presented for time and frequency domain imbalances. These correction schemes are useful in radar and communication systems. In this paper, a digital I-Q scheme is also presented for a pulse Doppler radar, along with hardware configuration for implementation.

**Keywords.** Digital I-Q; quadrature demodulation; pulse doppler radar; time-frequency analysis.

## **Introduction**

In a coherent receiver, In-phase and Quadrature (I-Q) phase signals are derived by demodulating the Intermediate Frequency (IF) signal. The I-Q signals should match in gain and phase by 90 degrees. In the analog schemes, IF signal is demodulated using in-phase and quadrature phase carrier (Goldman 1986; Liu 1989; Tsui 1995) and is sampled in two channels. In the digital schemes (Liu *et al* 1989, Tsui), IF signal is sampled and demodulated using sampled cosine and sine of the carrier. These I-Q schemes are explained in the literature towards simplification in the implementation (Levanon 1988; Liu *et al* 1989). However, these schemes tend to develop amplitude and phase imbalances. In this work, we are proposing simplified schemes for correcting the imbalances in time and frequency domains with application to pulse Doppler radar.

In radar and communication systems, signals are sampled for digital processing. As per Nyquist criterion a signal must be sampled at a rate more than twice the bandwidth. In complex (I-Q) sampling, the signals can be sampled minimum at the rate of bandwidth. I-Q signals avoid blind phases in sampling. This complex sampling also improves signal-to-noise ratio (SNR) by 3-dB compared to the only real (I-channel) signal processing (Levanon 1988).

The analog I-Q detector has a limitation of matching the gain & phase in the I and Q channels which can be achieved only upto a certain level (Goldman 1986). The mismatch creates an unwanted image frequency with an amplitude 24 dB down to the main signal. To achieve further rejection, the penalty in terms of cost is very high (Goldman 1986). Correction algorithms are incorporated in the signal processors to reduce the imbalance.

In the literature (Liu *et al* 1989; Tsui 1995), digital I-Q schemes are presented. Analog I-Q imbalance corrections are explained by Churchill *et al* (1981) and Levanon (1988) and the calibration procedure is presented by Pierre & Fuhrmann (1995). Hilbert transform techniques are described by Oppenheim & Schafer (1975). Simplification of digital sampling is available by Brown (1979), Considine (1983), and Frerking (1994). Recent literature (Liu *et al* 1989; Tsui 1995) on I-Q, stresses the imbalance free demodulation. However, such demodulation creates an additional imbalance due to delay between I-Q samples for Doppler-shifted signals. For example, in radars, the image frequencies have to be rejected up to 50 dB to 60 dB down in severe clutter to signal levels of 30 to 40 dB. From the clutter signal, the image frequencies can be calculated, but ignoring of these image frequencies creates additional blind zones in the Doppler plane. So to avoid blind zones and false target detections, the image frequency level should be brought down to the noise background.

## 2. Modeling I-Q imbalances

I-Q channels are modeled in four ways depending on the presence of error terms either in I or Q channels. The most commonly used signal with errors is (Churchill *et al* 1981; Levanon 1988)

$$x(t) = a(t)[(1 + \varepsilon) \cos(\omega t) + j \sin(\omega t + \theta)], \quad (1)$$

where  $a(t)$  is the envelope, ' $\omega$ ' is the angular frequency, ' $\varepsilon$ ' is the amplitude imbalance, ' $\theta$ ' is the phase imbalance between I-Q channels and ' $t$ ' is the time. The imbalance ratio is derived for (1). For simplicity  $a(t)$  is taken as amplitude  $A$ .

$$\begin{aligned} x(t) &= A[(1 + \varepsilon) \cos(\omega t) + j \sin(\omega t + \theta)] \\ &= A/2 [(1 + \varepsilon)(e^{j\omega t} + e^{-j\omega t}) + (e^{j(\omega t+\theta)} - e^{-j(\omega t+\theta)})] \\ &= A/2 [e^{j\omega t}(1 + \varepsilon + e^{j\theta}) + e^{-j\omega t}(1 + \varepsilon - e^{-j\theta})]. \end{aligned}$$

The image frequency strength  $X(-\omega)$  to main component strength  $X(\omega)$  is given by

$$\begin{aligned} \frac{X(-\omega)}{X(\omega)} &= \frac{(1 + \varepsilon - e^{-j\theta})}{(1 + \varepsilon + e^{j\theta})} \\ &= \frac{[1 + \varepsilon - \cos(\theta) + j \sin(\theta)]}{[1 + \varepsilon + \cos(\theta) + j \sin(\theta)]} \\ &= \frac{[\varepsilon^2 + 2\varepsilon + j 2(1 + \varepsilon) \sin(\theta)]}{[2(1 + \varepsilon + \varepsilon^2/2 + \varepsilon \cos(\theta) + \cos(\theta))] \\ &\approx \varepsilon/2 + j\theta/2, \text{ for small values of } \varepsilon \text{ and } \theta. \end{aligned}$$

ver ratio  $P_{-\omega}/P_\omega$  is derived by taking  $|X(-\omega)|^2/|X(\omega)|^2$  and is given by (Churchill 1981; Levanon 1988; Liu *et al* 1989)

$$P_{-\omega}/P_\omega \approx (\varepsilon^2 + \theta^2)/4.$$

similarly we can derive expressions for the remaining three cases. For the four possible balance cases, the image to main signal strength is given by

$$\begin{array}{ll} \text{Signal model } x(t) = & X(-\omega)/X(\omega) \approx \\ A[(1+\varepsilon)\cos(\omega t) + j\sin(\omega t + \theta)], & (\varepsilon/2 + j\theta/2), \end{array} \quad (2a)$$

$$A[\cos(\omega t) + j(1+\varepsilon)\sin(\omega t + \theta)], \quad (-\varepsilon/2 + j\theta/2), \quad (2b)$$

$$A[\cos(\omega t + \theta) + j(1+\varepsilon)\sin(\omega t)], \quad (-\varepsilon/2 - j\theta/2), \quad (2c)$$

$$A[(1+\varepsilon)\cos(\omega t + \theta) + j\sin(\omega t)], \quad (\varepsilon/2 - j\theta/2). \quad (2d)$$

balance errors can be estimated and corrected using frequency domain data while performing calibration. In order to calibrate, reference input is given at different frequencies preferably covering the whole band. Depending on the selected model, the ratio  $X(-\omega)/X(\omega)$  is considered with proper polarity. This is useful in automated calibration of receivers (Pierre & Fuhrmann 1995).

### Imbalance correction to the analog I-Q demodulators

In the analog I-Q, imbalances exist while demodulating the input using sine and cosine carriers at intermediate frequency. Imbalance correction for analog I-Q detector is presented below.

#### *Imbalance correction in the time domain*

The I-Q signals with imbalances of case-1, (2a) is modeled as

$$\begin{aligned} I(t) &= A(1+\varepsilon)\cos(\omega t), \\ Q(t) &= A\sin(\omega t + \theta). \end{aligned} \quad (3)$$

These can be corrected digitally by transforming the data as (Levanon 1988)

$$\begin{aligned} I1(t) &= E I(t), \\ Q1(t) &= P I(t) + Q(t), \end{aligned} \quad (4)$$

where  $E = \cos(\theta)/(1+\varepsilon)$  and  $P = -\sin(\theta)/(1+\varepsilon)$ .

After transformation,

$$\begin{aligned} I1(t) &= A\cos(\theta)\cos(\omega t), \\ Q1(t) &= A\cos(\theta)\sin(\omega t). \end{aligned}$$

The scheme mentioned above requires correction both in I & Q channel paths. Alternatively, we propose to correct this imbalance in the Q-channel path only by

modifying (4). This modified scheme is suitable for easy implementation in the signal processors.

$$\begin{aligned} I1(t) &= I(t) \quad (\text{remains same as input}), \\ Q1(t) &= (P/E) I(t) + (1/E) Q(t). \end{aligned} \quad (5)$$

### *3.2 Imbalance correction in the frequency domain*

In this scheme, analog baseband I-Q signals are sampled and the error correction is applied in the frequency domain. Normally, frequency transformation like discrete fourier transform (DFT) will be performed on the sampled data. The image frequency component appears after transformation. Hence, the correction is applied uniformly for all the bins. In the frequency domain, the frequency bins beyond  $f_s/2$  are complex-conjugates of the bins upto  $f_s/2$  and vice versa (Oppenheim & Schafer 1975) ( $f_s$  is the sampling frequency). Hence, both amplitude scaling and phase rotation, i.e.  $(\varepsilon/2 + j\theta/2)$  is provided uniformly on all the bins after conjugation operation.

For  $N$ -point DFT, let  $X(k)$  denote the transformed output and  $X^*(k)$  its conjugate; index  $k$  goes from 0 to  $N - 1$ . The correction data  $XM$  is generated as

$$XM(k) = (\varepsilon/2 + j\theta/2)X^*(k); \quad k = 1, 2, \dots, N - 1, \quad (6)$$

and the corrected data  $XC(k)$  is given by

$$XC(k) = X(k) - XM(N - k); \quad k = 1, 2, \dots, N - 1. \quad (7)$$

$XC(0) = X(0)$  in all  $XC$  computation equations.

With this type of correction, the image frequency component strength can be reduced by 30 to 40 dB below the main component strength.

## **4. Digital I-Q generation**

In a digital I-Q scheme, the carrier (IF) is offset at half the bandwidth  $B/2$  (Brown 1979; Considine 1983; Goldman 1986; Tsui 1995) and is sampled at  $2B$  frequency. Demodulation is performed using  $\cos(n\pi/2)$  &  $\sin(n\pi/2)$  which takes  $\{-1, 0, 1\}$  for integer values of ' $n$ '. Thus, demodulation is a simple operation of changing the polarity of the input depending on  $\{-1, 1\}$ . In this scheme,  $\cos(n\pi/2)$  is '1' when  $\sin(n\pi/2)$  is '0' and vice versa. So, Q-channel is a delayed version by a sampling interval. This delay creates an image frequency component. A fixed delay creates linear phase shift with frequency (Oppenheim & Schafer 1975). In analog I-Q scheme, phase shift is constant.

### *4.1 Imbalance correction in the frequency domain for digital I-Q scheme*

The sampled signals when analyzed in the frequency domain, give linearly varying phase shift with bin number. Hence, every correction scheme requires the frequency bin dependent phase correction. For a fixed sampling clock, correction coefficients are generated as function of the bin number.

Let  $f_s$  be the sampling frequency for I-Q signals and delay between I-Q samples is  $t_s$ . Sampling interval  $t_s$  and  $\delta t$  need not be related. Normally,  $\delta t$  is less than  $t_s$ . In pulse Doppler radars  $t_s$  is the pulse repetitive interval and  $\delta t$  is equal to  $1/2B$  for the signal sampled at 2B.

$$\begin{aligned}x(t) &= A[\cos(\omega t) + j \sin(\omega t + \omega \delta t)] \\&= A/2[(e^{j\omega t} + e^{-j\omega t}) + (e^{j(\omega t + \omega \delta t)} - e^{-j(\omega t + \omega \delta t)})] \\&= A/2[e^{j\omega t}(1 + e^{j\omega \delta t}) + e^{-j\omega t}(1 - e^{-j\omega \delta t})].\end{aligned}\quad (8)$$

The image strength  $X(-\omega)$  to main component strength  $X(\omega)$  is given by

$$\begin{aligned}X(-\omega)/X(\omega) &= (1 - e^{-j\omega \delta t})/(1 + e^{j\omega \delta t}) \\&= j[\sin(\omega \delta t)/(1 + \cos(\omega \delta t))] \\&\approx j\omega \delta t/2.\end{aligned}\quad (9)$$

$\omega \delta t$  is denoted as  $\Phi(k)$  in the discrete frequency domain. Phase error for a bin of one (e.  $f_s/N$ ) of  $N$ -point DFT is given by

$$\Phi_b = 2\pi(f_s/N)\delta t. \quad (10)$$

Phase error for other bins is given by

$$\Phi(k) = \Phi_b k; \quad k = 0, 1, \dots, N - 1$$

$$XM(k) = j[\sin(\Phi(k))/(1 + \cos(\Phi(k)))] X^*(k) \quad (11)$$

$$\approx j[\Phi(k)/2] X^*(k). \quad (12)$$

Equation (11) does not impose any constraint, and (12) limits the rejection for higher delays ( $\delta t$ ) between I-Q signals. Image-free components  $XC(k)$  are generated using (7). Windowing is applied on the time domain data to reduce the sidelobes. Figure 1a shows the input spectrum and figure 1b is the  $XM(k)$ . Figure 1c is the frequency reversal of  $XM$  and this is subtracted from input and indicated in figure 1d, which indicates the image-corrected spectrum. The main component is at bin 60 and image is at bin 4. Blackman window is used for this.

Due to windowing, frequency spread increases (Levanon 1988; Oppenheim & Schafer 1975). Let  $N - 2$  be the excitation bin and due to frequency domain broadening,  $N - 3$  and  $N - 1$  bins are also excited. For all these three bins, phase shift is  $(N - 2)\Phi_b$ . For  $(N - 1)$ th bin, phase correction weight is  $(N - 2)\Phi_b$ . But, the correction applied is given as  $(N - 1)\Phi_b$  in (12). The error rejection is  $((N - 1) - (N - 2))/(N - 2) \approx (1/N)$ , hence, at higher bin numbers, the rejection improvement is limited to  $20 \log(N)$ .

For example, using a 64-point FFT, the possible rejection is around  $20 \log(64) = 36$  dB. Prior to correction, the image frequency ratio is of the order of  $-14$  dB for the bin number 4 (image bin at 4) and  $-18$  dB image for bin number 61 (image bin at 3) as shown in figure 1a. After correction, the image is reduced by approximately 36 dB. With this technique, the image to main component strength is  $-54$  dB as shown in figure 1d. All the graphs are normalized with respect to the input spectrum maxima. Smaller values of the spectrum are limited to  $-80$  dB in displaying figure 1.

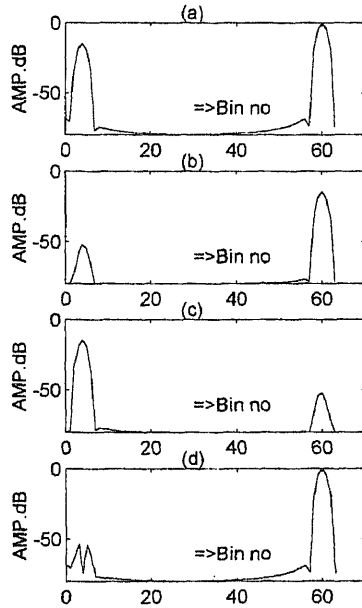


**Figure 1.** Frequency domain correction – magnitude plots. Phase is not indicated in the plots. (a) Input signal spectrum,  $X(k)$ , main component at bin 60 & its image at bin 4. (b) Correction spectrum,  $XM(k)$ , this takes care of phase also. (c) Frequency reversed of  $XM(k)$ . (d) Corrected spectrum. This is generated by subtracting  $XM(-k)$  from  $X(k)$ .

#### 4.2 Imbalance correction in the time domain for the modified digital scheme

The time delay between I-Q signals requires frequency dependent correction. As explained in the previous section in the frequency domain, correction vector is generated as frequency reversed conjugated spectrum with bin dependent coefficients. Thus, this forms multiplication in the frequency domain. Multiplication in the frequency domain reflects as convolution in the time domain. Convolution operation on the input gives correction signal in the time domain.

The corrected spectrum is given by,

$$XC(k) = X(k) - XM(N - k); \quad k = 1, 2, \dots, N - 1.$$

$$\text{Let } H(k) = j[\sin(\Phi(k))/(1 + \cos(\Phi(k)))],$$

$$\text{and } h(n) = IDFT[H(k)],$$

where IDFT denotes the inverse DFT operation. The number of significant coefficients in  $h(n)$  are much less compared to  $N$ . The image free signal  $xc(n)$  is generated as,

$$xc(n) = x(n) - xm(n),$$

$$xm(n) = h(-n) \odot x^*(n),$$

where  $\odot$  denotes circular convolution. Circular convolution is a computationally involved operation compared to the frequency domain correction. Also, time domain correction scheme lacks the facility for auto-calibration of the receiver.

While utilizing this scheme the following observations are to be noted

- (a) Filter consists of only few significant coefficients. Hence, the filter coefficients can be truncated to 5 to 8 coefficients, which saves computation time.

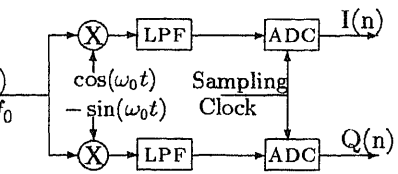


Figure 2. Analog I-Q scheme.

Circular convolution is performed on the finite data block.

The number of filter weights along with FFT size determine the possible imbalance reduction.

### I-Q scheme for pulse doppler radar

Pulse Doppler radars, carrier at transmitted frequency is pulse modulated and received signal is first converted to the intermediate frequency(IF). While converting the signal from IF to baseband, I-Q signals are generated as indicated in figure 2. In this scheme, carrier signal F is demodulated using  $e^{-j\omega_0 t}$  and the output is filtered using a low-pass filter (LPF) with bandwidth approximately equal to the reciprocal of the pulse width. I-Q signals are sampled using two Analog to Digital Converters (ADCs) at sampling interval less than or equal to the transmitted pulse width ( $\tau$ ).

Digital equivalent of the scheme is indicated in figure 3. In this scheme IF is generated at  $f_0 (= 1/\tau)$  and sampled at  $4f_0$ . This signal is multiplied with a carrier signal  $[-j(2\pi f_0 n(1/4f_0))] = \cos(n\pi/2) - j \sin(n\pi/2)$  and is suitably low-pass filtered down sampled to generate the required output sampling rate.

As an example, transmitter pulse width of 400ns. is considered. The steps involved here are as below.

Create IF ( $f_0$ ) at 2.5 MHz, one cycle is created in 400 ns. width.

Sample at 10 MHz ( $4f_0$ ).

Generate  $\cos(n\pi/2)$  [1 0 -1 0 1 0 -1 0 ...] period of 4 samples.

Generate  $\sin(n\pi/2)$  [0 1 0 -1 0 1 0 -1 ...] period of 4 samples.

Pass through LPF to pass signals up to  $f_0$  and remove components greater than  $2f_0$ . The filter should have maximum of 4 taps (equal to pulse width).

Decimate the filtered output by 2 to 4, to generate the I-Q signals at the required sampling frequency.

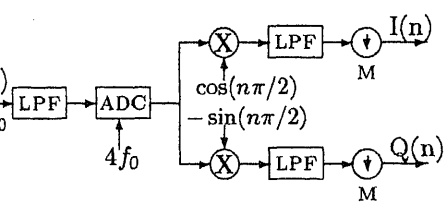


Figure 3. Digital I-Q scheme.

### 5.1 Choice of filter weights

Transmitted pulse is contained in approximately 4 samples. Matched filtering keeps the filter with samples comparable to the input. Filtering extends the signal due to convolution. Hence, the filter taps have to be limited to maximum of 4. Two simple filters selected are  $h = [1 \ 1]$  or  $[0.5 \ 1 \ 0.5]$ . First filter is a Haar smoothing filter with minimum number of taps. Second filter is a convolution of  $[1 \ 1]$  &  $[1 \ 1]$  with normalization. The main advantage gained through this choice is the scope for multiplication-less implementation.

### 5.2 Implementation

Block configuration for digital I-Q is indicated in figure 3 and implementation in figure 4.

In this, sampled signal at  $4f_0$  is demodulated using  $\cos(n\pi/2)$  &  $\sin(n\pi/2)$ . This sampled carrier takes the values  $\{+1, 0 \text{ & } -1\}$ . For multiplication by +1, 2's complement block passes on the input to its output. For -1, it is reversed in polarity using 2's complement operation. Multiplication by zero is performed in association with Reg1 by resetting Reg1. Reg1, Reg2, Reg3 outputs form 3-tap filter  $[0.5 \ 1 \ 0.5]$  (register is a latch/delay element denoted as 'Reg' in this paper). For multiplication by 0.5, adder  $\sum_1$  inputs are given with a right shift.  $\sum_1$  performs addition of first and the third sample.  $\sum_2$  performs combined operation. This output is considered with suitable down sampling from 2 to 4. Decimation operation is indicated as a down arrow with  $M$  in the diagram. For the decimation factor  $M$ , PRI has to  $i\tau M/4$ , where  $i$  is an integer. With this condition for PRI an integer number of range bins are obtained and  $M = 4$  corresponds to one sample/pulse width. One sample per pulse width gives straddling loss and to avoid this loss, it is preferred to keep  $M = 3$ .

For a selected  $M$ , hardware can be further simplified by optimizing the number of registers and adders. The main advantage of this scheme is the feasibility of configuring the whole hardware after ADC in Erasable Programmable Logic Devices (EPLD) or Field Programmable Gate Array (FPGA) without any multiplication operation. Hence, this type of scheme reduces hardware complexity.

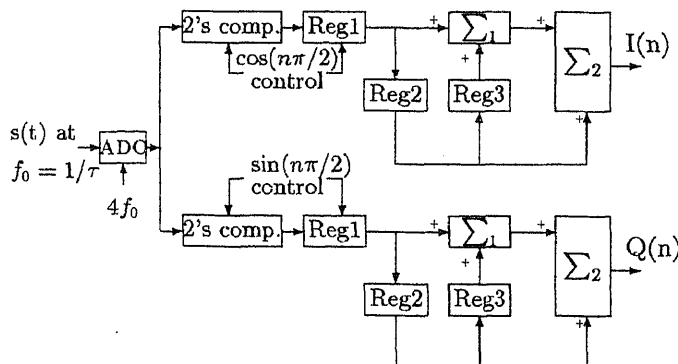


Figure 4. Digital I-Q implementation.

### 3 Imbalance correction

As explained in the previous sections, digital I-Q requires frequency bin dependent correction. This has to be incorporated in the signal processors. However, this imbalance correction may not be required in the ground based and clutter Doppler locked pulse Doppler radars.

### 4 Options

- ) Sampled signal is demodulated using  $\cos(n\pi/2)$  &  $\sin(n\pi/2)$ , passed through a low pass filter and decimated suitably.
- ) Sampled signal is demodulated as above and decimated by 2 or 4 in synchronism with the demodulating waveform (Liu *et al* 1989).
- ) Sample at highest possible frequency  $n(4f_0)$  to reduce phase imbalance, where 'n' is greater than or equal to 1.
- ) For pulse compression waveforms like linear FM, the block LPF can be merged with the pulse compression filter in digital pulse compression schemes. This I-Q scheme is hardware intensive and so the possible options are to be considered depending on the application.

## Conclusions

In this paper, different types of I-Q imbalance correction techniques are presented in time and frequency domains. These imbalance correction schemes are easy to implement both hardware and software and avoid the use of matched I-Q detectors which are costly. It may be easier to implement these schemes in the frequency domain and the frequency domain data can be utilized for amplitude and phase imbalance estimation in the automated calibration procedure. This is an added advantage. The computations required in the above schemes are negligible compared to computation involved in DFT/FFT and other signal processing operations. For digital I-Q, it is preferred to go for frequency domain correction. Digital I-Q schemes are useful for radar and communication applications. These schemes with higher image rejection will be useful for air-borne Doppler radars. The optimum hardware can be configured for the desired parameters depending on specific application.

The authors would like to thank Prof. V U Reddy, for his invaluable suggestions. The authors would also like to thank Dr K V S S Prasada Rao and their colleagues for their support and encouragement.

## References

Brown J L 1979 On quadrature sampling of bandpass signals. *IEEE Trans. Aerosp. Electron. Syst.* AES-15: 366–371

Churchill F E, Ogar G W, Thompson B J 1981 The correction of I and Q errors in a coherent processor. *IEEE Trans. Aerosp. Electron. Syst.* AES-17: 131–137

Considine V 1983 Digital complex sampling. *Electron. Lett.* 19: 608–609

Frerking M E 1994 *Digital signal processing in communication systems* (New York: Van Nostrand Reinhold) pp 113–151

Goldman S 1986 Understanding the limits of quadrature detection. *Microwave & RF* (Penton) Vol. 25, no. 13, pp 67–70 & 178

Levanon N 1988 *Radar principles* (New York: John Wiley)

Liu H, Ghafoor A, Stockman P H 1989 A new quadrature sampling and processing approach. *IEEE Trans. Aerosp. Electron. Syst.* AES-25: 733–747

Oppenheim A V, Schafer R W 1975 *Digital signal processing* (Englewood Cliffs, NJ: Prentice-Hall)

Pierre J W, Fuhrmann D R 1995 Consideration in the autocalibration of quadrature receivers. *Proc. Int. Conf. Acoust., Speech Signal Process.*, pp 1900–1903

Tsui J 1995 *Digital techniques for wideband receivers* (Norwood: Artech House)

# Interpolation of erasure bursts via cosine-modulated filterbanks

S JAYASIMHA and C G HIREMATH

Signion Systems Pvt. Ltd., 6-3-569/1/2, Rockdale Compound, Somajiguda,  
Hyderabad 500 082, India  
e-mail: signion@hotmail.com

**Abstract.** A novel and low-complexity approach for reconstructing periodic erasure bursts in data sampled at greater than the Nyquist rate, using cosine modulated filterbanks, is described. In the case of interpolation of erasure singlets or doublets periodically repeated over  $2M$  samples, the cosine modulated filterbank approach is shown to have a lower complexity (for a given restoration error) than a standard FIR interpolator. In the case of erasure triplets or quadruplets, periodically repeated over  $2M$  samples, the restoration error is primarily related to whether the  $M$ -channel filterbank's stopband suppression is better than the condition number of a  $2 \times 2$  matrix, where  $M$  is determined by the oversampling factor of the data. While the method used for erasure triplets and quadruplets extends to arbitrary erasure bursts, the condition numbers of the associated (larger dimension) matrices deteriorate rapidly with the increase in erasure length, posing practical problems such as the design of very high-attenuation filterbanks and large required implementation word-lengths.

**Keywords.** Chebyshev filters; discrete cosine transforms; equiripple filters;  $M$ -channel filterbanks; quadrature mirror filters; signal restoration; signal sampling/reconstruction.

## Introduction

The restoration of erasure bursts in oversampled multimedia data has assumed increased significance in the context of cell loss in ATM networks. Many heuristic methods, such as linear interpolation, repetition, or muting, are recommended in many multimedia standards. Other systematic approaches, however, have been considered in the recent years. While Vaidyanathan & Liu (1988) examine the feasibility of correcting long error bursts in the context of the sampling theorems, Marks and Radbel (Marks 1983; Marks & Radbel 1984), by considering the condition number of sub-matrices of a DFT matrix, exposed the

limitation<sup>1</sup> of the DFT method of signal restoration. The cosine modulated filterbank approach to burst erasure restoration described herein shows similar limitations. However, a poor condition number of a submatrix of a DCT matrix may be overcome by the design of a high stopband attenuation filterbank (in terms of achieving the desired restoration error). It is also shown that the approach proposed applies even to very slightly oversampled signals by increasing the number of channels  $M$ , albeit at the expense of the condition number of a submatrix of a DCT matrix. The method described is limited by practical considerations such as the design of very high stopband attenuation filterbanks and large required arithmetic word-lengths (for longer erasure bursts in signals approaching the Nyquist bandwidth). The method may be used to correct erasures either for isolated bursts (separated by at least the order of the prototype filter) or for either  $M$ - or  $2M$ -periodic erasure bursts. The method described is also *computationally efficient*, and in the simplest single  $2M$ -periodic erasure case, obtains a factor of 2 in reduced complexity as compared to an ordinary FIR interpolator.

## 2. New restoration method

The restoration method uses a typical  $M$ -channel maximally decimated filter bank as shown in figure 1, where  $H_k(z)$  and  $F_k(z)$ ,  $0 \leq k \leq M - 1$  are analysis and synthesis filters, respectively.

Here the cosine modulated filter bank is used which is attractive with respect to implementation cost and design ease. The cosine modulation may be either of type II or type IV<sup>2</sup>. The impulse response of the analysis and synthesis filters  $h_k(n)$  and  $f_k(n)$  are cosine modulated versions of the prototype filter  $h(n)$ . For type IV cosine modulation:

$$\begin{cases} h_k(n) = 2h(n) \cos \left( (2k+1) \frac{\pi}{2M} \left( n - \frac{N-1}{2} \right) - (2k+1) \frac{\pi}{4} \right), \\ f_k(n) = 2h(n) \cos \left( (2k+1) \frac{\pi}{2M} \left( n - \frac{N-1}{2} \right) + (2k+1) \frac{\pi}{4} \right), \\ 0 \leq n \leq N-1, \\ 0 \leq k \leq M-1, \end{cases} \quad (1)$$

where  $N$  is the length of  $h(n)$ . Here the cosine modulation uses a phase shift of  $(2k+1)\pi/4$  and satisfies the alias cancellation constraint given (Vaidyanathan 1993). The analysis

<sup>1</sup>Quoting from Strang & Nguyen (1996): "The Discrete Cosine Transform (DCT) improves on the DFT for the same reason that symmetric extension improves upon periodic extension. *The symmetric extension is continuous.*"

<sup>2</sup>The kernel for the modulation matrix is

$$\cos \left[ \left( (2k+1) \frac{\pi}{2M} \left( n - \frac{N'}{2} \right) \right) \theta_k \right],$$

where  $\theta_k$  is the phase shift determined by the alias canceling constraint (Vaidyanathan 1993). For type II modulation,  $N'$  is the length of the filter and for the type IV modulation,  $N'$  is the order of the filter.

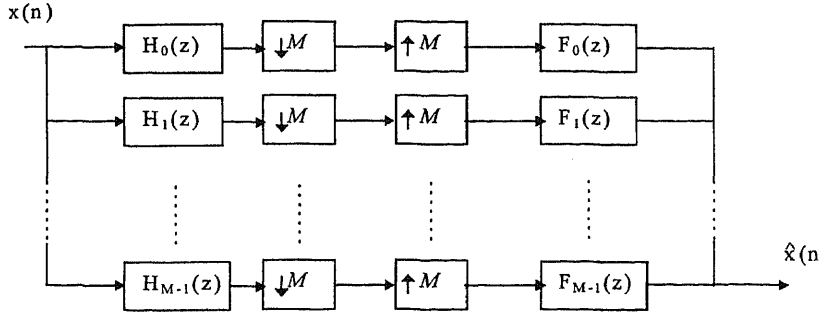


Figure 1.  $M$  channel maximally decimated filter bank.

or with these impulse responses can be separated into  $2M$  polyphase components

$$\begin{aligned}
 H_k(z) &= \sum_{i=0}^{2M-1} \sum_{q=0}^{(N/2M)-1} 2h(2qM + i) \\
 &\quad \times \cos \left( (2k+1) \left( i - \frac{N-1}{2} \right) \frac{\pi}{2M} - (2k+1) \frac{\pi}{4} \right) (-z)^{-2qM} z^{-i} \\
 &= \sum_{i=0}^{2M-1} G_i(-z^{2M}) \\
 &\quad \times \cos \left( (2k+1) \left( i - \frac{N-1}{2} \right) \frac{\pi}{2M} - (2k+1) \frac{\pi}{4} \right) z^{-i}, \tag{2}
 \end{aligned}$$

$$\text{where } G_i(-z^{2M}) = \sum_{q=0}^{(N/2M)-1} 2h(2qM + i)(-z)^{-2qM}
 \begin{cases} 0 \leq q \leq (N/2M) - 1, \\ 0 \leq k \leq M - 1. \end{cases}$$

an efficient implementation of this filter bank, the length of the prototype filter  $N$  is assumed to be an even multiple of  $M$ , i.e.,  $N = 2mM$ , where  $m$  is an even integer; this condition is not restrictive as a prototype of any length can be padded with an appropriate number of zeroes. This simplifies the filter transfer function to:

$$\begin{aligned}
 H_k(z) &= \sum_{i=0}^{2M-1} 2G_i(-z^{2M}) \cos \left( (2k+1)(2i+1-M) \frac{\pi}{4M} \right) z^{-i}, \\
 &0 \leq k \leq M - 1. \tag{3}
 \end{aligned}$$

A fast algorithm for implementing this filter bank using the IDCT-IV like modulation matrix (the modulation matrix used here are same as the DCT-IV matrix without the initial scaling factor for the first coefficient) can be obtained by reordering the polyphase components as follows:

$$G'_i = \begin{cases} z^{-M/2} G_{i+(M/2)}, & \text{for } i = 0, 1, \dots, (3M/2) - 1, \\ -z^{3M/2} G_{i-(3M/2)}, & \text{for } i = 3M/2, \dots, 2M - 1. \end{cases} \tag{4}$$

In terms of this new sequence, the analysis filters are expressed as follows:

$$H_k(z) = \sum_{i=0}^{M-1} 2(z^{-i} G'_i(-z^{2M}) - z^{-(2M-1-i)} G'_{2M-1-i}(-z^{2M})) \\ \times \cos\left((2k+1)(2i+1)\frac{\pi}{4M}\right), \quad 0 \leq k \leq M-1. \quad (5)$$

In matrix notation, the analysis filter bank vector  $\mathbf{h}(z)$  becomes:

$$\mathbf{h}(z) = \mathbf{Tg}(z), \quad (6)$$

where

$$\mathbf{h}(z) = \begin{bmatrix} H_0(z) \\ H_1(z) \\ \vdots \\ H_{M-1}(z) \end{bmatrix},$$

$$\mathbf{g}(z) = \begin{bmatrix} G'_0(-z^{2M}) - z^{-(2M-1)} G'_{2M-1}(-z^{2M}) \\ z^{-1} G'_1(-z^{2M}) - z^{-(2M-2)} G'_{2M-2}(-z^{2M}) \\ \vdots \\ z^{-(M-1)} G'_{M-1}(-z^{2M}) - z^{-M} G'_M(-z^{2M}) \end{bmatrix}$$

and  $\mathbf{T}$  is an  $M \times M$  IDCT IV like modulation matrix with elements:

$$t_{ki} = 2 \cos\left((2k+1)(2i+1)\frac{\pi}{4M}\right).$$

The corresponding synthesis filters  $F_k(z)$ , can also be expressed in terms of the DCT IV like modulation matrix:

$$F_k(z) = \sum_{i=0}^{M-1} 2z^{-K} (z^{-i} G'_i(-z^{-2M}) - z^{-(2M-1-i)} G'_{2M-1-i}(-z^{-2M})) \\ \times \cos\left((2k+1)(2i+1)\frac{\pi}{4M}\right), \quad 0 \leq k \leq M-1, \text{ where } K=N-2M, \quad (7)$$

In matrix notation, the synthesis filter vector  $\mathbf{f}(z)$  is written as

$$\mathbf{f}^T(z) = z^{-N} \mathbf{g}^T(z^{-1}) \mathbf{T}^T, \quad (8)$$

where,  $\mathbf{f}^T(z) = [F_0(z) \ F_1(z) \ \dots \ F_{M-1}(z)]$ .

Similarly, the analysis filter and synthesis filter vectors for type II modulation kernel can be expressed in terms of the DCT II modulation matrix as given below:

$$\mathbf{h}_{II}(z) = \mathbf{T}_{II} \mathbf{g}_{II}(z), \quad (9)$$

where

$$\mathbf{h}_{II}(z) = \begin{bmatrix} H_0(z) \\ H_1(z) \\ \vdots \\ H_{M-1}(z) \end{bmatrix},$$

$$\mathbf{g}_{II}(z) = \begin{bmatrix} G'_0(-z^{2M}) \\ z^{-1}G'_1(-z^{2M}) - z^{-(2M-2)}G'_{2M-2}(-z^{2M}) \\ \vdots \\ z^{-(M-1)}G'_{M-1}(-z^{2M}) - z^{-M}G'_{M+1}(-z^{2M}) \end{bmatrix}$$

$\mathbf{T}_{II}$  is an  $M \times M$  IDCT II like modulation matrix with elements

$$t_{ki} = 2 \cos \left( (2k+1)i \frac{\pi}{2M} \right).$$

synthesis filter vector  $\mathbf{f}(z)$  is written as

$$\mathbf{f}_{II}^T(z) = z^{-N} \mathbf{g}_{II}^T(z^{-1}) \mathbf{T}_{II}^T \quad (10)$$

polyphase structure, similar to the one given, that implements the analysis filterbank for IV modulation is shown in figure 2.

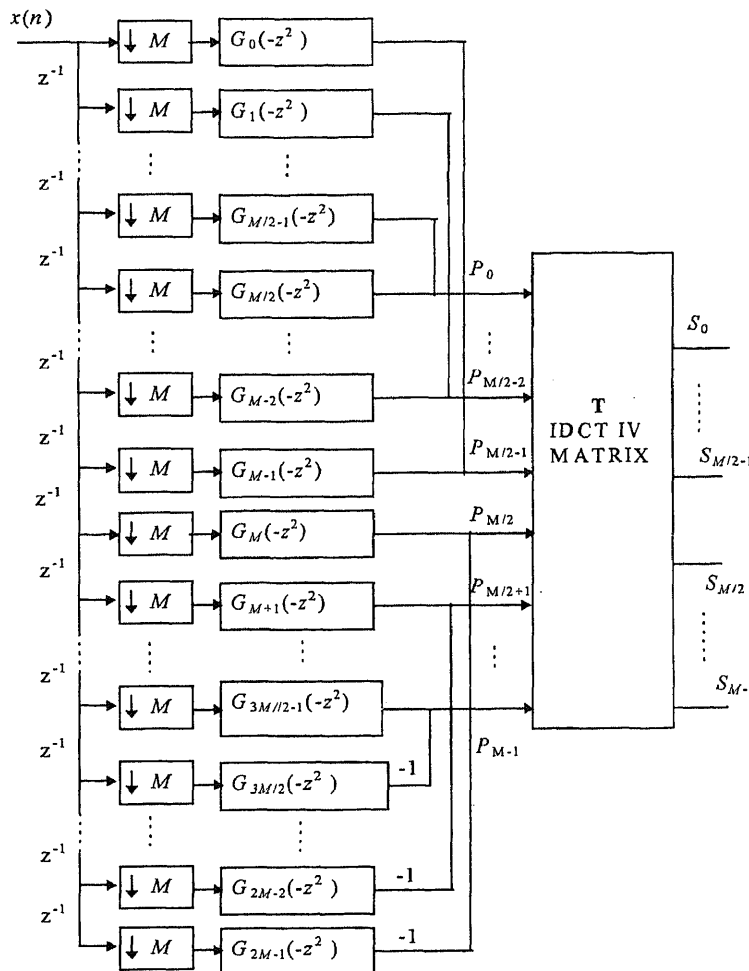


Figure 2. Cosine modulated analysis filter bank in terms of IDCT IV.

The analysis filters  $H_k(z)$  channelize the input signal into  $M$  subband signals  $S_k$ , which are in turn decimated by  $M$ . These subband components can also be expressed in matrix form in terms of the IDCT matrix and polyphase components as:

$$\mathbf{S} = \mathbf{T}\mathbf{P} \quad (11)$$

where  $\mathbf{S} = [S_0, S_1, \dots, S_{M-1}]^T$  is a vector of subband components  $S_k$  and  $\mathbf{P} = [P_0, P_1, \dots, P_{M-1}]^T$  is the vector of polyphase components  $P_i$  (i.e.,  $\mathbf{P} = \mathbf{g}(z)\mathbf{X}(z)$ , where  $\mathbf{X}(z) = [x(z) z^{-1}x(z) \dots z^{-M+1}x(z)]^T$ ) and  $\mathbf{T}$  is a  $M \times M$  orthogonal IDCT IV matrix. For an oversampled signal with a normalized bandwidth of  $r$  ( $2.F/F_s$ , where  $F$  is the bandwidth of the signal and  $F_s$  is the sampling frequency), and the last  $K = \lceil(1-r) \cdot M - 1\rceil$  subband samples are not present.

The  $p$  missing (or lost) samples are so aligned that a minimum number of polyphase components are unknown. In the case of a burst of erasures, the erased sample indices range from  $M - p/2 \pmod{M}$  to  $M + p/2 \pmod{M}$ , so that only  $\lceil p/2 \rceil$  polyphase components are unknown. Then the number of channels of the filter bank  $M$  are chosen according to:

$$M = \left\lceil \frac{(p+1)}{2} \right\rceil / (1-r) \Big|_2, \quad (12)$$

where,  $\lceil \cdot \rceil_2$  denotes rounding to an even number towards infinity.

For the filterbank with DCT-II modulation matrix, the number of unknown polyphase components is  $\lceil(p+1)/2\rceil$ . Therefore, when the length of erasure burst is even the number of unknown polyphase components for the filter bank with DCT-IV modulation matrix is one less than that for the filter bank with DCT-II modulation matrix.

Next, split the polyphase vector into a vector of known components  $\mathbf{P}_1$  and a vector of unknown components  $\mathbf{P}_2$ , so that

$$\begin{bmatrix} \mathbf{S}_1 \\ \mathbf{S}_2 \end{bmatrix} = \begin{bmatrix} \mathbf{T}_{11}^P & \mathbf{T}_{12}^P \\ \mathbf{T}_{21}^P & \mathbf{T}_{22}^P \end{bmatrix} \begin{bmatrix} \mathbf{P}_1 \\ \mathbf{P}_2 \end{bmatrix} \quad (13)$$

where,  $\mathbf{T}_{11}^P$ ,  $\mathbf{T}_{12}^P$ ,  $\mathbf{T}_{21}^P$  and  $\mathbf{T}_{22}^P$  are the submatrices of a permuted IDCT IV matrix. The columns of the modulation matrix  $\mathbf{T}$  are permuted according to the known and unknown polyphase components. As the input signal is bandlimited, the subband component vector  $\mathbf{S}_2$  can be set to zero. This results in a system of linear equations which are solved to determine the unknown polyphase components  $\mathbf{P}_2$ .

$$[\mathbf{T}_{22}^P] \mathbf{P}_2 = -[\mathbf{T}_{21}^P] \mathbf{P}_1. \quad (14)$$

As shown in figure 2, when the erased sample burst indices range from  $M - p/2 \pmod{M}$  to  $M + p/2 \pmod{M}$ , the first  $p/2$  components of the polyphase vector  $\mathbf{P}_{2F} = [P_0, P_1, \dots, P_{p-1}]$  will have to be determined for the first  $M$ -sample input block. When the next  $M$ -sample block is the input, the last  $p/2$  components of the polyphase vector  $\mathbf{P}_{2L} = [P_{M-p-1}, P_{M-p}, \dots, P_{M-1}]$  are unknown. The unknown polyphase component vectors alternate in this manner until all the erased samples are restored.

In the preceding paragraphs, we have considered  $2M$  periodicity in determining  $M$  from the given normalized bandwidth of  $r$  and burst length  $p$ . An alternate view of figure 2 is to consider a periodicity of  $M$  in determining  $M$  from the oversampling factor and burst

length. In this case, each missing polyphase component in the top  $M$  polyphase components ( $-z^{2M}$ ), has a counterpart, separated by  $M$  from it, that is also missing. In this case, DCT submatrix is always constant for every  $M$ -sample block during the restoration process. The number of subbands  $M$  is determined by

$$M = \left\lceil \frac{p+1}{1+r} \right\rceil_2 . \quad (15)$$

number of channels of the analysis filter bank obtained using (15) is less than twice the number of channels obtained using (12). Therefore, the interval between the error bursts using  $2M$ -periodicity (with  $M$  given by (12)) can, in some cases, be reduced by using  $M$ -periodicity (with  $M$  given by (15)).

## Error in restoration of erased samples

estimated polyphase components are passed through the polyphase structure of the synthesis filter bank to determine the erased samples. Therefore, the error in the restored samples is given by:

$$\|\delta\mathbf{x}\| = \|\mathbf{g}_e(z^{-1}\delta\mathbf{P}_2(z))\| \leq \|\mathbf{g}_e(z^{-1})\| \|\delta\mathbf{P}_2(z)\| \quad (16)$$

$$\|\delta\mathbf{P}_2(z)\| = \begin{vmatrix} \delta\mathbf{P}_{2F} + z^{-2}\delta\mathbf{P}_{2F} + \dots + z^{-\frac{N}{2M}}\delta\mathbf{P}_{2F} \\ \delta\mathbf{P}_{2L} + z^{-2}\delta\mathbf{P}_{2L} + \dots + z^{-\frac{N}{2M}}\delta\mathbf{P}_{2L} \end{vmatrix}$$

$\|\mathbf{g}_e(z^{-1})\|$  is the norm of the polyphase components in  $g(z)$  corresponding to  $\mathbf{P}_{2F}$  and

the error of the estimates of the unknown polyphase components using (14) is due to error introduced into (14) by the assumption that the subband vector  $\mathbf{S}_2$  is zero. The error in the restoration of  $\mathbf{P}_2$ ,  $\delta\mathbf{P}_2$  satisfies:

$$\|\delta\mathbf{P}_2\| \leq \kappa(\mathbf{T}_{22}^p) \frac{\|\mathbf{S}_2\|}{\|\mathbf{T}_{21}^p \mathbf{P}_1\|} \|\mathbf{P}_1\| \quad (17)$$

where,  $\kappa(\mathbf{T}_{22}^p)$  is the condition number of matrix  $\mathbf{T}_{22}^p$ <sup>3</sup> and  $\|\cdot\|^4$  denotes the norm of matrix or vector (Kreyszig 1993). For error vector  $\delta\mathbf{T}_{22}^p$  to be small, both the condition number of  $\mathbf{T}_{22}^p$  and the norm subband vector  $\mathbf{S}_2$  should be small. If the condition number of the matrix  $\mathbf{T}_{22}^p$  can be controlled (through the choice of  $M$ ), the norm of the subband vector  $\mathbf{S}_2$  can be reduced by using a filter bank with higher stop-band attenuation.<sup>5</sup> It should also be noted that as the condition number of the matrix  $\mathbf{T}_{22}^p$  increases, the word-length required

<sup>3</sup> condition number of matrix  $A\kappa(A)$ , is the ratio of largest singular value of  $A$  to the smallest singular value of  $A$ . The norm of matrix  $A$  is the largest singular value of  $A$ .

<sup>4</sup> assuming a perfectly bandlimited signal in  $[0, (M-K)\pi]$ , the  $L^\infty$  norm of the decimated signal in any high band (that will be set to zero) has an upper bound of  $M-K$  times the supremum of the  $L^\infty$  norms of the signals in the first  $M-K$  subbands multiplied by the supremum of stopband gain of the  $K$  high subband filters. This again will be small if the maximum stopband gain of the prototype is small.

$M$	$\kappa(\mathbf{T}_{22}^p)$ $\mathbf{P}_{2F}$ DCT IV	$\kappa(\mathbf{T}_{22}^p)$ $\mathbf{P}_{2L}$ DCT IV	$\kappa\mathbf{T}_{22}^p$ $\mathbf{P}_{2F}\text{DCT}$ II	$\kappa(\mathbf{T}_{22}^p)$ $\mathbf{P}_{2L}$ DCT II
8	91.2789	11.2485	24.4259	41.5830
12	225.6398	27.2672	56.7647	108.2118
24	954.6982	114.6825	231.7052	472.3874
32	1711.200	205.4472	413.3550	850.5666

**Table 1(b).** Condition numbers for DCT II and DCT IV submatrices  $\mathbf{T}_{22}^p$  for different  $K$  with  $M = 8$ .  $\mathbf{T}_{22}^p$  for different  $M$  with  $K = 2$ .

$K$	$\kappa(\mathbf{T}_{22}^p)$ $\mathbf{P}_{2F}$ DCT IV	$\kappa(\mathbf{T}_{22}^p)$ $\mathbf{P}_{2L}$ DCT IV	$\kappa\mathbf{T}_{22}^p$ $\mathbf{P}_{2F}\text{DCT}$ II	$\kappa(\mathbf{T}_{22}^p)$ $\mathbf{P}_{2L}$ DCT II
2	91.2789	11.2485	24.4259	41.5830
3	667.0022	40.2057	133.4108	190.1040
4	1059.4000	58.7428	260.1650	236.5874

for solving (14) also increases and imposes practical constraints on use of the usefulness of the algorithm. In the case of a large erasure burst, the reconstruction (psuedo-QMF, perfect, or near-perfect) properties of the prototype filter has only a negligible effect on restoration error.<sup>6</sup> Consequently, in the following examples used to illustrate lost-sample restoration, we have used the near-equiripple pseudo-QMF bank designed using the method described in by Jayasimha & Hiremath (1998).

The condition number of the matrix  $\mathbf{T}_{22}^p$  deteriorates with increasing  $M$  and with the number of missing polyphase components (i.e., the length of the lost-sample burst). The condition number of the matrix  $\mathbf{T}_{22}^p$  used while estimating  $\mathbf{P}_{2F}$  and  $\mathbf{P}_{2L}$  vectors is tabulated in tables 1a and b, respectively. As can be observed from the table, the maximum condition number is for the DCT-IV modulation matrix. Therefore, when the condition number is large, the filter bank with the DCT-II modulation matrix is used (in particular, for odd  $p$ ).

To compensate for the ill-conditioning of matrix  $\mathbf{T}_{22}^p$ ,  $\|\mathbf{S}_2\|$  should be small and the prototype filter must be designed to have high stopband attenuation. A method to design high-order, large even  $M$ , filterbanks (where  $M$  is an even composite number) is discussed by Hiremath & Jayasimha (1997).

#### 4. Interpolation of periodic erasure singlets and doublets

A block diagram for the efficient restoration of periodic, erasure singlets, compared with the restoration of periodic erasure singlets using a type II maximally-decimated  $M$ -channel (where  $M$  is divisible by 4) cosine modulated filterbank, is illustrated by an example in figure 3 for periodic erasure singlets with periodicity of  $I = 4$  and  $M = 12$ .

<sup>6</sup>In pseudo-QMF banks, the stopband attenuation; however, the restoration error is of the order of the stopband attenuation

Table 2. Restoration ESR for erasure bursts of various lengths ( $M = 8$ ).

Structure	Actual samples	Restored samples	ESR upper bound	ESR practical
Singlet	3352	3353	0.0026	0.00029
Doublet	3666, 3352	3668, 3345	0.004629	0.001465
Triplet	3666, 3352, 2855	3668, 3345, 2873	0.006688	0.001317
Quadruplet	3806, 3666, 3352, 2855	3779, 3651, 3352, 2871	0.005827	0.005057
Triplet	3806, 3666, 3352, 2855, 2248	3779, 3651, 3352, 2871, 2229	0.007171	0.005477

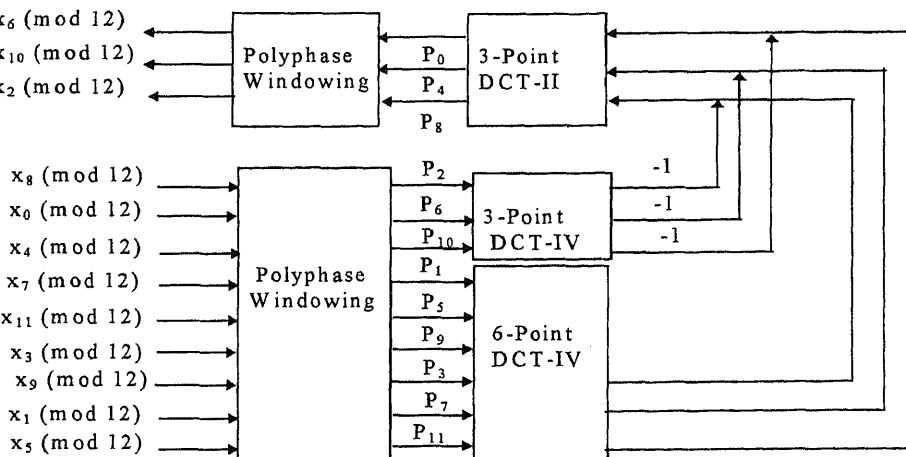
the complexity per interpolated point for the restoration of singlets with  $M = 12, I = 4$  ( $N = 128$ ) is given by  $C = I/M (\text{DCT}_{\text{IV}}^6 + \text{DCT}_{\text{IV}}^3 + 3 \cdot \text{adds} + \text{DCT}_{\text{II}}^3) + W/M$ . It requires approximately 25 multiplications and 35 additions.

The usual FIR interpolator derived from a 4th band filter (Adams 1991) for the restoration (with similar performance) of these periodic erasure singlets has 89 taps and uses 67 additions and 34 multiplications.

In a similar manner, doublets can be restored using the modulation matrix of DCT-II for which no FIR interpolator is proposed by Adams (1991). Note that the condition number  $\kappa(\mathbf{P}_{22}^p)$  is one and the error in the estimation depends upon the subband component  $\mathbf{x}_1$ .

### Erasure burst restoration example

The randomly selected position in audio data sampled at 44.1 kHz (an example from 'The Straits'), bandlimited to 13.23 kHz, is used to test the described restoration method. A  $M = 8, N = 128$  low-pass prototype with specifications: Passband edge normalized frequency: 0.01042 Stopband edge normalized frequency: 0.11458 Stopband attenuation: 40 dB was designed (Jayasimha & Hiremath 1998). This odd-length prototype padded with a leading zero, and used with a DCT-II modulation matrix for fast implementation, has a construction error of  $-54$  dB. The average restoration error to signal ratio, a measure

Figure 3. Restoration of singlet  $s$  ( $M = 12, I = 4$ ).

of the restoration's accuracy, is:

$$ESR = \left( \left\{ \sum_n (x(n) - \hat{x}(n))^2 \right\} / \left\{ \sum_n x^2(n) \right\} \right)^{1/2}. \quad (18)$$

The restoration ESR's for isolated bursts of various lengths for  $M = 8$  are given in table 2.

## 6. Conclusion

A novel, low-complexity cosine-modulated filterbank approach to short-burst erasure interpolation has been described. Potential applications areas of short-erasure burst restoration are in removal of lightning-induced impulsive noise in VLF and LF communications (detected by short-duration saturation of amplifiers and ADCs) and the extension of the ADC dynamic range when the bandlimited signal being acquired is slightly oversampled. One example of the latter application is that saturated signals in short regions of some 16-bit compact disk recordings may be restored and played back on 18-bit DACs.

## References

Adams R W 1991 Non-uniform sampling of audio signals. Preprint 3140 (E-1) of the 91st convention of the Audio Engineering Society, New York

Hiremath C G, Jayasimha S 1997 Design of large order prototype filter for composite M-channel filterbanks. *Proc. of the Third National Conference on Communications and Networking, NCC-97*, pp 63–65

Jayasimha S, Hiremath C G 1998 Pseudo-QMF banks with near-equiripple performance. *IEEE Trans. Signal Process.* SP-46: 209–214

Kreyszig E 1993 *Advanced engineering mathematics* (New York: John Wiley & Sons) p 998

Marks R J II Restoring lost samples from an oversampled band-limited signal. *IEEE Trans. Acoust. Speech Signal Process.* ASSP-31: 752–755

Marks R J II, Radbel M 1984 Error of linear estimation of lost samples in an oversampled band-limited signal. *IEEE Trans. Acoust. Speech Signal Process.* ASSP-32: 648–654

Strang G, Nguyen T 1996 *Wavelets and filter banks* (Wellesley, MA: Wellesley-Cambridge Press) pp 276–287

Vaidyanathan P P 1993 *Multirate systems and filter banks* Signal Processing Series (Englewood Cliffs, NJ: Prentice Hall) pp 370–372

Vaidyanathan P P, Liu V C 1988 Classical sampling theorems in the context of multirate and polyphase digital filter structures. *IEEE Trans. Acoust. Speech Signal Process.* ASSP-36: 1480–1495

# Comparative performance analysis of versions of TCP in a local network with a mobile radio link

ANURAG KUMAR<sup>1</sup> and JACK HOLTZMAN<sup>2</sup>

<sup>1</sup> Department of Electrical Communication Engineering, Indian Institute of Science, Bangalore 560 012, India

<sup>2</sup> WINLAB, Rutgers University, Piscataway, NJ 08855, USA

e-mail: anurag@ece.iisc.ernet.in; holtzman@winlab.rutgers.edu

**Abstract.** The scenario is that a bulk data transfer is being performed over a TCP connection, from a host on a local area network (LAN) to a mobile host attached to the LAN by a radio link. In an earlier work we had assumed that packet losses in a TCP connection over a radio link are statistically independent. In this paper, we extend this analysis to a Rayleigh fading link, which we model by a two-state Markov model. The bulk throughputs of TCP-OldTahoe and TCP-Tahoe are compared with and without fading, for various average signal-to-noise ratios. We also study the performance with a link protocol on the wireless link, and study the effect of varying the link packet size, the number of link packet attempts, and the vehicle speed. For the parameters of the BSD UNIX implementation, over a 1.5 Mbps wireless link, we find that, with fading, a signal-to-noise ratio of at least 30 dB is required to get reasonable throughput with TCP Tahoe or OldTahoe; this corresponds to at least 100 times more power than is needed without fading.

For fixed signal-to-noise ratio, as the vehicle speed varies there are roughly 3 regions of performance: at very low speeds (pedestrian speeds) the throughput is very good; at low vehicular speeds the throughput deteriorates, and again becomes very good at higher vehicle speeds. The speeds corresponding to the various regions depend on the parameters of the link protocol.

**Keywords.** Mobile internet; mobile computing; TCP modelling; TCP over fading channels.

## Introduction

The network scenario (figure 1) is motivated by the many recent experimental studies of performance over wireless mobile links (Bakre & Badrinath 1995; Cáceres & Iftode

work was done while the first author was on Sabbatical at WINLAB, Rutgers University

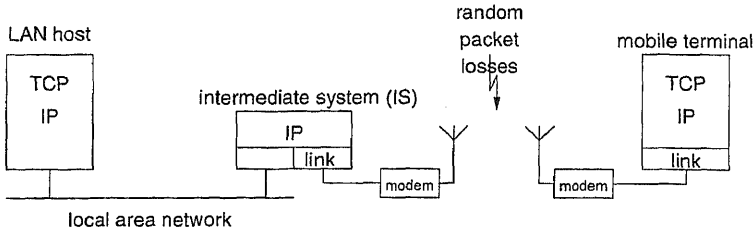


Figure 1. A LAN host with a TCP connection to a mobile host.

1995; Balakrishnan *et al* 1997). We are interested in the data throughput, from the LAN host to the mobile terminal, that can be achieved by various versions of TCP, when the wireless link introduces random packet losses. In our earlier work on this problem (Kumar 1996) (see also Mishra *et al* 1993, Lakshman & Madhow 1997) a simple loss model was assumed: TCP packets were transmitted in their entirety over the wireless channel, and each packet was lost independently of anything else with probability  $p$  (i.e., the Bernoulli loss model). The Bernoulli loss model would correspond to a nonfading channel with additive white Gaussian receiver noise. It is well known (Jakes 1974; Parsons 1992) that when the mobile and the transmitter are not in line-of-sight, the mobile receiver antenna observes a superposition of multiple reflected and diffracted signals that are out of phase with each other. The phase relationship between the interfering multipath signals is continuously changing as the vehicle moves. Destructive interference of these signals leads to "fading". The fade durations depend on the velocity of the vehicle and the radio carrier frequency. For high speed radio transmission (e.g., 1.5 Mbps), typical carrier frequencies (e.g., 900 MHz), and the usual vehicle speeds, the fade durations are comparable to the transmission times of TCP packets, or are multiples of transmission times of typical link packets. Thus the packet losses cannot be modelled as being independent of one other.

In this paper, we model the losses using a two state Markov model. We assume that a packet succeeds with probability 1 in the Good state, and with probability 0 in the Bad state. The TCP protocol alternates between packet transmission periods and loss recovery periods. It was shown by (Kumar 1996) that the TCP packet transmission process can be modelled as a Markov Renewal-Reward process (Wolff 1990), the Markov renewal instants being the epochs at which the first packet loss occurs in a transmission period, and the "reward" corresponding to successful packet transmissions. With the simple fading model, this Markov renewal-reward analysis is easily adapted. We obtain numerical results for the same parameters as by Kumar (1996).

In a previous work, Gilbert has used a two state Markov model to model bursty error rates in digital transmission links (Gilbert 1960). Wang and Moayeri (1995) have studied multistate Markov chain models for radio channels, and have, in particular, developed a finite state Markov model for a Rayleigh fading channel. Recently, Chaskar *et al* (1996) have analysed a wide area TCP connection in which the receiver end system is connected to the wireline network by a wireless mobile link. A Rayleigh fading model is assumed for the wireless link, and a two state Markov model is used. It is assumed that the link protocol on the wireless channel repeatedly retransmits the link packets until they succeed. Since this implies an increase in the effective transmission time of TCP packets,

main concern in the paper is the additional buffer requirement (at the wireline-to-wireless router) as a result of wireless channel losses. It is argued that for a Markovian fading model (implying exponentially distributed fade durations) TCP will yield reasonable throughputs if the buffer space grows only as fast as the logarithm of the bandwidth-delay product.

In our analysis, we assume that there are adequate buffers at the wireless router so that buffer overflow is not a concern. On the other hand, we permit the possibility of packet loss on the wireless link, either because there is no link protocol, or because the link protocol limits the number of retries. The effect of losses on the TCP throughput is studied. We provide results for throughput performance of TCP-OldTahoe and Tahoe as the signal-to-noise ratio varies, and compare the situations with and without Rayleigh fading. For a fixed signal-to-noise ratio, we then study the variation of TCP throughput with the vehicle speed. Varying the vehicle speed effectively varies the duration of the fades and the good conditions on the radio link, and results in interesting behaviour of the TCP throughput as a function of the vehicle speed.

This paper is organised as follows. In § 2 we develop the two state Markov loss model. In § 3 we describe TCP's window adaptation protocol. In § 4 we adapt the throughput analysis developed earlier (Kumar 1996) to the Markov loss model. In § 5 some numerical results and their discussion are presented.

## A Markov model for Rayleigh fading

### *Review of the Rayleigh fading model*

If the radio carrier is digitally modulated; for Pulse Amplitude Modulation (PAM), the transmitted signal is written as

$$x(t) = \sqrt{2} \operatorname{Re} \left\{ \sum_{k=-\infty}^{\infty} s_k e^{j\theta_k} p(t - kT) e^{j2\pi f_c t} \right\}$$

where  $p(\cdot)$  is the baseband pulse,  $f_c$  is the carrier frequency, and  $(s_k, \theta_k)$  is the complex modulating sequence (see, for example, (Lee & Messerschmitt 1988)). Analysis of the relative position of multipath signals, in the presence of receiver mobility, yields the following model for the received signal (Rappaport 1996):

$$y(t) = \sqrt{2} \operatorname{Re} \left\{ \sum_{k=-\infty}^{\infty} s_k r(t) e^{j(\theta_k + \phi(t))} \cdot p(t - kT) e^{j2\pi f_c t} \right\} \quad (1)$$

where  $r(t)$  is the random attenuation and  $\phi(t)$  is the random phase noise process. If the power fading phenomena (power law attenuation, and log-normal fading (Rappaport 1996)) are compensated for by power control, and the multipath phenomenon is spatially uncorrelated, then the process  $r(t)$  is stationary with a Rayleigh marginal distribution  $R$ , with density

$$p_R(r) = \frac{r}{\sigma^2} \exp \left( -\frac{r^2}{2\sigma^2} \right).$$

We note that  $E(R^2) = 2\sigma^2$ . The time variations in the process  $r(t)$  are of the order of the Doppler frequency  $f_d$ , which is related to the carrier frequency  $f_c$ , and the vehicle speed  $v$ , by the formula

$$f_d = \frac{vf_c}{c}, \quad (2)$$

where  $c$  is the speed of light. For a 900 Mhz carrier frequency, for example, the above formula yields a Doppler frequency of 3 Hz/m/sec, or 10.8 Hz/km/hr. Thus, for the signalling rates used in high speed wireless transmission (e.g., Mbps), Rayleigh fading can be taken to be roughly constant over several bits (see also Rappaport 1996, pp 165–166).

From (1), the predetection signal-to-noise ratio (SNR), say  $\psi(t)$ , at the receiver is given by

$$\psi(t) = (r(t))^2 \left( \frac{E_b}{N_0} \right)_{xmit}, \quad (3)$$

where  $(E_b/N_0)_{xmit}$  is the “transmitted” SNR. Denote the marginal random variable for the stationary process  $\psi(t)$  by  $\Psi$ ; then we have

$$\Psi = R^2(E_b/N_0)_{xmit}, \quad (4)$$

where  $R$  is the marginal of the process  $r(t)$ , as defined above. The *average* effective received SNR is then given by

$$\begin{aligned} E(\Psi) &= 2\sigma^2 \left( \frac{E_b}{N_0} \right)_{xmit} \\ &=: \left( \frac{E_b}{N_0} \right). \end{aligned}$$

In dB units we can now write (4) as

$$(\Psi)_{dB} = \left( \frac{E_b}{N_0} \right)_{dB} + (A)_{dB} \quad (5)$$

where  $A := R^2/2\sigma^2$ , and the distribution of  $A$  is known to be given by  $P(A > a) = e^{(-a)}$  (Rappaport 1996). As observed above, the SNR  $\psi(t)$  varies slowly as compared to the signalling rate. When the SNR is low (i.e., a large negative values of  $(A)_{dB}$ ), this situation persists for a while and the bit error rate (BER) is high; then the SNR improves and stays high for a while, yielding a low BER. This view motivates a Markov model for packet loss; we develop the model in the next subsection.

## 2.2 The Markov packet loss model

For a given average SNR  $(E_b/N_0)$  (say 30 dB) we determine the amount by which the SNR must drop below the average so that the channel enters the “Bad” state (say 20 dB, i.e., a factor of .01); call this “margin”  $\alpha$ , in dB units. Then, defining  $\delta := 10^{-\alpha/10}$  (i.e.,  $\delta = .01$  for  $\alpha = 20$  dB), the fraction of time that the channel is in the Bad state is given by  $P(A \leq \delta) = 1 - e^{-\delta}$ . Thus, fixing  $\alpha$  fixes the fraction of time that the channel is in the Bad state. To obtain the mean durations in each state, we use results from level crossing

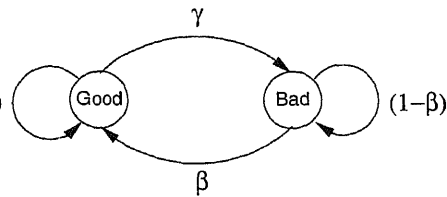


**Figure 2.** Transition structure of the Markov loss model.

ysis of the process  $r(t)$  (see, Parsons 1992). Defining  $G(\delta)$ , and  $B(\delta)$ , as the mean times in the Good and Bad states, respectively, the following formulas are obtained

$$G(\delta) = \frac{f_d^{-1}}{\sqrt{2\pi\delta}}, \quad (6)$$

$$B(\delta) = \frac{f_d^{-1}(e^\delta - 1)}{\sqrt{2\pi\delta}}, \quad (7)$$

where  $f_d$  is given by (2). For small  $\delta$ ,  $e^\delta - 1 \approx \delta$ , hence (6) and (7) yield

$$B(\delta) \approx \delta G(\delta). \quad (8)$$

The loss model is a discrete “time” Markov chain whose transitions are embedded at packet boundaries; thus we express the Good and Bad periods in units of packet transmission time on the link. The transition structure of the model is depicted in figure 2. The chain is assumed to be embedded at the *beginnings* of packet transmissions. Thus, if a number of packets are being transmitted back to back, and if the chain is in the Good state when the next packet is about to be transmitted then this packet will be Good, and the next packet will be Good or Bad with probabilities  $1 - \gamma$  and  $\gamma$ , respectively. It follows, from (8), that

$$\frac{\gamma}{\beta} \approx \delta.$$

In our calculations we will use the above approximation, as  $\delta \leq 0.1$  (i.e.,  $\alpha > 10$  dB) in our numerical results. Observe that we are making the tacit assumption that the durations during which the SNR is above or below the threshold level are exponentially distributed; this is not true (see Rice 1958), but the minimal Markov model that we have considered does not model any additional characteristic of the fading process.

Given  $\alpha$ , equivalently  $\delta$ , the individual values of  $\gamma$  and  $\delta$  in the Markov model are determined from the Doppler frequency  $f_d$  (2), and (6) and (7). For example, consider packet transmission times of 7.5 ms (e.g., 1.5 Mbps link, and 1400byte packets),  $f_c = 900$  MHz,  $\alpha = 20$  dB. For a speed of 5 kmph,  $f_d = 4.17$  Hz, the mean good period is about 1.8 packets, the mean bad period is about 1.28 packets, and  $\gamma = 0.0078$ ; at a speed of 10 kmph,  $f_d = 83.3$  Hz, the mean good period is about 6.4 packets, the mean bad period is about 0.064 packets, and  $\gamma = 0.156$ . Thus, clearly, some care is needed in using this model for high vehicle speeds at which the fade duration is smaller than one packet length. Without a link protocol, whenever there is a fade during a packet transmission, that packet is lost, even though the channel is good during some parts of the packet. For high speeds, for which the fade durations are smaller than a packet (but not so high that  $G + B <$  mean

pkt xmission time), we take  $\beta = 1$  (i.e., exactly one packet is lost in each fade), and  $\gamma$  is obtained from the following equation

$$\gamma = \left( \frac{G + B}{\text{mean pkt xmission time}} - 1 \right)^{-1}.$$

Thus, at low speeds, the probability that a packet is bad is just  $\delta/1 + \delta$ , whereas for high speeds, when the fades are shorter than the packet transmission time, the probability that a packet is bad *increases* with increasing speed, even though  $\delta$  is fixed.

### 2.3 The loss model with a link protocol

The round trip propagation delay on terrestrial mobile radio links is typically smaller than the packet transmission time. Consequently, a stop-and-wait link protocol suffices. We characterise a link protocol by the link packet length and the number of times it attempts a packet.

Observe that with 128byte link packets and 1.5 Mbps transmission, the link packet transmission time is about 0.68 ms. For 1400byte TCP packets, there are 11 link packets in a TCP packet and for speeds above 30 or 40 kmph the mean fade duration is less than 2 or 3 link packets. Thus, with a link protocol, we embed the Markov packet loss model (figure 2) at the beginnings of link packet transmissions. We use the loss model to obtain the probability of TCP packet loss, and assume that TCP packet losses are independent at the TCP packet level. This assumption is adequate if the link packets are small and the number of link packets in a TCP packet is large. We assume that the first link packet in a TCP packet finds the Markov model in its stationary distribution. The probability of TCP packet loss is then the probability that for at least one link packet all attempts fail. The link protocol also causes an increase in TCP packet transmission time; we use the link level Markov loss model to obtain the inflated mean TCP packet transmission time.

Let  $N$  denote the maximum number of attempts of a link packet; and  $L$  denote the number of link packets in a TCP packet. Recalling that the Markov process is embedded at the beginnings of link packet transmissions, we define

$$p_n = \text{Prob}\{\text{at least 1 out of } n \text{ link packets fails, given that the initial state is Good}\}$$

$$q_n^{(k)} = \text{Prob}\{\text{at least 1 out of } n \text{ link packets fails, given that the first link packet has already had } k (< N) \text{ bad attempts and the initial state is Bad}\},$$

$$p = \text{Prob}\{\text{a TCP packet is bad}\}.$$

Assuming that the first link packet in a TCP packet finds the Markov process in its stationary distribution, we have

$$p = \frac{\beta}{\gamma + \beta} p_L + \frac{\gamma}{\gamma + \beta} q_L^0.$$

The values of  $p_n$ ,  $1 \leq n \leq L$  and  $q_n^{(k)}$ ,  $1 \leq n \leq L$ ,  $0 \leq k \leq N-1$  are easily obtained from the following equations by recursive substitution, with the boundary conditions:  $p_1 = 0$ ,  $q_n^{(N-1)} = 1$ ,  $1 \leq n \leq N$ , and  $q_1^{(k)} = (1-\beta)^{(N-1)-k}$ ,  $0 \leq k \leq (N-1)$ . For  $n > 1$  and

$k < N - 1$

$$\begin{aligned} p_n &= (1 - \gamma)p_{n-1} + \gamma q_{n-1}^{(0)}, \\ q_n^{(k)} &= \beta p_n + (1 - \beta)q_n^{(k+1)}. \end{aligned}$$

obtaining the mean effective TCP packet transmission time, taking into account the  $k$  retransmissions, define

$m_n =$  mean number of link packets that will be sent for transmitting a TCP packet of length  $n$  link packets, given that the state at the beginning is Good,

$m_n^{(k)} =$  mean number of link packets that will be sent for transmitting a TCP packet of length  $n$  link packets, given that  $k$  link packets have already been sent for the first link packet and the current state is Bad,

$l =$  mean number of link packets that will be sent for transmitting a TCP packet of length  $L$  link packets.

As for the loss probability, we have

$$l = \frac{\beta}{\gamma + \beta} l_L + \frac{\gamma}{\gamma + \beta} m_L^0.$$

With the boundary conditions  $l_1 = 1$  and  $m_1^{(N-1)} = 1$ , we have the following equations,  $n \geq 1$  and  $0 \leq k < N - 1$ ,

$$\begin{aligned} m_n^{(k)} &= 1 + (1 - \beta)m_n^{(k+1)} + \beta l_n, \\ l_n &= 1 + (1 - \gamma)l_{n-1} + \gamma m_{n-1}^{(0)}, \\ m_n^{(N-1)} &= 1 + (1 - \beta)m_{n-1}^{(0)} + \beta l_{n-1}. \end{aligned}$$

These equations can also be solved recursively.

## TCP window adaptation

At any time  $t$  there is a *lower window edge*  $A(t)$ , which means that all data numbered up to, and including  $A(t) - 1$  has been transmitted and acknowledged. The transmitter sends data numbered  $A(t)$  onwards. There is also the transmitter's *congestion window*  $W(t)$ , which, at time  $t$ , is the maximum amount of data that the transmitter is permitted to send, starting from  $A(t)$ . Under normal data transfer,  $A(t)$  has nondecreasing sample paths, whereas the adaptive window mechanism causes  $W(t)$  to increase or decrease, but never exceed  $W_{\max}$ . The receipt of an acknowledgement (ack) packet that acknowledges some data will cause a jump in  $A(t)$  equal to the amount of data acknowledged, but the change in  $W(t)$  would depend on the particular version of TCP and the state of the congestion control process.

At the transmitter, round-trip time measurements of some packets are used to obtain a running estimate of the packet round-trip time (rtt) on the connection. Each time a new packet is transmitted, the transmitter starts a timer and *resets* the already running transmission timer, if any. The timer is set for a round-trip time-out (rto) value that is

derived from the rtt estimation procedure. Whenever a time-out occurs, retransmission is initiated from the next packet after the last acknowledged packet (i.e., from the sequence number  $A(t)$ ). It is important to note that the TCP transmitter process measures time and sets timeouts only in multiples of a *timer granularity*; for example, BSD UNIX based systems have a timer granularity of 500 ms. Further, there is a minimum timeout duration of 2 or 3 timer “ticks” in most implementations. We will see, in the analysis, that coarse timers have a significant impact on TCP performance. For details on rtt estimation, and the setting of rto values, see Desimone (1993) or Stevens (1994).

The following basic window adaptation procedure (Van Jacobson 1988) is common to all the TCP versions; our description follows that of (Lakshman & Madhow 1997). At all times  $t$  the following are defined for all the protocol versions:

$W(t)$  = the transmitter’s congestion window at time  $t$ ,

$W_{th}(t)$  = the slow-start threshold at time  $t$ .

The evolution of these processes is triggered by acks (only first acks; not duplicate acks) and timeouts as follows.

1. If  $W(t) < W_{th}(t)$ , each ack from the receiver causes  $W(t)$  to be incremented by 1. This is called the *slow start* phase.
2. If  $W(t) \geq W_{th}(t)$ , each ack from the receiver causes  $W(t)$  to be incremented by  $1/W(t)$ . This is called the *congestion avoidance* phase.
3. If *timeout occurs* at the transmitter, at epoch  $t$ ,  $W(t^+)$  is set to 1,  $W_{th}(t^+)$  is set to  $\lceil W(t)/2 \rceil$ , and the transmitter begins retransmission from the packet after the last packet acknowledged.

Note that the transmissions after a timeout always start with the first lost packet. We will call the “window” of packets transmitted from the lost packet onwards, but before retransmission starts as the *loss window*.

If a packet is lost, then the ack number from the receiver will cease to be advanced, and *the transmitter at the LAN host will continue sending packets until the current window is exhausted, or a packet gets through to the receiver and an ack is received*. The last packet transmitted will have a timeout associated with it; in TCP-OldTahoe, retransmission will start only upon the expiry of this timer. Later versions of TCP, i.e., Tahoe, Reno, and NewReno, implement a *fast-retransmit* scheme. Observe that, even if a packet is lost, if subsequent packets get through, the receiver will continue to send back acks, but the “expected packet” number is not incremented. If several (an integer parameter  $K$ , e.g., 3) such “duplicate” acks are received at the LAN host, then it can assume that the loss is a random loss, and not due to congestion. When the number of duplicate acks received reaches the threshold  $K$ , then the packet next expected by the receiver is retransmitted. A complicated recovery phase then follows. In particular, in TCP Tahoe (Fall & Floyd 1996) if the transmitter receives the  $K$ th duplicate ack at time  $t$ , before the timer expires, then the transmitter behaves as if a timeout has occurred and begins retransmission, with  $W(t^+)$  and  $W_{th}(t^+)$  as given by the basic algorithm.

## TCP throughput analysis with the Markov loss model

Assume that, at  $t = 0$  the connection starts with  $W(0) = 1$  and  $W_{th}(0) = \lceil W_{max}/2 \rceil$ , where  $W_{max}$  is the maximum window limit set by the receiver; this usually depends on the receiver's buffer size (typical values are 32 kbytes or 64 kbytes, i.e., several 10's of TCP packets). The protocol starts at time 0 in slow start. Let  $\ell_1$  be the epoch at which the first packet loss occurs, and let  $U_1 = W(\ell_1)$ . As described above, timeout or fast recovery follows and at some later epoch transmission resumes with the first lost packet. If this epoch finds the wireless channel in its Bad state, then a loss occurs immediately, the timeout is doubled, and the next cycle starts with  $W = 1$  and  $W_{th} = 2$ , the minimum value of  $W_{th}$  (Stevens 1994). No successful packet is sent in such a period. Hence, we merge such periods, if any, into the recovery period of the previous cycle. Thus at the beginning of the next cycle, denoted by  $t_1$ , the channel is in the Good state. Again an epoch  $\ell_2$  can be identified at which the first loss occurs in this transmission cycle. For  $k \geq 1$ , let  $t_k$  denote the  $k$ th epoch at which a new transmission cycle starts as described above. For  $k \geq 1$ , we call the interval  $(t_{k-1}, t_k]$  the  $k$ th cycle. In the  $k$ th cycle, let  $\ell_k$  be the epoch at which the first packet is lost in the cycle (this is an end of a packet transmission epoch from the computer). Further, for  $k \geq 1$ , let  $U_k = W(\ell_k)$  denote the transmitter's window size at which packet loss takes place. We take  $U_0 = W_{max}$ . Since the first packet transmitted in each cycle is always good, the state space of the process  $\{U_k\}$  is  $\{2, 3, \dots, W_{max}\}$ .

If the first retransmission after a recovery period finds the channel in the good state, then for TCP-OldTahoe and Tahoe, the value of  $U_k$  determines the values of  $W(t_k^+)$  and  $W_{th}(t_k^+)$ , according to  $W(t_k^+) = 1$  and  $W_{th}(t_k^+) = \lceil U_k/2 \rceil$ . We know that at the beginning of the transmission of the packet that is lost, the channel is in the Bad state. It is thus clear that the evolution of the congestion window process after the first loss epoch in the  $k$ th cycle depends only on the value of  $U_k$ ; thus the process  $\{U_k\}$  is a discrete time Markov chain over the state space  $\{2, \dots, W_{max}\}$ . We can obtain the stationary distribution of this chain. Note that a more complex analysis ensues if losses can occur in either state of the channel.

The mean number of packets successfully transmitted in each cycle, before the first lost packet, is just  $1/\gamma$ . When a loss occurs at the lossy link, there would be some packets queued in the lossy link transmitter and the TCP transmitter at the LAN host will continue sending packets till the congestion window ( $U_k$ ) is exhausted (even if fast-retransmit is implemented, by the time 3 duplicate acks are received, a fast sender would already have exhausted the window). Some of the packets that are transmitted on the lossy link, after the first lost packet, will get through, and will not need to be resent. We denote the mean number of such packets as *residual\_good*.

Thus, for each TCP version, we have a Markov renewal reward process (Wolff 1990), embedded at the epochs  $t_0, t_1, t_2, \dots$ , the reward being the number of good packets put through in each cycle. Then the throughput  $T$  is given by

$$T = \frac{1/\gamma + \text{residual\_good}}{\text{mean\_cycle\_duration}}. \quad (9)$$

With a link protocol and high vehicle speeds, we assume a Bernoulli loss model at the TCP packet level. Hence, for this case the analysis in (Kumar 1996) carries through directly, after accounting for the fact that TCP packet transmission times are longer.

We will assume that the minimum timeout is large compared to the other time scales in the local network; this is true for the numerical parameters that we used (Kumar 1996) (0.75 s minimum timeout, as in BSD and 7.5 ms packet transmission time). Then, if the loss in a cycle is followed by a timeout, we assume that the beginning of the next cycle finds the Markov loss process in its stationary distribution. This is always the case for OldTahoe, since it recovers only after a timeout. In the case of Tahoe, however, if fast retransmission takes place then we need to know the state of the Markov loss process at the beginning of the next cycle.

The following analysis also assumes that the LAN host can transmit much faster than the wireless link. Hence, during the packet transmission periods in a cycle, the wireless link is assumed to be continuously busy. This assumption facilitates the carrying over of the channel state from one packet to the next.

#### 4.1 Analysis of the markov chain $\{U_k\}$

Owing to the above viewpoint, the transition probabilities of  $\{U_k\}$  are slightly different from the ones in our earlier paper (Kumar 1996). For  $M \in \{2, \dots, W_{\max}\}$ , define

$$\theta_M = \text{Prob}\{\text{the next cycle starts with } W_{th} = \lceil M/2 \rceil, \text{ given that the loss window in this cycle is } M\}$$

$$\bar{\theta}_M = \text{Prob}\{\text{the next cycle is forced to start with } W_{th} = 2, \text{ owing to additional timeouts, given that the loss window in this cycle is } M (= 1 - \theta_M)\}.$$

Following the earlier development (Kumar 1996) we can now write down the transition probabilities. Given that  $U_k = M \in \{2, \dots, W_{\max}\}$  (and  $m := \max(2, \lceil M/2 \rceil)$ ), recalling the Markov loss model, and writing  $\bar{\gamma} = 1 - \gamma$ , define two transition probability matrices  $P$  and  $Q$  as follows:

$$p_{M,j} = \begin{cases} \bar{\gamma}^{(j-1)-1}\gamma & 2 \leq j \leq m-1 \\ \bar{\gamma}^{d(k)-1}(1 - \bar{\gamma}^{m+k}) & j = m+k, \\ & 0 \leq k \leq (W_{\max} - 1 - m) \\ \bar{\gamma}^{d(W_{\max}-m)-1} & j = W_{\max} \end{cases}$$

$$q_{M,j} = p_{3,j} (= p_{2,j} = p_{4,j}) \quad \text{for } 2 \leq j \leq W_{\max}$$

where

$$d(k) = (k+1)((m-1)+(k/2\dots)).$$

Note that  $P$  corresponds to the case in which the next cycle starts with  $W_{th} = \lceil M/2 \rceil$  and  $Q$  corresponds to the case in which the next cycle is forced to start with  $W_{th} = 2$ . Finally, we define the vector

$$\Theta = (\theta_2, \dots, \theta_{W_{\max}}),$$

and then the transition probability matrix of  $\{U_k\}$  is written as

$$\text{diag}(\Theta)P + (I - \text{diag}(\Theta))Q, \tag{10}$$

where  $I$  is the  $(W_{\max} - 1) \times (W_{\max} - 1)$  identity matrix.

The matrices  $P$  and  $Q$  are common to the OldTahoe and Tahoe versions with the same values of  $W_{\max}$  and Markov loss model transition probabilities  $\gamma$  and  $\beta$ ; as shown below depends on  $\gamma$  and  $\beta$  for both OldTahoe and Tahoe.

*OldTahoe:* Since we assume that after a timeout the Markov channel model is found in its stationary distribution, for  $M \in \{2, \dots, W_{\max}\}$ ,

$$\theta_M = \frac{\beta}{\gamma + \beta} = 1 - \phi_M.$$

*Tahoe:* Define, for  $M \in \{2, \dots, W_{\max}\}$ ,

$\phi_M = \text{Prob}\{\text{the good transmission period in a cycle is followed by fast retransmission, if the loss window is } M\}$

$\phi_M^{(G)} = \text{Prob}\{\text{the good transmission period in a cycle is followed by fast transmission, and at this epoch the channel is in the Good state}\}$

$\phi_M^{(B)} = \text{Prob}\{\text{the good transmission period in a cycle is followed by fast transmission, and at this epoch the channel is in the Bad state (i.e., } \phi_M^{(B)} = \phi_M - \phi_M^{(G)})\}$ .

follows that

$$\phi_M = \phi_M^{(G)} + (1 - \phi_M) \frac{\beta}{\gamma + \beta}.$$

Recursive equations were developed for computing  $\phi_M^{(G)}$  and  $\phi_M^{(B)}$ ; owing to lack of space here we refer the reader to the full report (Kumar & Holtzman 1996).

Thus the transition probabilities of the process  $\{U_k\}$  can be calculated by first computing  $\phi_M$ ,  $\phi_M^{(G)}$ ,  $\phi_M^{(B)}$ , and  $\theta_M$ , and finally using (10). The stationary distribution can be obtained by any of the many standard techniques. Denote the stationary distribution

$$u_M, 2 \leq M \leq W_{\max}.$$

## 2 Throughput analysis

Given that the loss window is  $M$ , the probability that  $k \leq (M - 1)$  of the remaining packets get through is just  $g_{M-1}^{(k)} + b_{M-1}^{(k)}$ . Given the stationary distribution  $u_M, 2 \leq M \leq W_{\max}$ , the mean number of good packets transmitted in a cycle after the first loss occurs can thus be calculated. This is what we had called *residual\_good* (see (9)).

We adopt the approximate mean cycle time analysis discussed in § 4.2 of Kumar (1996). Letting  $Z$  denote the mean of the loss window distribution, we take the average window during packet transmissions to be  $0.75Z$ , and take the network throughput to be  $r = r(\lambda, 0.75Z)$  ( $\lambda$  is the LAN packet transmission rate normalised to the wireless link transmission rate), where  $r(\lambda, w) = (\lambda^{(w+1)} - \lambda)/(\lambda^{(w+1)} - 1)$ , if  $\lambda \neq 1$ , and  $r(1, w) = w/(1 + w)$ .

We assume that the timeout is always the minimum timeout ( $rto\_min$ ) (a good assumption for a large coarse timeout and the local network situation). It follows that the

recovery time due to repeated, exponentially growing timeouts, is given by  $rto\_min/[1 - 2\gamma/(\gamma + \beta)]$  (for this equation to hold, we must have  $\gamma/(\gamma + \beta) < 0.5$ ).

It follows that the throughput of OldTahoe is given by

$$T_{\text{OldTahoe}} = \frac{(1/\gamma) + \text{residual\_good}}{(1/\gamma r) + rto\_min/[1 - 2\gamma/(\gamma + \beta)]},$$

where the first term in the denominator is the mean time for transmitting  $1/\gamma$  good packets. The throughput of Tahoe is given by

$$\begin{aligned} T_{\text{Tahoe}} = & (1/\gamma + \text{residual\_good}) \\ & \div \left( \frac{1}{\gamma r} + \sum_{M=2}^{W_{\max}} u_M \left( (1 - \phi_M) \frac{rto\_min}{1 - 2(\gamma/(\gamma + \beta))} \right. \right. \\ & \quad \left. \left. + \phi_M^{(G)} \frac{M}{r} + \phi_M^{(B)} \left( \frac{M}{r} + \frac{rto\_min}{1 - 2\gamma/(\gamma + \beta)} \right) \right) \right). \end{aligned}$$

Here the second term in the denominator is an expectation over the loss window distribution; the term corresponding to each  $M$  is the sum of the recovery durations for three possibilities: the first, if fast retransmit fails, the second, if fast retransmit succeeds and the next cycle finds the channel in the Good state, and the last, if fast retransmit succeeds but the channel is found in the Bad state, necessitating a timeout-based recovery.

## 5. Numerical results and discussion

We present numerical results for the same numerical parameters as in Kumar (1996). The wireless link speed is 1.5 Mbps (all rates are normalised to this rate) and the LAN host can transmit at 5 times the wireless link rate (i.e.,  $\lambda = 5$ ). The TCP packet length is 1400 bytes; i.e., its transmission time on the wireless link is 7.5 ms; various times are normalised to this transmission time. The minimum timeout is 750 ms; or 100 packet service times on the wireless link. The fast retransmit threshold is  $K = 3$ . The carrier frequency  $f_c$  is taken to be 900 Mhz.

We consider DPSK (differential phase shift keying) modulation. In this analysis we do not consider forward error correction coding, or bit interleaving. The link protocol operates directly over the modulation scheme, and has an error detection code. With AWGN the BER for DPSK is given by

$$\epsilon = 0.5 \exp[-(E_b/N_0)]. \quad (11)$$

Thus without a link protocol, in AWGN, the TCP packets can be assumed to be lost independently with probability  $p$  given by

$$p = 1 - (1 - \epsilon)^{\text{packet\_length}} \quad (12)$$

We will provide numerical results with AWGN for comparison purposes. In figure 3 we plot the throughput of TCP OldTahoe and Tahoe versus the average SNR, with and without fading (i.e., AWGN). There is no link protocol; thus, whenever a packet encounters a fade

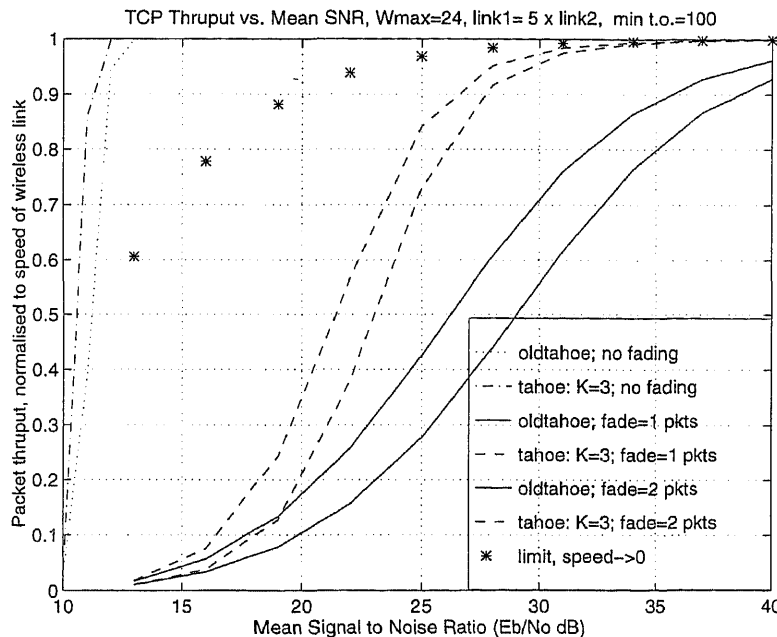


**Figure 3.** Throughput of versions of TCP vs. mean signal to noise ratio; no link protocol;  $K$  is the fast retransmit threshold.

at packet is certainly lost. In the case of fading, two curves are shown for each version, corresponding to average fade durations of 1 and 2 packets. The Bad state corresponds to an SNR  $\leq 10$  dB.

Figure 3 shows that with AWGN an SNR of about 12 dB yields very good throughput, whereas, with fading, an SNR of about 30 dB is required to obtain a throughput better than 90% from TCP Tahoe. TCP OldTahoe requires an SNR of 40 dB. For a given SNR, increasing the fade length appears to improve the TCP throughput. This observation is explained as follows. The ‘‘fade limit’’ of 10 dB, taken together with the average SNR, fixes  $\alpha$  (see Section 2.2), and hence fixes  $\delta$ ; i.e., for a given value of  $E_b/N_0$  the ratio of the good and the bad periods is fixed (see (8)). It follows that, for fixed  $E_b/N_0$ , if the fade duration is increased from 1 to 2 packets then the good periods also increase by a factor of two. Thus, although increasing the fade duration results in a greater frequency of consecutive losses, since the good duration also increases, the TCP window can build large values before losses do occur. This yields a larger throughput for increasing fade duration. These observations hold for low speeds at which the fade durations are comparable to the packet transmission times (e.g.,  $E_b/N_0 = 20$  dB implies speeds of about 10 to 20 kmph).

Consider what would happen if the vehicle speed was allowed to reduce to zero. For example, if  $E_b/N_0 = 30$  dB then the probability that a connection *starts* in the bad state is 0.01 (see (8)). For very low speeds, during the entire duration of the connection, the channel will be in the same state as it was found at the beginning of the connection. Thus if the initial state found is bad the throughput is 0, otherwise the throughput is 1. Hence, averaged over connections, the average throughput seen by a TCP connection will be

0.99. It follows that in figure 3, for a fixed SNR of 30 dB, as the vehicle speed decreases the throughput of both Tahoe and OldTahoe will converge to 0.99. Similar calculations can be done for each value of SNR; these results are plotted as “limit, speed  $\rightarrow 0$ ” in figure 3. Note that we have no link protocol in the model for which results are shown in figure 3. With a link protocol, the throughput should be no worse than without one. Thus, we see that for speeds approaching zero the average throughput increases and converges to the throughput obtained from a “quasistatic” analysis assuming very long fade durations and good durations but with the appropriate probabilities. This observation is consistent with the results with a link protocol that we present next. We now fix the average SNR (to 30 dB or 25 dB), and, for a fixed fade limit of 10 dB, we study TCP throughput as a function of vehicle speed. We now include the link protocol model in our analysis (see Section 2.3).

In figures 4 and 5 we show the TCP throughout versus vehicle speed. The link packet length is 128 bytes; thus there are 11 link packets in a TCP packet. In figure 4 each link packet is attempted  $N = 2$  times, whereas in figure 5 each packet is attempted  $N = 8$  times.

Figure 4 shows that, as the vehicle speed increases from a small value, first the throughput (for both versions) decreases, hits a minimum, and then it increases. This is explained as follows. Note that if the fade duration is longer than the number of attempts made for a link packet then that link packet and the corresponding TCP packet is surely lost. To the left of the minimum point, the mean fade duration is longer than 2 link packets, and increases as the speed decreases; however, as observed earlier, the good period length increase too, hence the throughput increases. To the right of the minimum point, the fade duration is

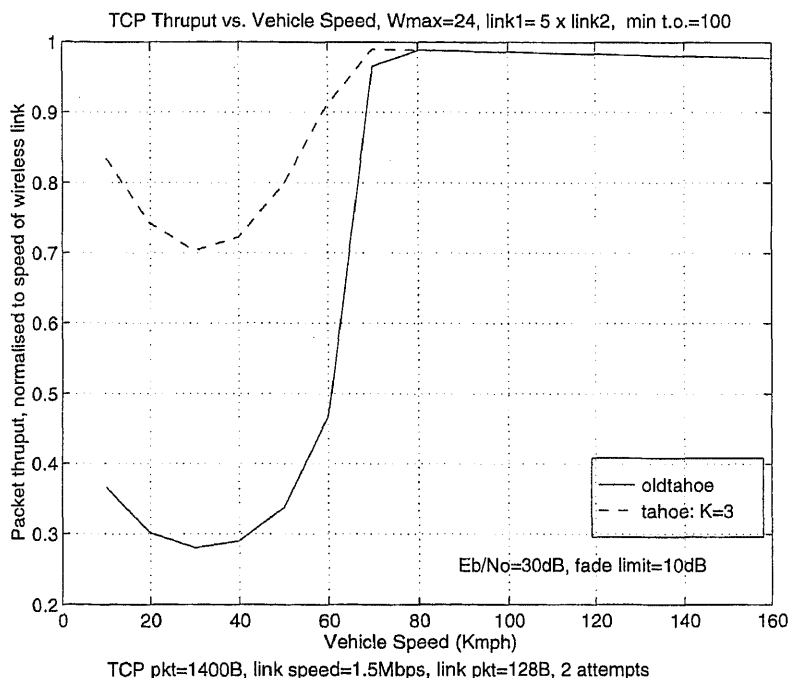


**Figure 4.** Throughput of versions of TCP vs. vehicle speed, for fixed  $E_b/N_0 = 30$  dB and fade limit = 10 dB; each link packet is attempted 2 times.

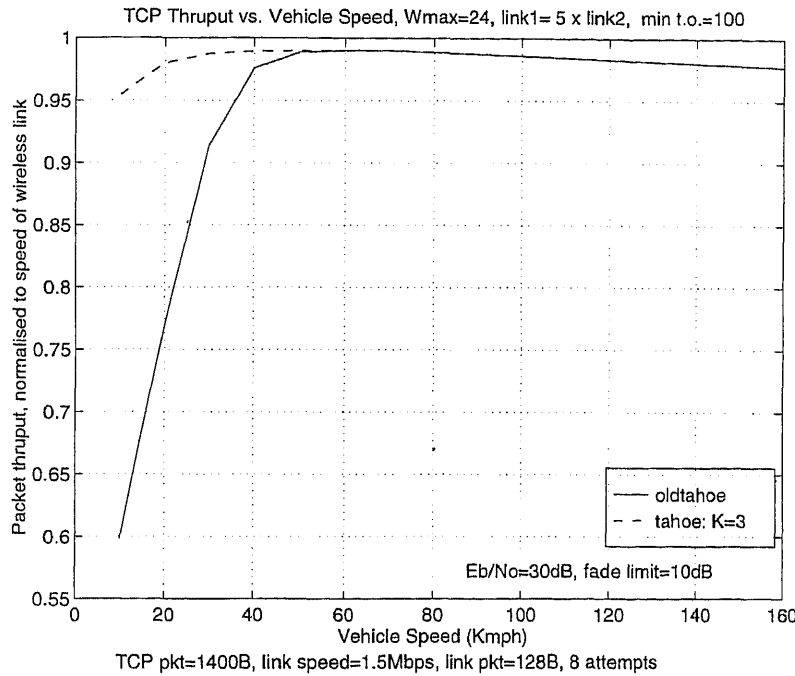


Figure 5. Throughput of versions of TCP vs. vehicle speed, for fixed  $E_b/N_0 = 30$  dB, and fade limit = 10 dB; each link packet is attempted 8 times.

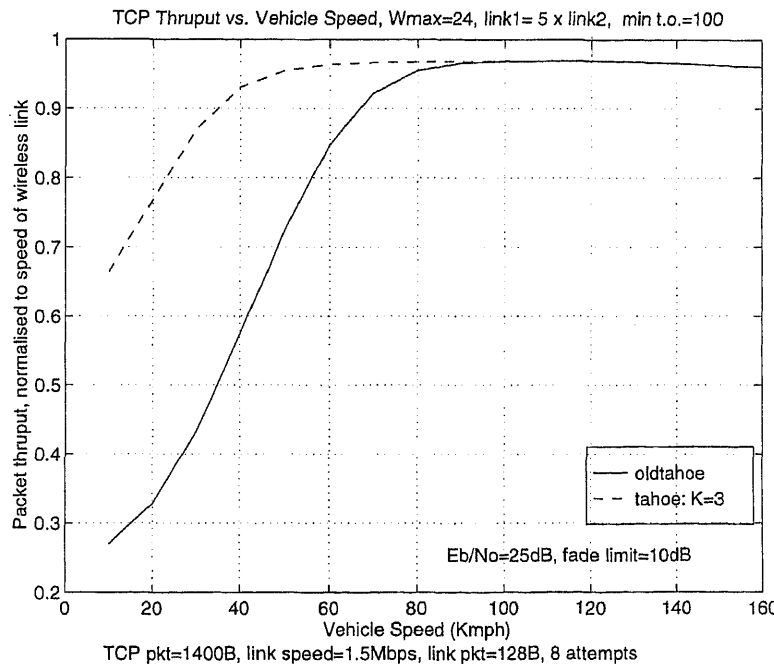


Figure 6. Throughput of versions of TCP vs. vehicle speed, for fixed  $E_b/N_0 = 25$  dB, and fade limit = 10 dB; each link packet is attempted 8 times.

smaller than 2 packets, and for larger vehicle speeds there is increasing probability that not all attempts of a link packet fail.

We note that the behaviour of throughput versus vehicle speed, for fixed SNR, in figure 4 is consistent with our discussion for low speeds in the context of figure 3. The throughput does increase for low vehicle speeds. If the curves in figure 4 are extrapolated as speed goes to zero, however, the limit will not match that obtained in the context of figure 3. This is because the model used to obtain the results in figure 4 (fading model at the link packet level, but Bernoulli losses across TCP packets) does not apply for very low vehicle speeds for which there is significant fade correlation between TCP packets.

Figure 5 shows that each link packet needs to be attempted 8 times for Tahoe to yield a good throughput for a large range of vehicle speeds. In figure 6 we show the effect of reducing the SNR by 5 dB. We find that 8 attempts are no longer enough even for Tahoe. The number of link packet attempts need to be increased to 16 for Tahoe to provide reasonably good performance (see Kumar & Holtzman 1996).

## 6. Conclusion

For the default parameters of the BSD implementation of TCP, over a 1.5 Mbps wireless link, as a general observation, we find that (without physical level enhancements, such as forward error correction and bit interleaving\*) an SNR of 25 dB to 30 dB is required to obtain from Tahoe a throughput greater than 90% of the wireless link speed. Without a link protocol, OldTahoe requires 40 dB; and with a link protocol OldTahoe suffers at low vehicle speeds, for which the fade durations are large. When using a link protocol, the choice of link packet length and the number of attempts for each packet are important parameters. Basically, the attempts have to “outlast” the fade. Since very large link packets defeat the idea of using link packets, small link packets have to be attempted several times. For a fixed SNR, a given link packet length, and a given number of link packet attempts, we find that throughput varies in an interesting way with vehicle speed. At very low speeds (e.g., pedestrian speeds) the throughput is high; it decreases with increasing vehicular speed until the fade durations become shorter than the number of link packet attempts. Beyond this speed, again the throughput increases, and is limited only by the expansion of the TCP packet transmission time owing to link-level retransmissions.

Much work remains to be done to develop more comprehensive protocol analyses even with the simple two state Markov loss model. Our analysis at present does not apply to many situations of interest; e.g., link protocols at very low speeds, or with large link packets. The Markov model can also be enhanced to include a nonzero loss probability in the Good state. Both these situations will require a more complex analysis, as the state of the Markov loss model will need to be included in the evolution of the TCP window process. Such enhancements of the analysis will be fruitful as future research. Other TCP versions, such as Reno and NewReno, also need to be analysed.

---

\*In any case, forward error correction and interleaving are not much help when there is slow fading.

## References

Bakre A, Badrinath B R 1995 I-TCP: Indirect TCP for mobile hosts. *Proc. 15th International Conf. on Distributed Computing Systems (ICDCS)*, pp 136–143

Balakrishnan H, Padmanabhan V N, Seshan S, Katz R H 1997 A comparison of mechanisms for improving TCP performance over wireless links. *Proc. ACM Sigcomm'96*, Stanford, CA

Cáceres R, Iftode L 1995 Improving the performance of reliable transport protocols in mobile computing environments. *IEEE J. Selected Areas Commun.* 13: 850–857

Chaskar H, Lakshman T V, Madhow U 1996 On the design of interfaces for TCP/IP over wireless. *Proc. IEEE MILCOM'96*; (also to appear in *IEEE J. Selected Areas Commun.*)

Desimone A, Chuah M C, Yue O C 1993 Throughput performance of transport layer protocols over wireless LANs. *Proc. IEEE Globecom'93*

Fall K, Floyd S 1996 Comparisons of Tahoe, Reno, and Sack TCP. manuscript, <ftp://ftp.ee.lbl.gov>

Gilbert E N 1960 Capacity of a burst-noise channel. *Bell Syst. Tech. J.* 39: 1253–1265

Jacobson V 1988 Congestion avoidance and control. *Proc. ACM Sigcomm'88*, August

Jakes W C 1974 *Microwave mobile communications* (New York: John Wiley and Sons)

Kumar A 1996 Comparative performance analysis of versions of TCP in a local network with a lossy link. WINLAB Technical Report No. 129, Rutgers University (Also submitted for publication to *IEEE Trans. Networking*)

Kumar A, Holtzman J M 1996 Comparative performance analysis of versions of TCP in a local network with a lossy link: Rayleigh Fading Mobile Radio Link. WINLAB Technical Report No. 133, Rutgers University, Piscataway, NJ

Lakshman T V, Madhow U 1997 The performance of TCP/IP for networks with high bandwidth delay products and random loss. *IEEE/ACM Trans. Networking* 5: 336–351

Lee E A, Messerschmitt D G 1988 *Digital communication* (Boston: Kluwer Academic)

Mishra P P, Sanghi D, Tripathi S K 1993 TCP flow control in lossy networks: Analysis and enhancements. In *IFIP Transactions C-13 Computer Networks, Architecture and Applications*, (eds) S V Raghavan, G Bochmann, G Pujolle (Amsterdam: Elsevier, North Holland) pp 181–193

Parsons J D 1992 *The mobile radio propagation channel* (London: Pentech)

Rappaport T S 1996 *Wireless communications* (New York: IEEE Press)

Rice S O 1958 Distribution of the duration of fades in radio transmission. *Bell Syst. Tech. J.* 37: 581–635

Stevens W R 1994 *TCP/IP illustrated* vol. 1 (Reading, MA: Addison-Wesley)

Wang H S, Moayeri N 1995 Finite-state Markov channel – a useful model for radio communication channels. *IEEE Trans. Vehicular Technol.* 44: 163–171

Wolff R W 1990 *Stochastic modelling and the theory of queues* (Englewood Cliffs, NJ: Prentice Hall)



# ACADEMY PUBLICATIONS IN ENGINEERING SCIENCES

Volume 1. The Aryabhata Project (eds UR Rao, K Kasturirangan)

Volume 2. Computer Simulation (eds N Seshagiri, R Narasimha)

Volume 3. Rural Technology (ed. A K N Reddy)

Volume 4. Alloy Design (eds-S Ranganathan, V S Arunachalam, R W Cahn)

...written by eminent scientists of India and abroad...Academy deserves all praise in bringing out these [papers]

*Powder Metall. Assoc. India, Newslett*

Volume 5. Surveys in Fluid Mechanics (eds R Narasimha, S M Deshpande)

An informal and stimulating publication...provides a survey of many important topics in Fluid Mechanics...All the papers are of excellent technical content and most are very well written. Many include lengthy reference lists, which are as useful as the body of the paper...The publishing quality is very good...

*IEEE J. Ocean Eng.*

...The general level (of papers) is high...Several are likely to have wide appeal...

*J. Fluid Mech.*

Volume 6. Wood Heat for Cooking (eds K Krishna Prasad, P Verhaart)

...interesting and stimulating account of technical thinking on the wood stove problem up to date...excellent collection of valuable and thought-provoking investigations.

*Rev. Projector (India)*

Volume 7. Remote Sensing (eds B L Deekshatulu, Y S Rajan)

Several contributions are specifically addressing topics of national interest, however, the majority of the papers is of general interest for a wide community. The book can serve not only as an inventory of the Indian activities, but also as a textbook on techniques and applications of remote sensing.

*Photogrammetria*

...particularly refreshing...

*Int. J. Remote Sensing*

Volume 8. Water Resources Systems Planning (eds M C Chaturvedi, P Rogers)

...well got up and very well printed...forms a valuable addition to our limited literature on Water Resources of India.

*Curr. Sci.*

Volume 9. Reactions and Reaction Engineering (eds R A Mashelkar, R Kumar)

...eighteen portraits of some major frontiers of research in CRE by a Micro-Who's Who of contemporary CRE researchers...good mix of theory and experiment that will provide many a good read for the specialist as well as the generalist researcher..."must-buy" for all research libraries, corporate or personal that contain CRE titles.

*Can. J. Chem. Eng.*

Volume 10. Reliability and Fault-Tolerance Issues in Real-Time Systems (ed. N Viswanadham)

...should help the reader to obtain a global view of the design of real-time systems with specifications in reliability and fault tolerance.

*IEEE Control Syst. Mag.*

11. Composite Materials and Structures (ed. K A V Pandalai)

...will surely find its place in libraries dealing with applied research.

*Bull. Electrochem.*

Volume 12. Developments in Fluid Mechanics and Space Technology (eds R Narasimha, A P J Abdul Kalam)

Volume 13. Advanced Ceramics (ed. E C Subbarao)

...presents a comprehensive view of advanced ceramics...should be of interest to students, research scientists, development engineers and to those engaged in the modern ceramic industry.

*Ind. Ceram.*

...most of the chapters put stress not only on the science, but also on the technological aspects.

*Trans. Indian Ceram. Soc.*

Volume 14. Modelling and Control of Stochastic Systems (eds N Viswanadham, V S Borkar)

Volume 15. Parallel and Real-Time Distributed Computing (ed. R K Shyamasundar)

Volume 16. Surveys in Fluid Mechanics - III (ed. R Narasimha)



*(Continued from back cover)*

Interpolation of erasure bursts via cosine-modulated filterbanks	103	<i>S Jayasimha and C G Hiremath</i>
Comparative performance analysis of versions of TCP in a local network with a mobile radio link	113	<i>A Kumar and J Holtzman</i>

# SĀDHANA

Academy Proceedings in Engineering Sciences

## CONTENTS

### Special Issue on Signal Processing and Communications

Foreword	1	<i>V U Reddy and A Kumar</i>
Parameter estimation using a sensor array in a Ricean fading channel	5	<i>K V S Hari and B Ottersten</i>
Spatial smoothing with uniform circular arrays	17	<i>K M Reddy and V U Reddy</i>
Region-of-interest reconstruction from noisy projections using fractal models and Wiener filtering	29	<i>A K Roy Chowdhury, K Barman and K R Ramakrishnan</i>
Rotational invariance of two-level group codes over dihedral and dicyclic groups	45	<i>J Bali and B S Rajan</i>
Power spectrum estimation of complex signals and its application to Wigner–Ville distribution: A group delay approach	57	<i>S V Narasimhan, E I Plotkin and M N S Swamy</i>
Asymptotic equivalence of some adaptive biquad notch filters	73	<i>V V Krishna and C G Hiremath</i>
Convergence and bias in the LSG algorithm for adaptive lattice filters	83	<i>R Negi and P G Poonacha</i>
I-Q imbalance correction in time and frequency domain with application to pulse Doppler radar	93	<i>N Sivannarayana and K V Rao</i>

(Continued on inside back cover)